University of Alberta

Liquefaction and Seabed Instability in the Fraser River Delta

BY

ANNAJIRAO V. CHILLARIGE

A thesis submitted to the Faculty of Graduate Studies and Research in partial fulfillment of the requirements for the degree of Doctor of Philosophy

in

GEOTECHNICAL ENGINEERING

DEPARTMENT OF CIVIL ENGINEERING

Edmonton, Alberta

Fall 1995

National Library of Canada
Bibliothèque nationale du Canada

Acquisitions and Bibliographic Services Branch
Direction des acquisitions et des services bibliographiques

395 Wellington Street
Ottawa, Ontario
K1A 0N4

395, rue Wellington
Ottawa (Ontario)
K1A 0N4

Your file *Votre référence*

Our file *Notre référence*

THE AUTHOR HAS GRANTED AN IRREVOCABLE NON-EXCLUSIVE LICENCE ALLOWING THE NATIONAL LIBRARY OF CANADA TO REPRODUCE, LOAN, DISTRIBUTE OR SELL COPIES OF HIS/HER THESIS BY ANY MEANS AND IN ANY FORM OR FORMAT, MAKING THIS THESIS AVAILABLE TO INTERESTED PERSONS.

L'AUTEUR A ACCORDE UNE LICENCE IRREVOCABLE ET NON EXCLUSIVE PERMETTANT A LA BIBLIOTHEQUE NATIONALE DU CANADA DE REPRODUIRE, PRETER, DISTRIBUER OU VENDRE DES COPIES DE SA THESE DE QUELQUE MANIERE ET SOUS QUELQUE FORME QUE CE SOIT POUR METTRE DES EXEMPLAIRES DE CETTE THESE A LA DISPOSITION DES PERSONNE INTERESSEES.

THE AUTHOR RETAINS OWNERSHIP OF THE COPYRIGHT IN HIS/HER THESIS. NEITHER THE THESIS NOR SUBSTANTIAL EXTRACTS FROM IT MAY BE PRINTED OR OTHERWISE REPRODUCED WITHOUT HIS/HER PERMISSION.

L'AUTEUR CONSERVE LA PROPRIETE DU DROIT D'AUTEUR QUI PROTEGE SA THESE. NI LA THESE NI DES EXTRAITS SUBSTANTIELS DE CELLE-CI NE DOIVENT ETRE IMPRIMES OU AUTREMENT REPRODUITS SANS SON AUTORISATION.

ISBN 0-612-06192-2

Canada

University of Alberta

Library Release Form

Name of Author: AnnajiRao Venkata Chillarige

Title of Thesis: Liquefaction and Seabed Instability in the Fraser River Delta

Degree: Doctor of Philosophy

Year this Degree Granted: 1995

Permission is hereby granted to the University of Alberta Library to reproduce single copies of this thesis and to lend or sell such copies for private, scholarly, or scientific research purposes only.

The author reserves all other publication and other rights in association with the copyright in the thesis, and except as hereinbefore provided, neither the thesis nor any substantial portion thereof may be printed or otherwise reproduced in any material form whatever without the author's prior written permission.

2 - 14 - 148/C
1st Line, Shymala Nagar
Guntur - 522006, India.

Date Sep 28, 1995

University of Alberta

Faculty of Graduate Studies and Research

The undersigned certify that they have read, and recommend to the Faculty of Graduate Studies and Research for acceptance, a thesis entitled **Liquefaction and Seabed Instability in the Fraser River Delta** submitted by **AnnajiRao V. Chillarige** in partial fulfillment of the requirements for the degree of Doctor of Philosophy in Geotechnical Engineering.

Dr. N.R. Morgenstern (Supervisor)

Dr. P.K. Robertson (Co-Supervisor)

Dr. D.C. Sego (Committee Chairman & Examiner)

Dr. P. Steffler (Committee Member)

Dr. T. Moslow (Committee Member)

Dr. D. Prior (Committee Member)

Date Sep 28, 1995

Abstract

Flow liquefaction failures of sand deposits in the Fraser River Delta are a major concern for the stability of coastal structures. These failures are believed to be triggered by environmental processes, such as rapid sedimentation, surface waves, drawdown effects associated with large tidal amplitude changes, gas in the sediments, tidal currents, dredging and the interaction of these events. An investigation to evaluate the possible contributions of these triggering mechanisms in a major liquefaction failure that occurred in 1985 has been carried out in this thesis.

The background for explaining liquefaction failures in the Fraser River Delta (FRD) is based on steady state concepts. Flow liquefaction is the strain softening and collapse of a loose sand to its steady state. Steady state divides sand into two possible states, that is, contractive and dilative. A contractive sand with its driving stresses greater than its steady state strength has a potential for flow liquefaction. A dilative sand requires large strains to reach its steady state and, hence may not be susceptible to flow liquefaction. The concepts of collapse surface and contractant state boundary are discussed in explaining the triggering of flow liquefaction in contractive sands. Different processes influence the deposition of sand at the mouth of the Fraser River in the delta. Explanation of the triggering of the flow slides in sand deposits of the delta requires knowledge of steady state parameters. Laboratory test results on the Fraser River Delta sand are presented and discussed. A chart is developed to characterize the in-situ state of deposits of the FRD. In-situ test results, such as Cone Penetration Tests and Seismic Cone Penetration Tests are performed and evaluated for flow liquefaction susceptibility of the deposits in FRD. The evaluation shows that the sediments are prone to flow liquefaction.

The potential triggering mechanisms, such as rapid sedimentation, surface waves and low tides are evaluated. To evaluate the contribution of sedimentation as a triggering mechanism, the stress state in the deposits is established using finite element stress analysis. The stress state is evaluated using the chart developed from laboratory tests, conducted as part of this study. The analysis shows that the sedimentation builds up shear stresses, but can not initiate flow liquefaction failures. The evaluation for the effect of wind generated surface waves in causing deep seated liquefaction flow slide is aided by a field study for wave induced porewater pressures in the delta. The study indicates that no significant porewater pressures accumulate due to surface waves and hence, surface waves can not trigger deep seated flow liquefaction failures. The effect of tides in causing the flow slides in the sediments of FRD is evaluated. The tides can not initiate failure in submerged saturated sands. However, gas induces desaturation of the sediments and the effect of tides on gaseous sediments is investigated. It is found that the presence of gas induces residual pore pressures in the sediments during low tides and contributes to the triggering of flow liquefaction failures in the delta. These failures lead to retrogressive flow slides.

Acknowledgement

This research was conducted under the guidance of Professor N. R. Morgenstern and Professor P. K. Robertson of Geotechnical Engineering at the University of Alberta.

I am really indebted to Prof. Morgenstern for his guidance and support during these years of research. I am grateful for his exceptional patience and encouragement. His time, discussions, suggestions and expertise were invaluable in accomplishing this research. Without his constant support and enthusiasm, this research would not have been possible.

I am also grateful to Prof. Robertson for his valuable discussions, suggestions and guidance. His time, support, ideas and enthusiasm through out the course of this study are very much appreciated.

I wish to thank Prof. Sego for his help and suggestions.

I gratefully acknowledge the financial support provided by the Canadian Commonwealth Scholarship and Fellowship program and Prof. Morgenstern. I sincerely express my thanks to the Government of India for sponsoring me for the Canadian Common Wealth Scholarship which contributed significantly to my coming to Canada.

The field study in the Fraser River Delta was largely funded by the Geological Survey of Canada. My special thanks are to Mr. Harold Christian of the Atlantic Geoscience Center, Geological Survey of Canada for his invaluable comments in my thesis and help during field work at Sand Heads in the Fraser River Delta. Mr. Christian kindly provided soil samples for laboratory testing.

I wish to further thank Mr. Glenn Jolly, Addara Systems Ltd., Vancouver and Mr. David J. Woeller, ConeTec Investigations Ltd., Vancouver for helping in the field work at Sand Heads in the Fraser River Delta.

Special thanks are due to Mr. Gerry Cyre and Mr. Steve Gamble for their assistance during the laboratory work.

Many thanks are extended to Mr.Sam Proskin for reviewing the first draft and for his constructive criticism.

I also wish to thank Mr. Amin Touhidi for his help during the laboratory work. I very much enjoyed his company during my stay. I thank all the new friends, I met in Canada for making my stay very enjoyable, in particular, Sam Proskin, Richard Stahl, Peter Skopek, Hak Joon Kim, Ali Pak, Abbas Soroush, Barb Hoffman and Catherine Fear.

My thanks to Dr. Srinivas Mandalapu and his wife for their help during my stay in Edmonton.

The love and support of my parents, brother and sisters have always been an essential source of strength at all stages of my life. To them I am deeply grateful. I owe thanks to my maternal uncle and my aunt Dr. Vijaya Dhannawada for their constant encouragement.

I wish to express my greatest appreciation to my wife, Radhika. Without her love, patience, support and encouragement I could not have achieved this goal.

Table of Contents

Chapter		Page
1.	Introduction	
	1.1. General	1
	1.2. Basis of Framework for Liquefaction	2
	1.2.1. Liquefaction Phenomenon	2
	1.2.2. Liquefaction Terminology	3
	1.3. History of Submarine Liquefaction Flow Slides	4
	1.3.1. Flow Slides in The Netherlands	4
	1.3.2. Flow Slides in Norway	5
	1.3.3. Flow Slides in the United States of America	6
	1.3.4. Flow slides in Canada	6
	1.4. Observations from the Historical Slides	8
	1.5. Objective of the Present Work and Scope of the Thesis	10
2.	Developments in Steady State Concepts	
	2.1. Introduction	18
	2.2. Steady State Line	19
	2.2.1. Influence of confining stress on steady state	22
	2.2.2. Influence of sample preparation methods	23
	2.2.3. Influence of strain rate during the tests	24
	2.3. In-situ Strength of Soil	24
	2.4. Effect of permeability of soil deposits in liquefaction	24
	2.5. Mechanism of Flow slides	25
	2.6. Advances in steady state concepts	26

2.6.1. Collapse Surface 26

2.6.2. Contractant State Boundary Surface 27

2.6.3. Implications of Cyclic Loading on CSB 29

2.6.4. Dilative Boundary Surface 30

2.7. Application of CSB concept for flow slides 34

2.8. Summary 35

3. The Fraser River Delta

3.1. Introduction 49

3.2. Geographical and Geological Setting 49

3.3. Morphological Setting 50

3.4. Fluvial Setting 51

3.5. Progradation of the Delta 51

3.6. Oceanographical Setting 53

3.7. Sediment Dynamics at the Mouth 53

3.8. Influence of Dredging on Sedimentation 55

3.9. Influence of Mass Wasting Events 55

3.10. Morphological Features on the Fraser Delta Slope 57

3.10.1. Sea Valleys 57

3.10.2. Sand Waves 58

3.10.3. Foreslope Hills 58

3.11. Summary 59

4. Characterization of the Fraser River Delta Sands near Sand Heads

4.1. Introduction 63

4.2. Laboratory Testing on the Fraser River Delta Sand 64

4.2.1. Physical Properties of Material Tested 64

4.2.2. Testing apparatus 65

4.2.3. Sample Preparation 65

4.2.4. Testing Program and Results 66

4.3. Shear Wave Velocity Measurement 68

4.3.1. Laboratory Measurements of Shear Wave Velocity 69

4.3.2. Shear Wave Velocity Measurements in the Present Study 70

4.4. Coupling of Vs Measurements to the Steady State Line 71

4.4.1. e - p' - Vs Relationship for the Fraser River Delta Sand 72

4.5. In-situ Tests in the Fraser River Delta 74

4.6. Evaluation of liquefaction susceptibility of the Deposits at Sand Heads 75

4.6.1. Evaluation Based on Cone Penetration Tests 75

4.6.2. Evaluation from Seismic Cone Penetration Test (SCPT) 76

4.6.3. Evaluation Based on State Parameter Approach 77

4.7. Summary 79

5. Evaluation of Influence of Sedimentation

5.1. Introduction 96

5.2. Configuration of the Slope in the FRD 96

5.3. State of Stress in the Slope 97

5.3.1 Modeling the Slope Using SIGMA/W Program 98

5.3.2 Results from the Analysis 99

5.3.3 Characterization of the Stress State of the Soil in the Slope 101

5.3.4 Characteristics of the Sediments in the Slope 103

5.4. Summary 104

6. Evaluation of Surface Wave Effects

6.1. Introduction 120

6.2. Wave-induced Bottom Pressures on the Ocean Floor 120

6.2.1 Wave induced Stresses within the Seabed 122

6.3. Wave induced Porewater Pressures 122

6.3.1 Transient Pore Pressures 123

6.3.2 Residual Porewater Pressures 123

6.3.3 Distinction Between Transient and Residual Porewater Pressures 124

6.4. Additional Studies on the Effect of Surface Waves on Seabed Instability 124

6.5. Wave-induced Liquefaction Studies 125

6.6. Measurement of Wave-induced Pore Pressures in the FRD 125

6.6.1. Design of Probes 125

6.6.2. Data Acquisition 126

6.6.3. Probe Installation 127

6.6.4. Results from the Pore Pressure Probe Study 128

6.7. Wave Effects on the Seabed Instability at the FRD 129

6.7.1. Verification of Threshold Shear strain 129

6.7.2 Influence of Transient Pore pressures 131

6.8. Summary 131

7. Evaluation of the Effect of Tides

7.1. Introduction 141

7.2. Modeling Tidal Variations for One-Dimensional Flow Conditions 142

7.3. Evaluation of Tidal Drawdown on Saturated Sediments 144

7.4. Effect of Tidal Drawdown on Gaseous Sediments 146

7.4.1 Evaluation of Tidal Drawdown on Gaseous Sediments in the FRD 148

7.4.2. Stress Path Evaluation 151

7.4.3. Implication of the Stress path on the Contractant State Boundary Surface 153

7.5. Development of Flow Slides 154

7.6. Summary 155

8. Summary and Conclusions

8.1. Summary of Thesis 163

8.2. Conclusions 170

8.3. Recommendations 171

8.4. Further Research 172

Bibliography 174

Appendix A

Methods of Sample Preparation 187

Appendix B

Modeling Tidal Loading on Saturated Sediments 190

Appendix C

Modeling Tidal Loading on Gaseous Sediments 194

List of Tables

Table	Pages
1.1. Earthquake Induced Flow Slides in Submarine Deposits	13
1.2. Statically Induced Flow Slides in Submarine Deposits	15
4.1. Shear Wave Velocity Measurements during Consolidation and Stresses at Steady State	80
7.1. Compressibilities of Pore Fluid at Different Degrees of Saturation and Ratio of Compressibilities	156

List of Figures

Figure		Page
1.1	Liquefaction terminology	16
1.2	Morphology of The Fraser River Delta (after McKenna and Luternauer, 1987)	17
2.1	Undrinaed test on contractive sand	36
2.2	Drained test on contractive sand	36
2.3	Stress paths of contractive and dilative sand (after Sladen et al., 1985)	37
2.4	Undrained test on dilative sand (after Been et al., 1991)	38
2.5	Drained test on dilative sand (after Been et al., 1991, Lee and Seed, 1967)	38
2.6	Undrained test on contractive dilative sand	39
2.7	Steady state line - projections on planes	40
2.8	Influence of relative density on steady state line	41
2.9	Collapse surface (after Sladen et al., 1985)	42
2.10	Collapse surface in e-p'-q space (Sladen et al., 1985)	43
2.11	Contractant state boundary surface (Alarcon-Guzman et al., 1988; Ishihara et al., 1991)	44
2.12	Confirmation tests for contractant state boundary surface	45
2.13	Effect of cyclic loading on saturated liquefiable sands	46
2.14	Dilative state boundary surface	47
2.15	Instability line (Lade, 1993)	48
3.1	Geographical locations and physiography of the western delta front of the Fraser River	60
3.2	Surficial deposits in the Fraser River Delta	61
3.3	Deposition of sediment at a river mouth (Coleman, 1976)	62
4.1	Morphology of the Fraser River Delta foreslope off the Main Channel (after McKenna and Luternauer, 1987)	81
4.2	Grain size distribution curve of the Fraser River Delta Sand	82

4.3	Triaxial test set-up (after Cunning, 1994)	83
4.4	Results of consolidated undrained triaxial tests	84
4.5	Results of consolidated drained triaxial tests	85
4.6	Normalised stress paths of tests on the Fraser River Delta Sand	86
4.7	Typical undrained and drained stress paths	87
4.8	Steady state line - The Fraser River Delta Sand	88
4.9	Typical oscilloscope output	89
4.10	Normalised shear wave velocity against void ratio	90
4.11	Steady state line - Fraser River Delta Sand Measured shear wave velocities during consolidation Contours of shear wave velocities	91
4.12	CPT profile at site B (Figure 4.1) in the Fraser River Delta	92
4.13	CPT profile at site D (Figure 4.1) in the Fraser River Delta	93
4.14	Assessment of liquefaction potential of sand deposits from CPT2 profile	94
4.15	Assessment of liquefaction potential from shear wave velocity measurements	95
5.1	Areal extent of the flow slide in 1985 in the FRD	106
5.2	Slope along section 1-1	107
5.3	Finite element mesh (vertical exaggeration 10)	108
5.4(a)	Contours of effective X-stress state of the elements	109
5.4(b)	Contours of effective Y-stress state of the elements	110
5.4(c)	Contours of effective X-Y stress state of the elements	111
5.4(d)	Contours of mean confining stress (p') state	112
5.4(e)	Contours of deviatoric stress (q) state	113
5.4(f)	Contours of maximum shear stress state	114
5.5	Effective stress state of elements in the slope	115
5.6	Path of maximum shear stress due to sedimentation	116
5.7	Stress state of the node 616	117
5.8	Characterization of the stress state in the fresh deposits of the FRD	118

5.9	Evaluation of the stress state of fresh deposits in the FRD	119
6.1	Bottom pressures and stress changes from wave loads	132
6.2	The relationship between wave period, wave length and water depth (after Weigel, 1964)	133
6.3	The wave-induced pressure on ocean floor (Seed and Rahman, 1978)	133
6.4	Results of cyclic loading tests on saturated sands (Stokoe et al., 1987)	134
6.5	Pore pressure probe	135
6.6	Location of probes in the FRD	136
6.7	Pressures @ 4.17 p.m. - Probe No.1	137
6.8	Mudline and Tip pressures - Probe No.2	138
6.9	Significant wave heights (using Bretschneider's theory)	139
6.10	Variation of pore pressure due to a wave of 2.7 m and wave length 40 m	140
7.1	Tide conditions @ Sand Heads - June, July 1 - 11	157
7.2	Influence of a tide of 5 m with a period of 16 hr on saturated sediments	158
7.3	Pore air and pore water pressure responses to a change in total stress during undrained compression (Fredlund and Rahardjo, 1993)	159
7.4	Components of compressibility of an air-water mixture (Fredlund and Rahardjo, 1993)	159
7.5	Variation of pressures for a tide of 5 m with 16 hr period (S=98%)	160
7.6	Stress path due to a tide of 5 m (When S =98%)	161
7.7	Influence of tidal drawdown on the contractant state boundary surface	162

List of Symbols and Abbreviations

A	Intercept of the V_{s1} - e relationship at e = 0 (Shear wave velocity parameter)
B	Slope of the V_{s1} - e relationship (Shear wave velocity parameter)
c_v	Coefficient of consolidation of soil skeleton
c_{vg}	Coefficient of consolidation of gaseous sediments
D_{50}	Mean grain size
e	Void ratio
G	Shear modulus
G_0	Small strain shear modulus
H	Surface wave height (m)
Hz	Hertz
k	Coefficient of permeability of sediments
K	Wave number
K_o	Coefficient of earth pressure at rest
L	Wave length
m_v	Compressibility of soil skeleton
M	Slope of the steady state line in p'-q plane
n	porosity of the soil structure
p'_{ss}	Mean normal confining stress at steady state
p_c'	Mean normal effective consolidation stress
q	Deviatoric stress
q_c	Cone penetration resistance
q_{c1}	Normalized cone penetration resistance
r	ratio of consolidation coefficients
s	Slope of the contractant state boundary
S	Degree of saturation
t	Slope of the collapse surface in p'-q plane
T	Time Period of surface waves
u	Pore pressure
V_{s1}	Normalized shear wave velocity
V_s	Shear wave velocity
z	Depth below seabottom
α_l	Angle of the collapse surface in p'-q plane
α_{ss}	Angle of steady state line in p'-q plane
β	Compressibility of pore fluid
ϕ'	Angle of shearing resistance at steady state
γw	weight of water (kN/m^3)
Γ	Ordinate of the steady state line at p' = 1 kPa
λ_{ln}	Slope of the steady state line in the e- ln p' plane
σ	Total stress due to tidal loading
σ_1'	Major principle Stress
σ_2'	Intermediate principle Stress
σ_3'	Minor principle Stress
σ_{vo}'	Effective vertical overburden stress
ω	Circular frequency of surface waves

ASTM	American Society of Testing Materials
CPT	Cone Penetration Tests
CSB	Contractant State Boundary Surface
DFR	Drained test on the Fraser River Delta sand
DSB	Dilative State Boundary Surface
FRD	Fraser River Delta
FSH	Foreslope Hills
LVDT	Linear Variable Differential Transformer
SCPT	Seismic Cone Penetration Tests
SSL	Steady state line
UDFR	Undrained test on the Fraser Delta sand

1.0 Introduction

1.1 General

Instability in coastal and underwater slopes is a natural phenomenon and its impact is felt when human developmental activities extend into these subaqueous environments. Safety of coastal structures such as jetties, breakwaters, lighthouses, pipelines and offshore platforms is a major concern due to slope instability. A major source of instability in cohesionless sediments is the result of liquefaction flow slides. The flow slides are recurrent phenomena in the active river deltas in the world. These flow slides can be triggered by dynamic effects, such as earthquakes, blasting and vibrations due to pile driving operations and by static effects. The occurrence of flow slides due to static effects has usually been unexpected and unexplained. Terzaghi (1956) referred to the phenomenon of sudden or static liquefaction of loose sands by minor triggering mechanisms as spontaneous liquefaction. Several cases of liquefaction induced flow slides in subaqueous environment have been presented by Terzaghi (1956), Morgenstern (1967), Seed (1968), Schwarz (1982) and Chaney and Fang (1991). Table 1.1 presents cases of earthquake induced liquefaction flow slides in the marine environment. These flow slides are the result of undrained failures of sediments. Table 1.2 summarizes cases of spontaneous liquefaction failures of sediments in river deltas and in coastal deposits. An explanation for the static liquefaction flow slides in coastal zones is not well established in the literature and has resulted in speculation. Different environmental processes such as rapid sedimentation, low tides, surface waves, gas in the sediments, currents and dredging operations may trigger or contribute to the initiation of liquefaction flow slides in river deltas. Researchers studying the causes of triggering of flow slides in river deltas have not quantified the contributions of the triggering mechanisms. The present work investigates a liquefaction flow slide that occurred in 1985 in the Fraser River Delta and evaluates the

contributions of different environmental processes in triggering the flow slide. Background to the liquefaction phenomenon is required for explaining the causes of liquefaction flow slides. In the literature the generic term liquefaction is used to describe different mechanisms. However, the definition by Castro (1969) for liquefaction provides a strong basis to explain the phenomenon.

1.2 Basis of Framework for Liquefaction

1.2.1 Liquefaction Phenomenon

While explaining liquefaction failures of loose cohesionless sediments, studies have concentrated on defining liquefaction as the condition where effective stress approaches zero (Seed et al. 1983). An approach by Castro (1969) for defining liquefaction provided great insight into the phenomenon. He defined liquefaction as the behaviour of saturated, metastable sand immediately after collapse with increasing pore pressures which decrease the effective stresses resulting in a reduction in the shear resistance (called strain softening) to a constant value, called a steady state. During liquefaction the destructured mass of soil behaves as a thick viscous liquid. If the gravitational shear stresses are larger than the steady state strength of the soil deposit, liquefaction leading to large flow deformations can occur. When the failure occurs on slopes, a flow slide can develop. In level ground conditions, the soil loses its bearing capacity which affects structures founded on the soil. Catastrophic failures associated with liquefaction of sands have been observed just after earthquakes in Alaska and in Japan in 1964.

The research based on steady state concepts is important in understanding the behaviour of liquefiable soils. An explanation for the phenomenon has been established within the framework of critical state soil mechanics as developed by Roscoe et al. (1958). In the

framework, a state of soil at any time can be represented by a point in the space e-p'-q where e is void ratio, p' is mean normal effective stress and q is deviatoric stress. Response of the soil to the changes of stress is determined by following the appropriate stress path of the soil in the e-p'-q space. Laboratory testing of a soil specimen in the specified stress path measures the response of the soil. The specimen is initially subjected to the in-situ stresses and loaded with the subsequent stress changes that are expected in the field. The critical state is the state at which a soil can deform at constant state of stress at constant volume (no changes of void ratio). A critical state is uniquely defined as the state of failure for a given soil. The steady state condition is the critical state condition for sandy soil (Castro, 1975, Poulos, 1981). Shear behaviour of sand subjected to different drainage conditions is described and discussed in Chapter 2 in detail.

1.2.2. Liquefaction Terminology

To bring out the differences between different mechanisms of liquefaction, Robertson (1994) suggested specific liquefaction terminology. Flow liquefaction describes a strain softening response in undrained shear loading for the case of in-situ gravitational shear stresses greater than the steady state strength. Flow liquefaction follows closely the definition of liquefaction suggested by Castro (1969). Cyclic undrained shear loading can also induce flow liquefaction failures. This concept is illustrated in Figure 1.1 (Case 1).

If the gravitational shear stresses are smaller than the steady state strength in a soil deposit, the response of the soil for undrained shear loading will be strain hardening at large strains. If a slope or level ground is composed entirely of strain hardening soil, undrained collapse and flow failure cannot occur and deformation will, in general, be small. However, cyclic loading can induce cyclic softening of the material in the slope. If the amplitude of the

cyclic undrained shear stress is greater than the in-situ gravitational shear stress, shear stress reversal occurs with both shear stress and confining stresses approaching zero values. Figure 1.1 (Case 2) shows the zero effective stress state which is termed cyclic softening. At this state the soil has very little stiffness and large deformations can result under very small gravitational shear stress.

Cyclic mobility results when there is no shear stress reversal during undrained cyclic loading with limited deformation. Zero effective stress does not develop during cyclic mobility of the strain hardening material. Figure 1.1 (Case 3) illustrates this mechanism.

1.3. History of Submarine Liquefaction Flow Slides

A number of static liquefaction flow slides in the coastal environment have been reported. The slides have involved similar materials and have occurred under similar circumstances. A few historical cases of static liquefaction flow slides are presented below.

1.3.1. Flow Slides in The Netherlands

Flow slides are common during low tides on the shores of Zeeland province, Netherlands. The flow slides occurred on average slopes of 15 degrees (Koppejan et al, 1948, Terzaghi, 1956) and eroded material from dikes constructed to protect low lying areas from high waters. Enormous volumes of fine sand are involved in the flow slides. The fine sands are deposited by streams in the estuaries with porosities ranging from 47.5 to 48.5 percent and these fine sands are very metastable. A metastable structure collapses with slight provocation. Terzaghi (1956) suggested that the breakdown of the metastable structure of the sediment was caused by the seepage pressure of the ground water which returned to the ocean during the receding tide.

1.3.2. Flow Slides in Norway

The process of liquefaction may spread from the site of a local disturbance to progressively larger areas. The slides that occurred in Follafjord in Norway in 1952 confirmed the spreading of the disturbances in loosely deposited fine sands and silts (Bjerrum, 1971; Terzaghi, 1956). A dredger used for constructing a harbour suffered anchor cable breaks due to a small slide. After a few minutes a larger slide developed which towed the dredger for a distance of 300m. The consequence of these failures was the foundation failure of two landing piers. At the site of the slide events, a river formed an estuary where the bottom of the fjord sloped outward at about 5 to 7 degrees. The reason for the first failure was believed to be the dumping of material from the dredging operations.

The failed masses of the flow slides can attain high velocities and can have destructive effects on submarine cables. The flow slides in Orkadalsfjord, Norway resulted in the breakage of submarine cables in 1930 (Andresen and Bjerrum, 1967; Terzaghi, 1956). The River Orkla deposits loose fine sands, silt and silty clay in the fjord. The slopes in the fjord ranged between 5 -10 degrees. Three successive flow slides occurred in fine sands during exceptionally low tide periods.

A railway embankment constructed on loose fine sand and coarse silt was damaged due to a flow slide in the Finnivika fjord, Norway in 1940 (Bjerrum, 1971). Some 100 m of the embankment disappeared beneath the water surface as a result of the slide which occurred during a low spring tide. Within a few minutes another major slide occurred in the fjord destroying some harbour structures.

A large slide occurred in thick deposits of loose fine sand in and along the banks of Hommelvika Bay, Norway in 1942 (Bjerrum, 1971). The slide occurred after spring low tide and involved some material from a fill and a 450 m length of coastline.

Retrogressive flow slides in Trondheim harbour of Norway occurred in natural deposits of silty fine sands during low tide periods in 1888 (Bjerrum, 1971). They were initiated in the fjord where the slope angles ranged between 8 to 15 degrees. A railway embankment and a jetty were destroyed in the slides. The damage occurred when a flood wave of 5 to 7 m receded from the shores.

1.3.3. Flow Slides in the United States of America

A liquefaction flow slide was reported in Puget Sound during dredging operations for construction of an effluent system at the head of Duwamish River (Kraft et al. 1992). The slide occurred during a low tide period and involved large volumes of fine sand. The slopes at the site of the dredging operations were about 16 degrees.

In November, 1994, a flow slide occurred during extreme low tides (4m) near Skagway, Alaska destructing harbour dock facilities (Morgenstern, 1995; personal communication). Seabed slopes of about 25 -30 degrees are common at the slide area. About 10 - 20 million cubic meters of silty sands were estimated to be involved in the slide. Gas release was observed from the debris of the slide.

1.3.4. Flow slides in Canada

Terzhagi (1956) discussed a flow slide that occurred in 1955 in deltaic deposits of sand and gravel on the northern shore of Howe Sound in southern British Columbia. The Squamish

River deposits sediments in an estuary and the maximum tidal range in the Sound is about 5 m. The flow slide occurred on the slopes of the deposits during extreme low tide conditions. Following the slide, a portion of a warehouse was destroyed and piles supporting a dock lost their bearing strength and failed. The soundings in the area showed that the gradient of the delta front was uniform ranging from 27 to 28 degrees. It was believed that drainage was impeded from sandy sediment by perched silty sediments during low tides.

Five major liquefaction flow slides occurred in 1983 during the construction of a hydraulically placed subsea sand berm in the Beaufort sea (Sladen et al, 1985). Failures were triggered by the sand placement at locally oversteepened side slopes. The slide material came to a halt at very flat slopes of 1 to 2 degrees after runout distances of about 100 m. The void ratio of the sand within the berm was approximately 0.8 with a permeability of 10^{-5} m/ sec. The slopes ranged between 10 to 12 degrees with a height of 20 to 30 m before failure.

In April 1975, a very large submarine liquefaction flow slide involving very rapid movement of sandy silts occurred at the foreslope of the Kitimat River Delta in British Columbia (Morrison, 1984). The depth of the slide was about 35 m. The slide developed an 8 m high sea wave. The flowslide and the sea wave carried away piles and anchors supporting a dock. The slide happened during extreme low tides. The tidal range at the time of the slide was about 6 m. and the slope was at about 19 degrees.

Liquefaction flow slides are recurrent in the Fraser River Delta on the western coast of Canada. Coastal structures are at risk to foundation movements resulting from the failures. Five major slides between 1970 and 1985 are reported by McKenna et al (1992) on the upper delta slopes at the mouth of the main channel of the Fraser River. The failures of the

delta front sediments are the result of liquefaction of silty sand and are believed to be triggered by different environmental processes, such as rapid deposition at the mouth during high river discharges, drawdown effects associated with large spring tides, earthquakes, storm-waves, gas generation due to bio-degradation of organic matter, tidal currents causing erosion of sediments and dredging operations in the navigation channel at the mouth of the river. A well documented major failure involving one million cubic meters of the delta front sediments occurred during low tide periods in 1985 (McKenna and Luternauer, 1987). Figure 1.2 shows that the failure scarp was close to Sand Heads lighthouse and Steveston Jetty. Soundings at the mouth of the Fraser River at Sand Heads indicated that the slide occurred between 27 June and 11 July 1985. The upper part of the delta slope has a gradient of approximately 0.05 degrees and the lower part of the delta fore slope has an average gradient of approximately 1.5 degrees (Mathews and Shepard, 1962), but may be inclined as steeply as 23 degrees along its upper reaches. (Scotton, 1977).

1.4. Observations from the Historical Slides

The liquefaction flow slides in the coastal sediments involved remarkably similar materials and similar conditions. Table 1.2 summarizes the descriptions of soils involved and the circumstances surrounding the failures. Some slopes have very low gradients and might have been the post event gradients. Conventional slope stability analyses of the slopes as presented by Morgenstern (1967) result in high factors of safety and the slopes should be stable. The reasons for the failures are very intriguing and are comprised of interactive environmental processes.

Failures resulting from liquefaction are often characterized by their speed of occurrence, the flatness of the slopes before and after failures, the large displacements of liquefied materials and the progressive nature of their development (Kramer, 1988). The characteristic feature

of the fine grained cohesionless material in the flow slides is the metastable structure. The structure collapses on slight provocation. Collapse slumping could be a possible type of slumping associated with the metastable sediments in the subaqueous environment (Morgenstern, 1967). A collapse slump is defined as the one that fails initially under drained conditions, but the deformations associated with the failure bring about a large increase in pore pressures and reduces shearing resistance of the material and leads to liquefaction.

Most of the subaqueous liquefaction flow slides occurred on the upper slopes in fjords and river deltas. When rivers deposit sediments in the estuaries, coarse grained soils are deposited close to the mouth of the river and finer grained soils are transported further offshore. Apparent cohesion between the silt and sand particles maintain higher void ratios during deposition. Andresen and Bjerrum (1967) speculate that the presence of a small quantity of fine particles cause the uniform fine sands to settle out at higher porosities. Removal of either the finest or the coarsest constituents of the sand eliminates the capacity of the sand to form an abnormally porous aggregate (Terzaghi and Peck, 1948). Observations from the Norwegian flow slides indicate that the sands with a small amount of fines or organic matter posses the highest porosities. From the observed liquefaction failures due to earthquake loading in silty sands, Ishihara (1993) states that the potential for flow failure is considered to be much higher for a dirty sand than for a clean sand. When the content of fine particles with plastic properties increases in fine sands, the possibility of liquefaction in the sands decreases. Liquefaction flow slides in the Fraser River Delta involved fine silty sands. A metastable structure may be the characteristic of the sediments at the mouth of the Fraser River.

Many uncertainities exist for explaining the triggering of flow liquefaction in metastable sands. The inadequate understanding of liquefaction flow slides during low tides in river

deltas necessitates further study of the triggering of the failures. The contributions of enironmental processes have to be explored and quantified. This thesis will investigate the liquefaction flow slide that occurred in 1985 on the Fraser River Delta slopes within the framework of steady state concepts.

1.5 Objective of the Present Work and Scope of the Thesis

The purpose of this research is to critically evaluate the triggering mechanisms of the 1985 liquefaction flow slide of the subaqueous Fraser River Delta (FRD) and to establish a stress path explaining the initiation of flow liquefaction of silty sands in the FRD. The flow slides are believed to be triggered by the environmental processes including rapid sedimentation at the mouth of the delta, tidal drawdown, tidal currents, surface wave effects, earthquakes, gas generation due to the decay of organic matter and dredging operations. However, seismic activity was not observed in 1985 at the delta front (McKenna and Luternauer, 1985). Hence, earthquakes were not the cause of the flow slide.

The following requirements are to be met for a liquefaction flow slide to occur.

To trigger liquefaction of the silty sands in the FRD, the deposits must have a metastable structure (strain softening material). In-situ gravitational shear stresses in the deposits should be greater than the steady state strength of the sediments. The stress path caused by different environmental processes should be able to explain the triggering of liquefaction of silty sands using the framework of steady state concepts.

To satisfy these requirements, the following elements are necessary.

i) Establish the physical setting of the FRD and the existing environmental conditions at the time of the failure

ii) Establish the steady state line for the silty sands of FRD for determining steady state strength of the sediments

iii) Perform stress analysis of the slope of the delta before failure and characterize the state of sediments in terms of strain softening and strain hardening responses

iv) Evaluate the effects of different triggering mechanisms in initiating liquefaction failures of the sediments

The scope of each chapter is:

Chapter 2: This chapter reviews the steady state concepts for explaining the liquefaction phenomenon and introduces the concepts of contractant and dilative state boundary surfaces. It also discusses implications of the state boundary surfaces in initiating liquefaction failures.

Chapter 3: The physical setting of the FRD and its progradation due to the sedimentation in the delta are described. Processes influencing the distribution of sediments are also discussed.

Chapter 4: This chapter presents different laboratory tests and results on reconstituted samples of FRD silty sand for establishing its steady state line and its parameters. It also introduces the use of bender elements in triaxial test samples for obtaining shear wave velocity measurements. The chapter also presents coupling of void ratio - effective confining stress - shear wave velocity (e-p'-V_S) measurements and the development of a chart for the evaluation of the in-situ state of deposits in the FRD. It discusses the evaluation of in-situ tests such as Cone Penetration Tests (CPT) and Seismic Cone Penetration Tests (SCPT) for assessing liquefaction potential of deposits.

Chapter 5: Influence of sedimentation is evaluated in this chapter by performing stress analysis of the deposits in the slope. The analysis uses a finite element based program - SIGMA/W and incorporates drained linear elastic parameters. The in-situ stress state of the FRD deposits is determined and is characterized using the chart developed in Chapter 4. Available undrained shear strength (steady state strength) of the deposits for the in-situ stress state is also obtained using the derived steady state line in Chapter 3.

Chapter 6: The effect of surface waves in causing deep seated liquefaction failures is discussed in this chapter. The analysis is also assisted by field measurements of surface wave induced pore pressures in the shallow depths of the slope. The pore pressures are monitored at a depth of 2 m using pore pressure probes. Results from the field study are presented and discussed. A concept of Threshold Shear Strain has been used to investigate the development of residual pore pressures for the surface waves in the deposits. Comparison between the observations of the field study and the results of the analytical study is made.

Chapter 7: The influence of tidal drawdown on saturated sediments is investigated in this chapter. The effect of tides on the deposits is modelled as a one-dimensional consolidation problem. The analysis uses finite difference methods to arrive at the magnitudes of pore pressures during the tidal drawdown. The results of the analysis are discussed in the light of the initiation of the liquefaction failures. The effect of gas in the sediments on the effective stress state is also presented in this chapter. The influence of tidal drawdown on gaseous sediments is also explored as a one-dimensional problem. The analysis examines the development of residual pore pressures during low tide conditions and evaluates the response (stress path) of sediments for the residual pore pressures. The implication of the resulting stress path on the contractant state boundary is also examined.

Chapter 8: Final conclusions and suggestions for further research are presented.

Slides	Magnitude	Deposits	Nature of soils	Slope angles	Reference
New Madrid earthquake, 1811 (Mississippi River Banks)		River Bank	Sands		Seed (1968)
Alaska (Yakutat), 1899		Submarine deposit	Deltaic marine sediments (silty sand and gravel)		Seed (1968)
Alaska (Valdez), 1908		Submarine deposit	Deltaic marine sediments (silty sand and gravel)		Seed (1968)
Messina cone, 1908	7.5	Submarine deposit	Sand/silt	4 degrees	Ryan and Heezen (1965) Schwarz (1982)
Alaska (Valdez), 1911	6.9	Submarine deposit	Deltaic marine sediments (silty sand and gravel)		Seed (1968)
Alaska (Valdez), 1912	7.25	Submarine deposit	Deltaic marine sediments (silty sand and gravel)		Seed (1968)
Chile, 1922	8.3	Submarine deposit	Sand with silt	6 degrees	Morgenstern, (1967)
Sagami Wan, 1923		Submarine deposit	Sand		Menard(1964) Morgenstern (1967);
Kwanto (Tokyo), 1923	8.2	Coastal hill sides			Seed (1968)
Grand Banks, 1929	7.2	Submarine deposit	Fine sand and silt	3.5 degrees	Heezen and Ewing (1952)
Suva, Fizi, 1953	6.75	Submarine deposit	Sand	3 degrees	Houtz and Wellman (1962)
Orleansville, 1954	6.7	Submarine deposit	Sand	4-20 degrees	Heezen and Ewing (1965)
Sanfransico, 1957	5.3	Lake banks	Aeolin beach sands		Seed (1968)
Chile (Puertto Montt), 1960	8.4	Coastal deposits	Loose sands and silts		Seed (1968)

Table 1.1. Earthquake Induced Flow Slides in Submarine Deposits

Slides	Magnitude	Deposits	Nature of soils	Slope angles	Reference
Alaska (Valdez), 1964	8	Submarine deposit	Silty sand and gravel	15-20 degrees	Holish and Hendron (1975)
Alaska (Seward), 1964	8.3	Submarine deposit	Loose to medium sand, gravel	15 -20 degrees	Holish and Hendron (1975) Seed (1968)
Alaska (Valdez), 1964	8.3	Submarine deposit	silty sands and gravel	4-10 degrees	Morgenstern (1967) Seed (1968)
Seattle,1965	6.7	Coastal bluff			Seed (1968)
Klamath River Delta, 1980 (California)	6.5	Submarine deposit	Fine sand	0.25 degrees	Field et al. 1982

Table 1.1. Earthquake Induced Flow Slides in Submarine Deposits

Flow slide	Nature of soil	Failure conditions	Slope angles	Reference
The Netherlands	Loose fine sand	Low tides	15 degrees	Koppejan et al., (1948)
Magdalena River delta,1935	Sand and silts	Rapid sedimentation	2 to 3 degrees	Menard(1964); Morgenstern (1967)
Helsinki Harbour, 1935	Sand and silts	Rapid filling	4-5 degrees	Andresen and Bjerrum (1967)
Follafjord slides, 1952	Loose fine sand, silt	Dumping of dredged soils	5 to 7 degrees	Terzaghi (1956); Bjerrum, (1971)
Orkdalsfjord, 1930	Loose fine sand, silt	Low tides	5-10 degrees	Terzaghi (1956), Schwarz (1982) Andresen and Bjerrum (1967)
Finnivaka Slide, 1940	Loose fine sand, silt	Low tides		Bjerrum (1971)
Hommelvika, 1942	Loose fine sand	Low tides		Bjerrum (1971)
Trondheim 1888	Loose Fine sands, silt	Low tides	8-15 degrees	Terzaghi(1956); Bjerrum (1971)
Western Norwegian fjords	Fine sand and silt	River sedimentation	1.5-3 degrees	Aarseth,I et al. (1989)
Scripps Cayon, 1959/1960	Sand	Free gas and storm waves	25-35 degrees	Dill (1964); Morgenstern (1967)
Puget Sound, 1985	Loose sands	Low tides	16 degrees	Kraft, L.M. et al.(1985)
Skagway, Alaska, 1994	Loose silty sands	Low tides of 4m	35 degrees	Morgenstern, (1995, pers. comm)
Howe Sound, 1955	Fine sands and gravel	Low tides	27-28 degrees	Terzaghi(1956)
Kitimat fjord, 1975	Loose silty sands	Low tides of 6m	19 degrees	Morrison, K.J. (1984)
Nerlerk Sand berms,1983	Loose sands	Fill placement	10-12 degrees	Sladen et al. (1985,a)
Fraser River delta,1985	Loose fine sands, silt	Low tides of 5m	23 degrees	McKenna and Luternauer(1987)

Table 1.2. Statically Induced Liquefaction Flow Slides in Submarine Deposits

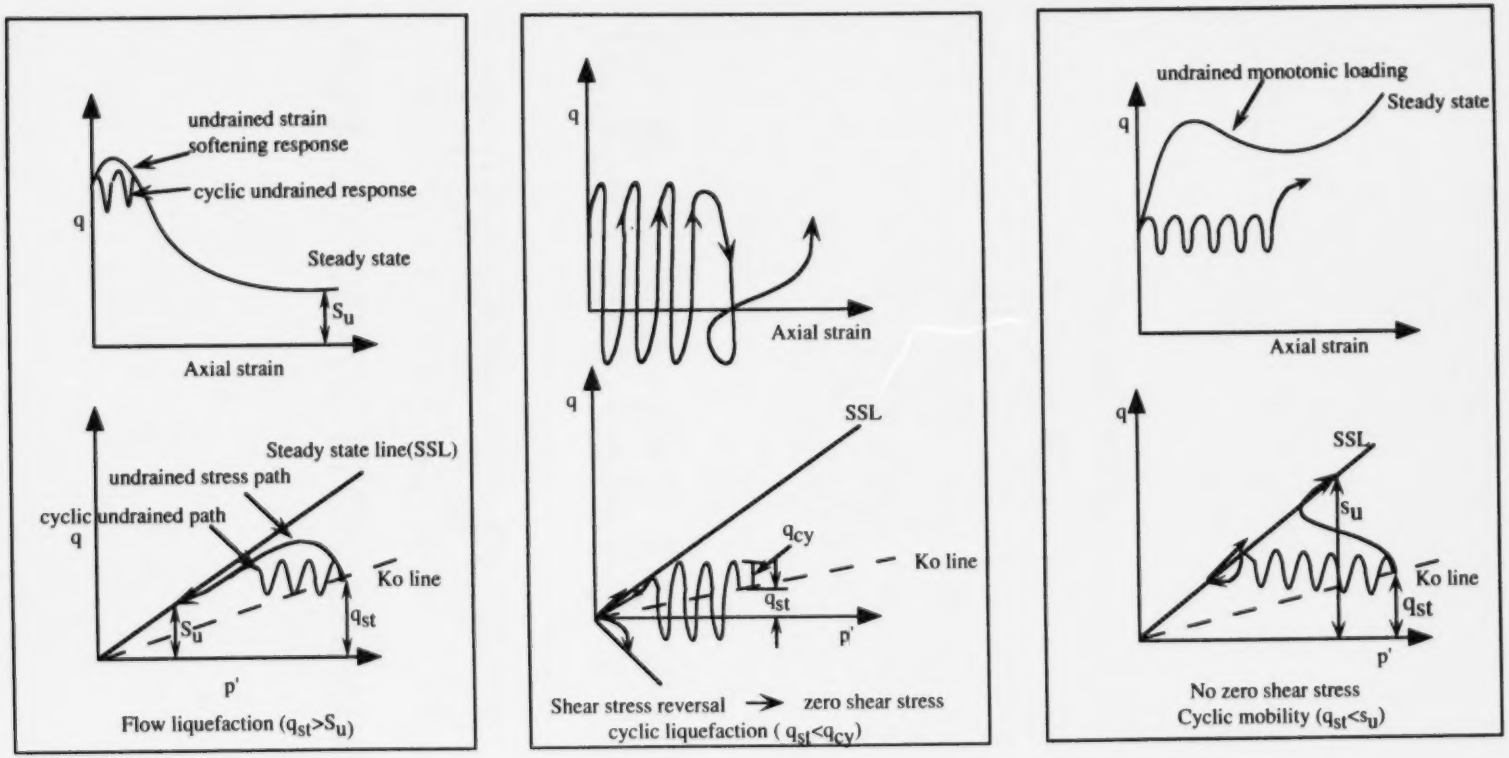

Figure 1.1. Liquefaction terminology

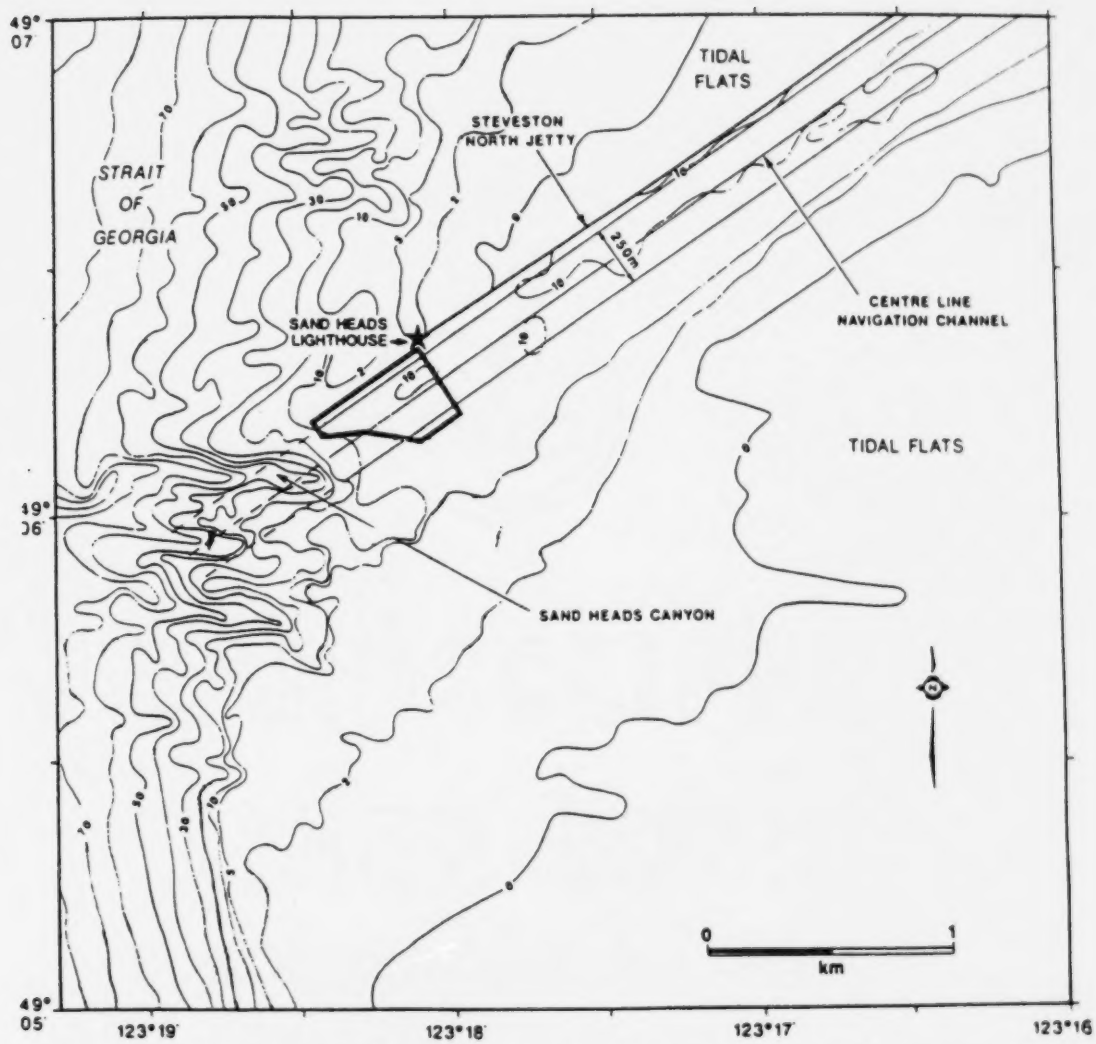

Figure 1.2. Morphology of the Fraser River Delta (after McKenna and Luternauer, 1987). Box indicates the area of the flow slide in 1985.

2.0 Developments in Steady State Concepts

2.1 Introduction

It is known is that liquefaction flow slides are triggered by either cyclic or static undrained loading in loose saturated sands. Catastrophic failures occurred following earthquakes in Alaska and Niigata, in 1964 and lead to the development of research studies based on the view that liquefaction occurs at zero effective stress state. However, this concept cannot adequately explain the flow slides in mine waste dumps and in river deltas of underwater slopes. In the Kersten lecture, Morgenstern (1994) referred to the definition of a liquefaction flow slide by Hutchinson (1988):

> " characterized by the sudden collapse and extensive, very to extremely rapid run-out of a mass of granular material or debris, following some disturbance. An essential feature is that the material involved has a meta-stable, loose or high porosity structure. As a result of the disturbance this collapse transfers the overburden load wholly or partly onto the pore fluid, in which excess pressures are generated. The consequent loss of strength gives the failing material, briefly a semi-fluid character and allows a flow slide to develop."

The collapse of the metastable structure may be triggered by cyclic loading or by some other mechanisms. An approach by Castro (1969) provided a better understanding of the phenomenon of liquefaction. He defined liquefaction as the strain softening and collapse of a loose structured sand to an ultimate state, called steady state. At the steady state of deformation, a mass of soil deforms at constant volume, constant shear stress, and constant velocity. The steady state of deformation is achieved only after all particle orientation has reached a statistically steady state condition and after all particle breakage, if any, is complete, so that the shear stress needed to continue deformation and the velocity of deformation remain "constant" (Castro and Poulos, 1977). However, the term constant

velocity of deformation is not well addressed (Been et al., 1990). Steady state methods have received much deserved attention in research studies of liquefaction failures. Recent developments in the approach provided a strong base for addressing liquefaction induced flow slides in both artificial fills and natural soils. This chapter presents and discusses the steady state concepts and limitations and also describes the application of the method in evaluating liquefaction flow slides.

2.2 Steady State Line

The void ratio at steady state is the critical void ratio as defined by Casagrande (1936) and Koppejan et al. (1948) whereby liquefaction can only take place in loose saturated sands with void ratio higher than the critical void ratio. It is difficult to observe liquefaction in the sands with void ratio lower than the critical void ratio. The critical void ratio distinguishes two states of sand as contractive and dilative.

A contractive sand is one which when loaded to failure from its initial state, exhibits a continuous increase in pore pressures for an undrained path or a continuous decrease in void ratio for a drained path. Figure 2.1 shows typical stress - strain behavior of an isotropically consolidated saturated contractive sand sample in an undrained triaxial compression test and the corresponding pore pressure development during the test. During the undrained test, void ratio remains constant implying that there is no volume change in the sand specimen (Been et al., 1991; Ishihara et al., 1991). After reaching a peak resistance, the sand strain softens to a constant resistance during which the effective stress state remains constant. Figure 2.2 presents typical stress - strain behavior in a drained triaxial compression test of a contractive sand consolidated to the same confining pressure as that in the undrained test and the corresponding volume changes. In the drained test, pore pressure remains unaltered and volume changes occur. The deviatoric stress

approaches a constant value with corresponding constant volume change (Been et al., 1991; Lee and Seed, 1967). Stresses in triaxial compression are defined in terms of mean normal effective stress $p' = (\sigma'_1+2\sigma'_3)/3$ and the deviatoric stress $q = (\sigma_1 - \sigma_3)$. In both tests, ultimate points attain a state of constant stress and constant volume which is the steady state condition. Stress paths for both tests plot as shown in Figure 2.3 in p' - q space and e - p' space where e is the void ratio. Stress changes during the test are reflected in the p' - q space and the volume changes are manifested in the e - p' space.

A dilative sand is one which exhibits a decrease in pore pressure when loaded in undrained loading or an increase in void ratio in drained loading. An undrained triaxial compression test on a dilative soil sample, which is isotropically consolidated to the same stress level as that of the contractive specimen, results in constant stress as shown in Figure 2.4. Pore pressures increase initially but eventually decrease to constant negative pore pressures at its ultimate state (Been et al., 1991; Ishihara et al., 1991). The sample contracts initially and then dilates with increasing negative pore pressures until it reaches its steady state. In a drained test on a dilative sample consolidated to the same confining pressure, the sample reaches an ultimate state with an associated increase in volume and a void ratio at the ultimate state higher than the initial void ratio (Been et al., 1991; Lee and Seed, 1967). The corresponding stress-strain curve and volume change characteristics are presented in Figure 2.5. When the stress paths for the tests on the dilative soil samples are superimposed in Figure 2.3, the ultimate states of the two drained tests terminate at the same void ratio in e-p' space and at the same steady state strength in p' - q space. The stress paths in e-p' space for the undrained tests essentially remain horizontal indicating that no volume changes are occurring during the tests.

In the literature certain sands at moderate initial confining pressures are found to exhibit contractive behaviour initially, but dilate at large strains in undrained loading. Dilation

continues until the sand reaches its steady state. This type of behaviour is observed with the samples prepared by water pluviation techniques (Vaid and Chern, 1985) and water sedimentation methods (Ishihara, 1993). Figure 2.6 illustrates this kind of behaviour. From the stress - strain curve, it can be seen that there is a temporary drop in shear stress accompanied by a large strain whereupon the sand changes its behaviour from contractant to dilative. This type of behaviour has been referred to as flow with limited liquefaction (Vaid and Chern, 1985), limited deformation (Ishihara, 1993) or limited strain softening (Robertson, 1994).

The stress path in p' -q space for this type of behaviour is also shown in Figure 2.6. The stress path represents a contractant behaviour followed by a dilative behaviour until steady state. Characteristic of this type of response is an "elbow" in the stress path which separates strain softening from strain hardening. The stage of elbowing has been identified as phase transformation (Ishihara, 1975) and quasi-steady state (Alarcon-Guzman et al., 1988; Been et al., 1991). The occurrence of quasi-steady state is governed by the void ratio and the confining stress at the time of consolidation (Ishihara, 1993).

From the steady state points in the e - p' space, it can be established that the locus of all the steady state points forms a curve (Figure 2.3). The curve is approximately a straight line on the logarithmic abscissa. Similarly the steady state points in p' - q space fall in a straight line passing through zero coordinates. As the steady state is a condition of Mohr-Coulomb shear failure, it follows that the effective normal and shear stresses at steady state are uniquely related by the angle of internal friction at the steady state and the effective cohesion intercept at the steady state is essentially zero. The steady state line in the e-p'-q space can be represented schematically as shown in Figure 2.7 with the corresponding projections of the line on the different planes.

Ishihara (1993) presented results of undrained tests on Toyoura sand samples, exhibiting zero residual strength (steady state strength). The void ratio corresponding to the zero residual strength is called the " Threshold Void Ratio". This void ratio marks the beginning of the state boundary in the contractant region in e - p' -q space. The in-situ void ratio at the surface of a deposit may correspond to this threshold void ratio. During undrained loading, this soil can have zero steady state strength.

It is argued that several factors influence the position of the steady state line. Castro and Poulos (1977) state that the position of the steady state line is a unique soil property. The inclination of the steady state line for many soils is such that small variations in void ratio can lead to rather large variations in steady state effective stress. The following section discusses the influences of some factors on the position of the steady state line.

2.2.1 Influence of Confining Stress on Steady State

In normal practice, the relative density of a soil determines the state of the soil as either loose or dense. However, the shear behavior of the soil is very much influenced by the effective confining pressure. A soil of low relative density can behave like a contractive soil at higher confining pressures or like a dilative soil at low confining pressures. This behavior is illustrated in Figure 2.8. When a loose soil with high void ratio (low relative density) is tested undrained at two different confining pressures A and B, the stress paths remain horizontal in the e-p' plane and terminate at the same steady state point A' and B'. The basic difference in the shear behavior is reflected in the p' - q space for the two tests. The drained test path for the soil at low confining pressure reaches the steady state line at a higher void ratio (pt. A") than the initial void ratio and the path for the soil at higher confining pressure reaches a lower void ratio (pt. B")

Similarly the shear behavior of a soil with a lower void ratio (high relative density) is different at different at confining pressures (pt. C and pt. D in Figure 2.8). Undrained test paths of the soil in the e - p' space of Figure 2.8 continue to stay on a straight line and converge at the same steady state point (pt. C' and pt. D'). In the p'- q space the shear behavior for the low and high confining pressure tests are clearly distinguishable. The drained stress paths for the soil in either case exhibit different characteristics as presented in Figure 2.8. The soil at low confining pressure dilates and moves to a higher void ratio (pt. C"), whereas the soil at high confining pressure contracts to a new state at a lower void ratio (pt. D").

2.2.2 Influence of Sample Preparation Methods

In laboratory studies different methods of sample preparation can be employed, such as moist tamping, water pluviation, air pluviation and water sedimentation. Preparation of samples with water sedimentation methods and water pluviation result in dilative samples (Ishihara et al. 1991; Vaid and Chern, 1985). Experience in the present study shows that a wide range of void ratios can be achieved with the moist tamping methods. The preparation of the moist tamped samples and the water pluviated samples is presented in Appendix A. Irrespective of sample preparation techniques, all samples reach their steady state values at large strains. The steady state line is independent of stress path, sample preparation methods and initial density, implying that the steady state is unique for a void ratio regardless of whether it is reached by drained or undrained loading (Been et al. 1991).

2.2.3 Influence of Strain Rate During the Tests

Sladen et al. (1985,a) studied the influence of stress controlled triaxial tests and strain controlled triaxial tests on the steady state line and stated that there was no significant difference between the results from load-controlled and strain controlled tests. Moreover, the frictional behavior of sand is largely independent of strain rate (Hungr and Morgenstern, 1984).

2.3 *In-situ* Strength of Soil

In-situ soil deposits are characterized by Ko - conditions (anisotropic stress state). Undrained shear strength is the governing strength during the flow liquefaction of a sandy soil deposit. The steady state strength is the available undrained shear strength of the soil at the in-situ void ratio as shown in the Figure 2.8. For a contractive sand whose in-situ driving shear stresses are higher than the available undrained shear strength, there exists a potential for flow liquefaction of the sand which may lead to catastrophic failures. However, for a dilative sand where the undrained shear strength is greater than the driving shear stress, flow liquefaction may not be a concern.

2.4 Effect of Permeability of Soil Deposits in Liquefaction

For flow liquefaction to occur in a saturated sand deposit, it must be contractive and the in-situ shear stresses must be greater than the available undrained shear strength at the commencement of liquefaction. As mentioned previously, flow liquefaction is due to the collapse of the metastable soil structure resulting in generation of pore pressures. From laboratory model studies of flow slides on contractive coking coal, Eckersley (1990) stated that the flow liquefaction of coal stocks is a consequence of collapse of the structure due to

the rise of the water table. However, there was no discussion of the effect of permeability of the material during liquefaction. During the collapse of the contractive material, the permeability of the material must be sufficiently low to impede the drainage of the excess pore pressures for flow liquefaction to begin. Hence, coarse grained gravelly deposits may not be subjected to flow liquefaction. However, some percentage of fine material can impede the drainage during collapse. Evans et al. (1992) quoted several case studies of flow liquefaction failures in gravelly soil deposits with about 30% sand. Sand contributed to the impedance of the drainage during collapse. Lade (1993) indicates that no statically triggered liquefaction flow slides are observed in saturated cohesionless soils with permeabilites greater than 10^{-4} m/sec. Dawson et al., (1992) observed that liquefaction flow slides occurred in mine waste dumps with permeabilties of about 10^{-4} m/sec. Skopek et al., (1994,b) also identifed that loose cohesionless soils with the permeabilities greater than 10^{-4} m/sec are not susceptible to flow liquefaction. However, a capping layer of fine material having a permeability less than 10^{-4} m/sec can impede the dissipation of pore pressures from more permeable lower deposits.

2.5 Mechanism of Flow Slides

Flow liquefaction initiation may not fully explain the development of a flow slide. The drainage capacity of a saturated deposit is extremely important in controlling the behavior during collapse. For a flow slide to develope there must be a sufficient volume of strain softening material. Collapse of some elements of soil generates pore pressures resulting in strain softening of these elements to their steady state. The strain softening of the elements can transfer the excessive load to the adjacent elements and bring them to collapse. Hence, progressive propagation of collapse leading to flow liquefaction of contractive deposits can result in catastrophic failures. The progressive nature of liquefaction is demonstrated by Gu et al. (1993) while explaining the liquefaction failures in the Lower San Fernando Dam.

For the collapse of soil elements, undrained conditions are not a prerequisite (Sasitharan et al., 1993).

2.6 Advances in Steady State Concepts

Sladen et al. (1985,a) introduced the concept of collapse surface to serve as a triggering criterion for flow liquefaction. They state that the necessary condition for liquefaction is that the soil state lie on the surface. A state boundary surface was defined by Alarcon-Guzman et al. (1988) and Ishihara(1991) which controls the behaviour of purely contractive sands. They state that a sandy soil cannot exist above the state boundary. Further research for validation and corroboration of the existence of the collapse surface lead to the confirmation of the state boundary surface for contractive sands (Sasitharan et al., 1993; Sasitharan et al., 1994; Skopek et al.,1993; Skopek et al.,1994). For dilative soils, the effective stress paths are bounded by a surface beyond quasi-steady state strength and this surface is analogous to the Hvorslev surface for over consolidated clays (McRoberts and Sladen, 1990). This state boundary surface controls the behaviour of dilative soils and it can be referred to as the dilative boundary surface.

2.6.1 Collapse Surface

From this discussion onwards, contractant sand will be referred to as loose sand and dilatant sand as dense sand for describing sand behavior. Figure 2.9 illustrates undrained effective stress paths of loose sand samples in p' - q space which are consolidated to the same void ratio and sheared at different initial confining pressures. All the stress paths converge to the same ultimate or steady state. The peak deviatoric stress of all the stress paths fall in a straight line that passes through the steady state strength of the samples. Sladen et al. (1985,a) referred to the line as the collapse line. Different undrained stress

paths of the same material tested at different initial void ratios yield collapse lines of approximately the same slope, but terminate at different ultimate states on the steady state line. All these collapse lines in the e-p'-q space generate a collapse surface (Figure 2.10) at which the collapse of a loose saturated material is initiated by undrained loading. The collapse surface is nominally independent of stress path and constitutes a trigger criterion regardless of whether it is approached by montonic or cyclic loading. There is a potential risk for the state of a soil to liquefy when it is close to the collapse surfce. Any static trigger, such as undrained dumping of fill material, could lead to flow liquefaction.

2.6.2 Contractant State Boundary Surface

An examination of Figure 2.9 shows that the post peak portions of the monotonic undrained stress paths appear to follow along the collapse surface to their ultimate states (Sladen et al., 1985,a). Further examination of the collapse surface concept revealed that post peak portions of the undrained stress paths are bounded by a 'State Boundary Surface' (Alarcon-Guzman et al.; 1988 and Ishihara et al, 1991). The state boundary surface is positioned above the collapse surface. A soil state can exist above the collapse surface and below the state boundary surface. The state boundary surface is the surface enveloping all the undrained effective stress paths of the contractive soil, irrespective of their consolidation stresses and void ratios (Figure 2.11). The surface can be approximated by parallel straight lines in the p' - q space for different void ratios (Sasitharan et al., 1994). Soils appear to be less brittle at higher stress states and the state boundary appears to flatten at the higher stress states. Since the state boundary controls the behaviour of contractant soils, it can be referred to as Contractant State Boundary (CSB).

Tests on contractant soil specimens have supported the postulation of the CSB. Sasitharan et al. (1993) presented a q - constant test in which the stress path of a loose saturated sand

remained in a constant shear stress plane in e - p'- q space and the specimen was brought to failure under fully drained conditions. During the test, the drained stress path attempted to cross the CSB resulting in collapse of the soil structure and rapid generation of pore pressures. The shear resistance fell along the CSB to the steady state, that is, flow liquefaction (Figure 2.12). This stress path simulates a rise of the water table in loose sands. During the rise, changes in the stress state of the soil will be induced under drained conditions, that is, the pore pressure remains hydrostatic. However, the deformations associated with the collapse cause increases in pore pressures, and the soil liquefies. This phenomenon is observed in the laboratory modeled flow slides in coal stock piles by Eckersley (1990). The stress path also explains the failures that occurred in the Rocky Mountain coal mine waste dumps (Dawson et al, 1994). The collapse of the specimen occurred on the CSB after the stress path crossed the collapse surface. These results demonstrate that an undrained loading is not a pre-requisite for collapse to occur.

Sasitharan et al. (1994) demonstrated in another laboratory test the existence of the CSB. A p' - constant path test was conducted on a loose saturated sand sample with its stress state on the post peak portion of the undrained effective stress path, that is, the sample is on its CSB. The stress path tried to cross the CSB vertically in p'-q space (Figure 2.12). The stress path stayed on the CSB and reached its steady state at a different void ratio.

From the above tests , it is evident that a loose sand cannot exist beyond the contractant state boundary surface and the surface conforms with the conditions assumed for a State Boundary Surface by Roscoe et al. (1958).

Additional compelling evidence for the existence of the CSB is derived from tests on a dry sand sample in a constant shear stress plane (Skopek et al., 1993, 1994,a). The stress path is similar to that described by Sasitharan et al. (1993). During the test the shear stress is

unchanged while reducing p' and the contractant behavior of the dry sand is consistent with the behavior of loose saturated sand. A saturated sample collapses on the CSB resulting in vigorous generation of pore pressures and liquefaction. For a dry sample, the stress path is forced to deflect on the CSB to accommodate the structural changes due to the loading as shown in the Figure 2.12. Shear stress remains constant on the CSB for the dry sample and the sample experiences rapid structural collapse on the CSB which further explains the dramatic rise of pore pressures in the saturated sample. If the pore pressures are released during the collapse, the stress path re-positions to a stable stress path either on the state boundary or away from the boundary. An instability exists on the boundary surface whenever a soil attempts to cross it.

Following collapse on the CSB due to the applied stresses in the q - constant plane, a saturated loose sand assumes the undrained path and attains the ultimate state on the steady state line which may result in catastrophic failure. In contrast, the dry sand travels along the fully drained path on the CSB for the applied stress changes in the q - constant plane. These two different stress paths on the state boundary represent two extreme cases of the same phenomenon. The stress path of a partly saturated loose sand sample for similar stress changes lies on the CSB in between the two extreme cases. Measurable volume changes for a dry soil sample in q - constant plane on the CSB can be used to quantify the pore pressure generation in a saturated soil sample for the same stress path (Skopek et al. (1994,b).

2.6.3. Implications of Cyclic Loading on the CSB

Cyclic loading may induce undrained failure leading to foundation instability of structures resting on loose saturated sand. For flow liquefaction to occur the sand must be contractive and saturated. The permeability of the sand should be sufficiently low to sustain generated

pore pressures. Amplitude of the cyclic loading, rate of loading and time span of the loading determines the occurrence of flow liquefaction. The in-situ state of the soil in the field can be represented on the K_O plane in the e - p' - q space. Studies show that the CSB forms a critical surface that can trigger liquefaction failures due to cyclic loading (Ishihara, 1991). Different cases may prevail before the initiation of liquefaction in the sands due to the loading as shown in Figure 2.13. Cyclic earthquake loading on soil deposits represent one type of behaviour (Case1). Undrained failures will result when the rate of loading is fast enough to take the state of the soil on to the CSB. The stress path can touch the state boundary in the first few cycles for large amplitudes of loading and follow along the surface to its steady state. A higher number of cycles of small amplitude may be required to move the stress path on to the boundary surface in the undrained plane. Case 2 of Figure 2.13 demonstrates cyclic loading due to surface waves on loose marine deposits of sand. Surface waves can induce partially dissipated residual pore pressures in loose sandy deposits (Seed and Rahman, 1978). These residual pore pressures may trigger liquefaction of the loose deposits. If the permeability is such that the partial dissipation of excess pore pressures occurs during the unloading phase, the stress path moves to an undrained plane at a different void ratio and may collapse in the plane on the CSB on further loading. Slow rates of loading can densify the state of soil.

2.6.4. Dilative Boundary Surface

The undrained behaviour of anisotropically consolidated sand samples at different confining pressures but at same void ratio is illustrated in Figure 2.14. As the steady state strength is uniquely related to void ratio, all the samples would reach the same steady state strength at large strains. The stress strain response of sample A exhibits a marked strain softening behaviour, that is, pure contractive behaviour (Type 1 response). The stress path shows the strain softening in p'-q space to its steady state. It is obvious that the initial state

of the sample should be in the contractive region of the e-p' space. It also can be observed that the in-situ shear stress is higher than the steady state strength in p'-q space. The sample possesses a potential for liquefaction.

The behaviour of sample B, whose initial state is also in the contractive region differs considerably at large strains. Sample B responds with limited strain softening (Type 2). The stress path in p'-q space shows a transition stage in which the strength of the specimen strain softens to quasi-steady state followed by strain hardening to its steady state. It can also be observed that the initial shear stress on the Ko line is lower than the steady state strength in p'-q space. The initial state of samples is in the contractive region relative to the steady state line in e-p' space, but the behaviour of the sample does not show a pure contractive response. Soil deposits with this initial state are not susceptible to flow liquefaction failures. However, the deformation of the soil deposits associated with this transition stage may cause considerable damage to the structures founded on such soils. Vaid and Chern (1985) believed that there is a major discrepancy in the separation of initial states into regions which are liquefiable (contractive) from those which are not (dilative). It may be appropriate to consider also the state of initial static shear stress relative to the steady state strength in p'-q space along with the consideration in the e-p' space.

The response of sample C is purely dilative behaviour (Type 3). The stress path in p'-q space shows that the sample exhibits strain hardening behaviour when it reaches its steady state strength.

Sands will generally dilate at a stress ratio, (q/p') higher than the ratios at the steady state (McRoberts and Sladen, 1990). Examination of the stress paths of the samples B and C shows that the effective stress paths are bounded by an envelope in the undrained plane in the strain hardening region (dilative region). The envelope represents a surface in e-p'-q

space. According to McRoberts and Sladen (1990), this surface is comparable to the Hvorslev surface indicated by Roscoe et al. (1958). Originally, the Hvorslev Surface was defined for the behaviour of over consolidated clays. It may be reasonable to refer to the surface as a " Dilative State Boundary Surface" (DSB), which envelopes the strain hardening undrained effective stress paths for dilative soils.

In nature many sand deposits are contractive, that is, they try to decrease in void ratio for an increase in shear stresses. The effective undrained stress paths in p'- q space moves up and to the left (contractive response). However, as the contractive stress path approaches DSB, a phase transformation occurs (from contractive to dilative). The strain required for the phase transformation depends on the angularity of grains. Following the phase transformation, the stress path follows the DSB and reaches its steady state. Little attention has been paid to the behaviour of dense (dilative) sands on the DSB. This is because shear loading induces negative pore pressures in undrained loading on the DSB and dilation in drained loading. The dense sand deposits require very large strains to reach steady state. Hence, it is believed that the dilative soils are not susceptible to flow liquefaction.

Ishihara (1993) presented several results of undrained tests of water sedimented samples of Toyoura sand. The samples appeared to be contractive in e-p' space. The initial confining stress is also close to the steady state line. However, all the samples reached quasi-steady state during undrained loading and dilated on the DSB to their respective steady state strength. Ishihara (1993) assumed that the quasi-steady state strength of the soil deposits was the governing strength of natural deposits in undrained loading. Quasi-steady state strength forms a line (Quasi-steady state line - QSSL) over a wide range of void ratios. However, the quasi-steady state condition is very dependent on the confining stress. Variability of the quasi-steady state makes it difficult to define the initial state of a sand deposit relative to the QSSL.

Vaid and Chern (1985) and Vaid and Thomas (1995) presented several undrained triaxial compression results of water pluviated samples. Void ratios resulting from water pluviated samples are always in the dilative region. Undrained stress paths of the samples showed initial contractive response followed by dilative response on the DSB. Vaid and Chern (1985) also reported stress paths resulting from anisotropic cyclic triaxial compression tests with shear stress reversal on water pluviated samples. The cyclic loading stress path takes the state of samples on to the DSB. As the stress path follows up the DSB, the sample dilates. However, the cyclic loading reverses the direction of dilation and brings the state of soil sample away from the DSB. Upon the reversal in the direction of shear straining, the number of contact points between the neighbouring grains is drastically reduced. Accordingly, the sand structure tends to collapse with positive pore pressures on further loading. During this phase, the sample may experience zero effective stress and zero shear strength. According to Vaid and Thomas (1995), this is the state which may correspond to the definition of initial liquefaction by Seed (1979). Robertson (1994) defined this state as cyclic softening.

Research studies have concentrated in studying the behaviour of contractive sands with respect to flow liquefaction, that is, unlimited deformations in level grounds and flow slides in slopes. The design concern for these contractive sandy deposits is stability. Hence, much attention has focussed on the implication of stress path on the CSB. The design concerns with dilative sands during cyclic loading are excessive deformations and the reduction of effective stress to zero . It may be necessary to study the influence of the structural arrangement of soil grains on the DSB during cyclic undrained loading.

2.7. Application of CSB Concept for Flow Slides

The collapse surface approach is a powerful concept to estimate the potential for catastrophic liquefaction failures. Sladen et al. (1985, b) explained the liquefaction failures of the Nerlerk berms in the Beaufort Sea using the concept. The construction of the berm by hydraulic filling brought the in-situ state of the soil on to the collapse surface. Additional dumping of the fill resulted in undrained flow slides. Similar observations were made by Lade (1993) for the berm failures. Lade proposed an instability line in the p' -q space (Figure 2. 15) passing through the peaks of undrained stress paths of samples at the same void ratio and through the origin. He concluded that the state of the soil in the berms was in the region of instability and undrained failures were initiated due to the dumping of the berm material. The two arguments by Sladen et al, (1985,b) and Lade (1993) agree with the conclusion that the state of the soil in the berms was on the verge of catastrophic collapse. The building of the berms increased shear stresses and confining pressures in the berms along the K_o - line. Before failure, the state of the soil approached very close to the CSB and further additions of the material in the berm brought the state of soil on to the CSB in an undrained manner. There was insufficient time for the dissipation of the pore pressures, which triggered the flow slides.

Kramer and Seed (1988) studied the factors affecting the undrained strength of cohesionless soils. They referred to liquefaction flow slides due to static loadings as static liquefaction. From the results of laboratory tests, they stated that for a loose sand consolidated to K_o - conditions, a small undrained increment of load is sufficient to trigger liquefaction. This test simulates the undrained failures in the Beaufort sea.

The failures of the materials leading to liquefaction flow slides can be best explained through CSB concepts based on steady state methods. This thesis explores the

effectiveness of the CSB frame work for explaining the liquefaction flow slides at the mouth of the Fraser River Delta.

2.8. Summary

Liquefaction flow slides are triggered by either static effects or cyclic effects. Liquefaction is explained using steady state concepts. When a loose saturated sand strain softens to its steady state, its structure collapses and liquefies. A steady state line is defined to differentiate between two possible states of soil deposits. A contractive state, in which a soil contracts during shear, has a potential to liquefy. A dilative state, in which a soil expands during shear, does not liquefy. An intermediate state which shows contractive response followed by dilative response also exists. Although liquefaction is not a problem with intermediate soils, the deformations associated with undrained loading have to be addressed. For flow liquefaction to occur, a contractive sand must have its static shear stresses higher than its steady state strength. Advances in the steady state concepts resulted in defining a collapse surface and a contractant state boundary surface for contractant sands. The contractant state boundary forms a surface controlling the shear behaviour of contractant sand. Any attempt to cross the contractant boundary surface by the soil results in flow liquefaction. The collapse surface concept helped to explain the undrained failures of artificially placed sand berms in the Beaufort Sea. These concepts also helped to explain the liquefaction flow slides in mine waste dumps. A dilative boundary surface can also be defined for dilative sands enveloping the undrained stress paths of dilative sands in the strain hardening region.

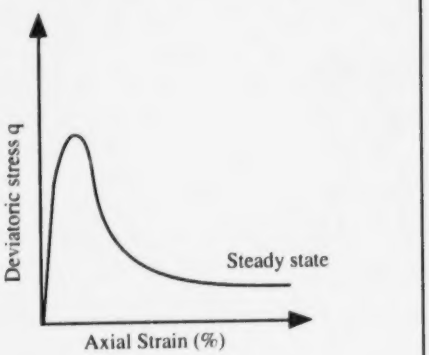

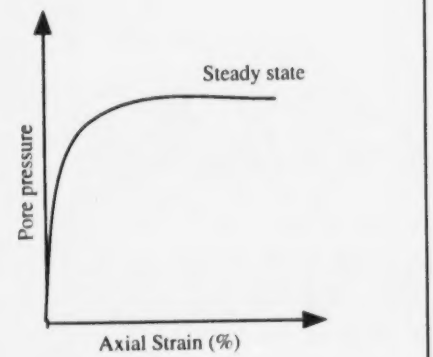

Figure 2.1 Undrained test on contractive sand

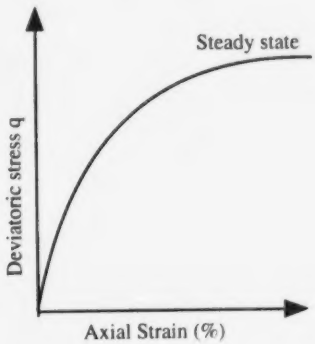

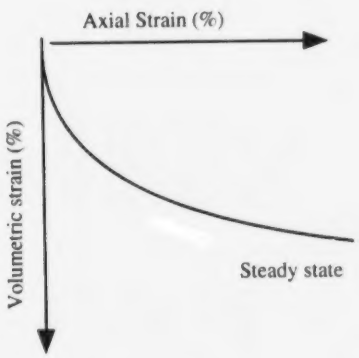

Figure 2.2. Drained test on contractive sand

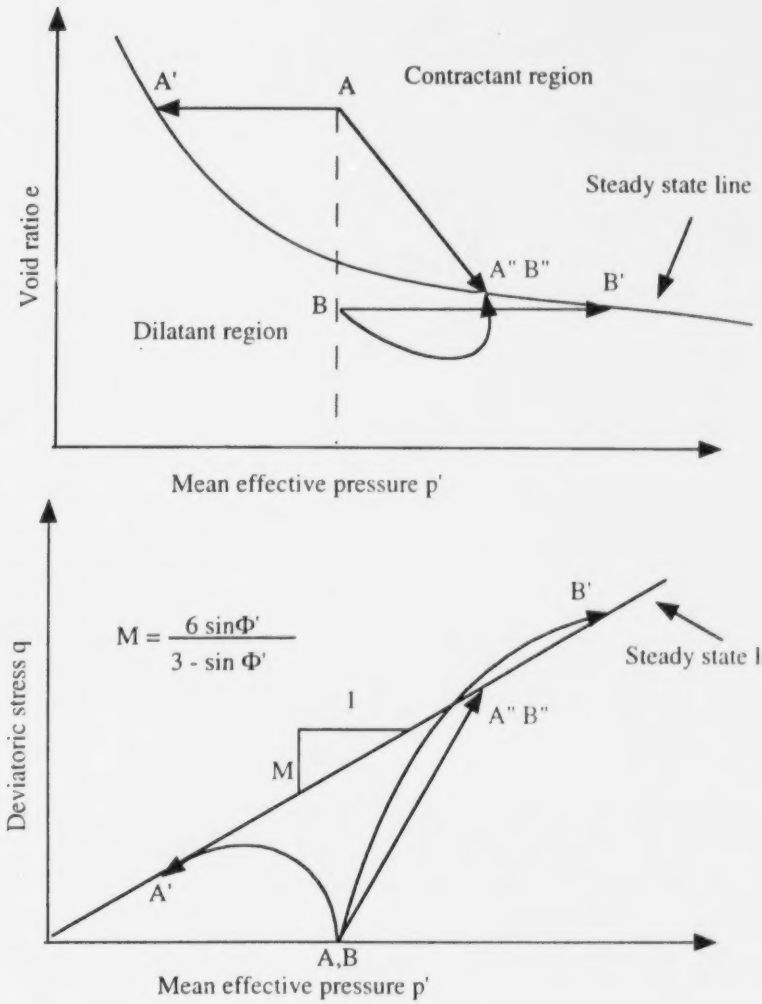

Figure 2.3. Stress paths of contractant and dilatant sand
(after Sladen et al. 1985)

Undrained stress paths --- AA', BB'

Drained stress paths --- AA", BB"

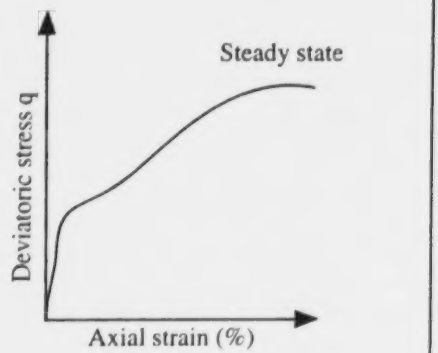

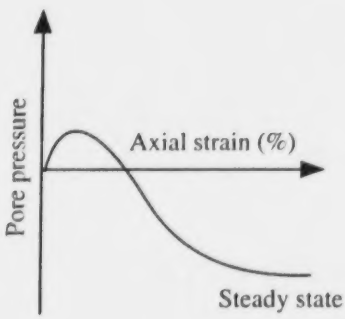

Figure 2.4. Undrained test on dilative sand
(after Been et al. 1991)

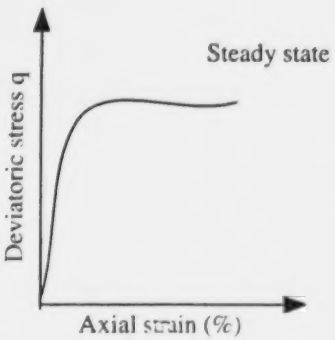

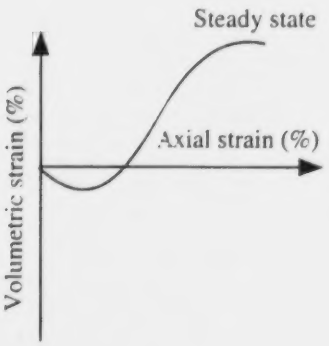

Figure 2.5. Drained test on dilative sand
(after Been et al., 1991; Lee and Seed, 1967)

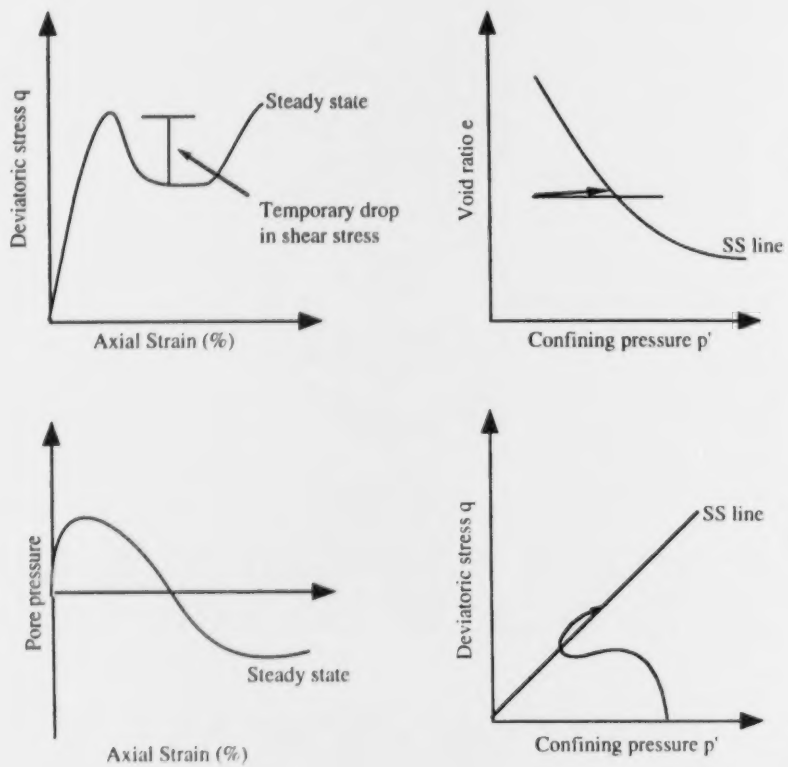

Figure 2.6 Undrained test on contractive dilative sand

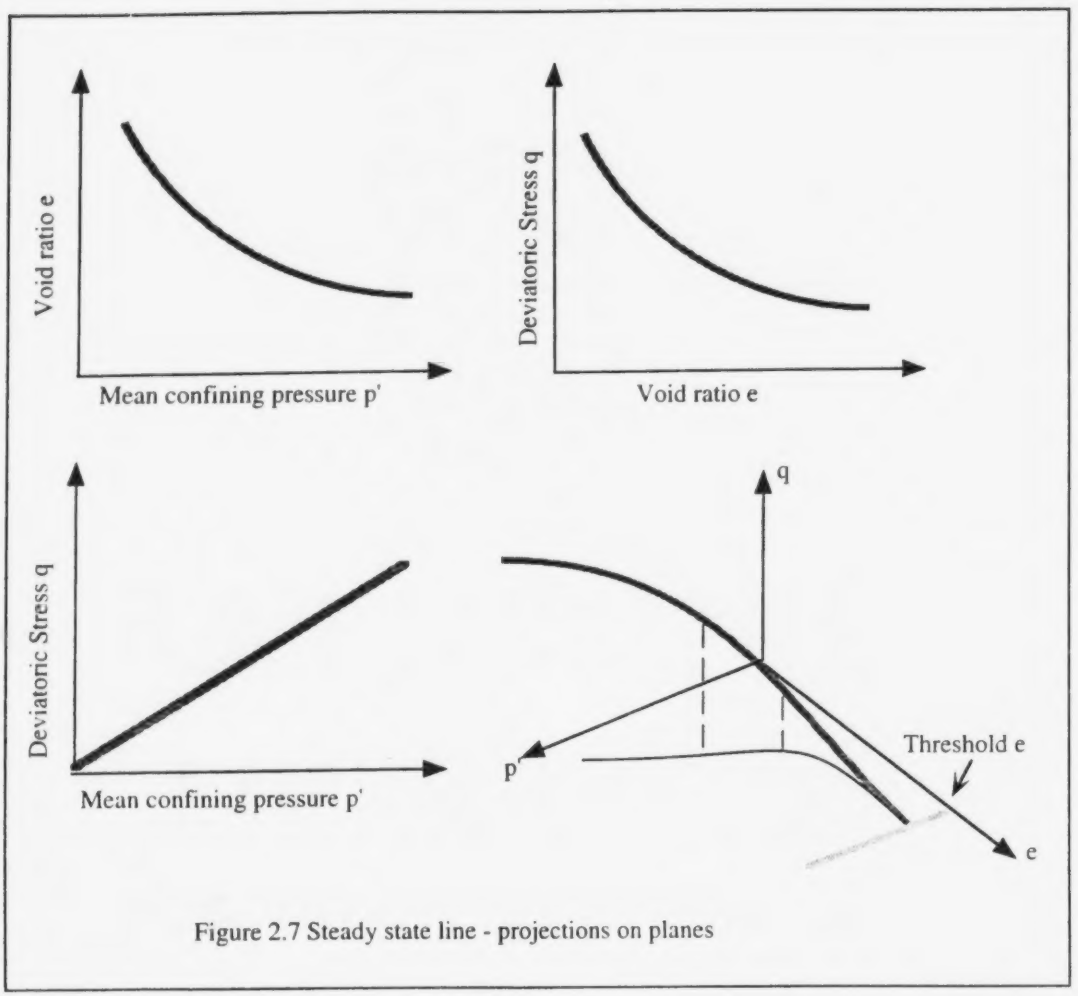

Figure 2.7 Steady state line - projections on planes

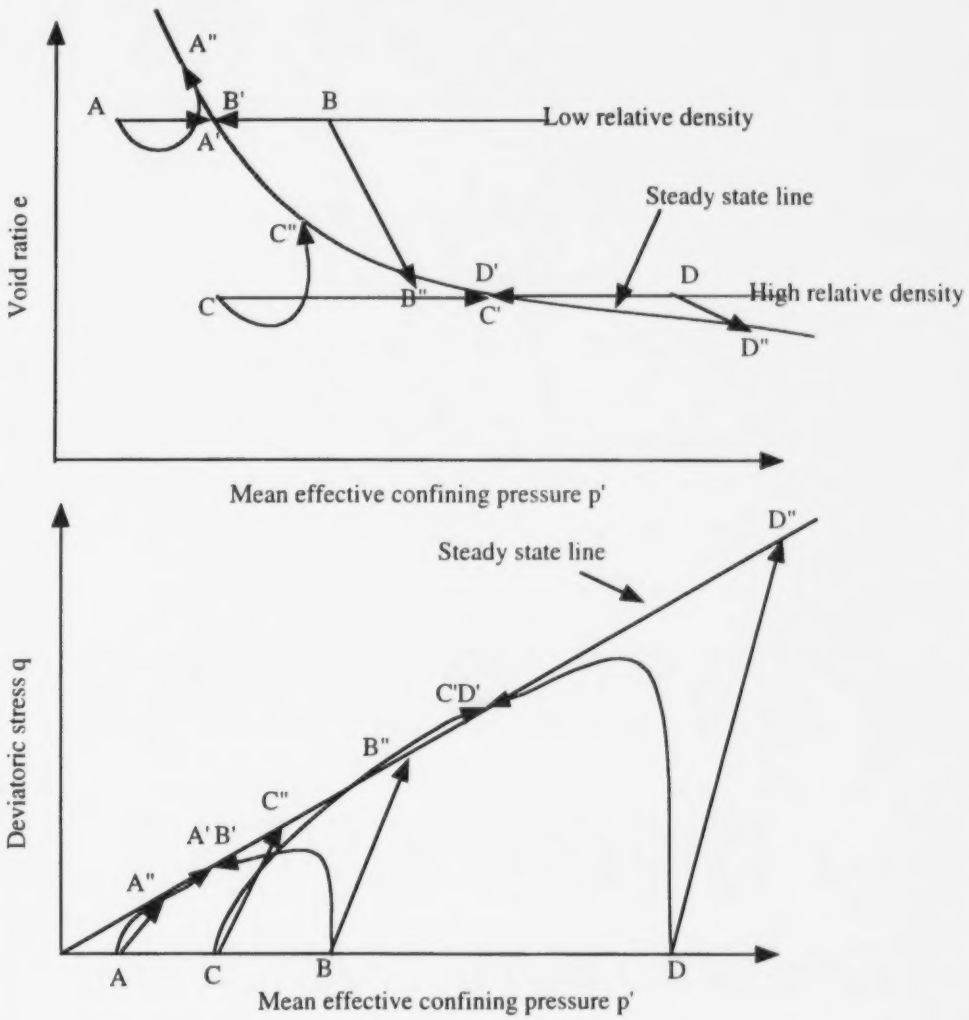

Figure 2.8. Influence of relative density on steady state line
(after Kramer and Seed, 1988)

Undrained stress paths --- AA', BB', CC', DD'
Drained stress paths --- AA", BB", CC", DD"

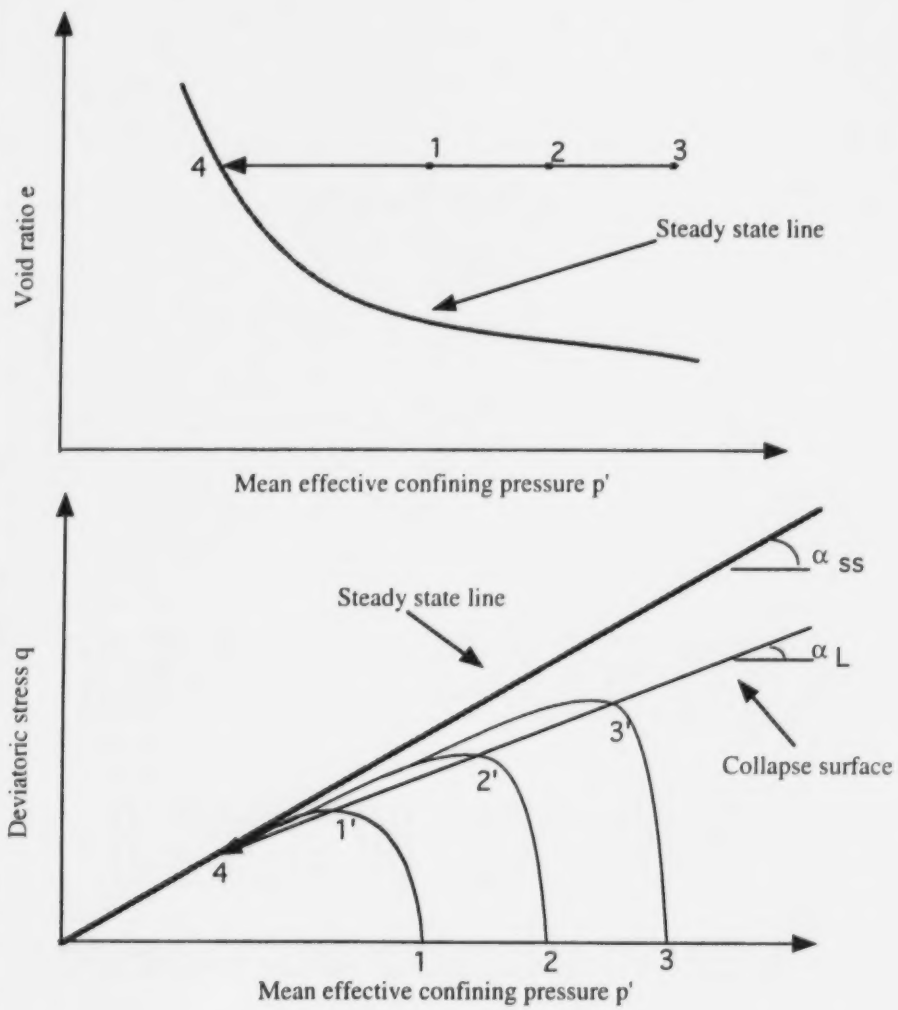

Figure 2.9. Collapse surface (after Sladen et al., 1985)

Undrained stress paths --- 1-1'-4, 2-2'-4, 3-3'-4

Peak points 1', 2', 3'

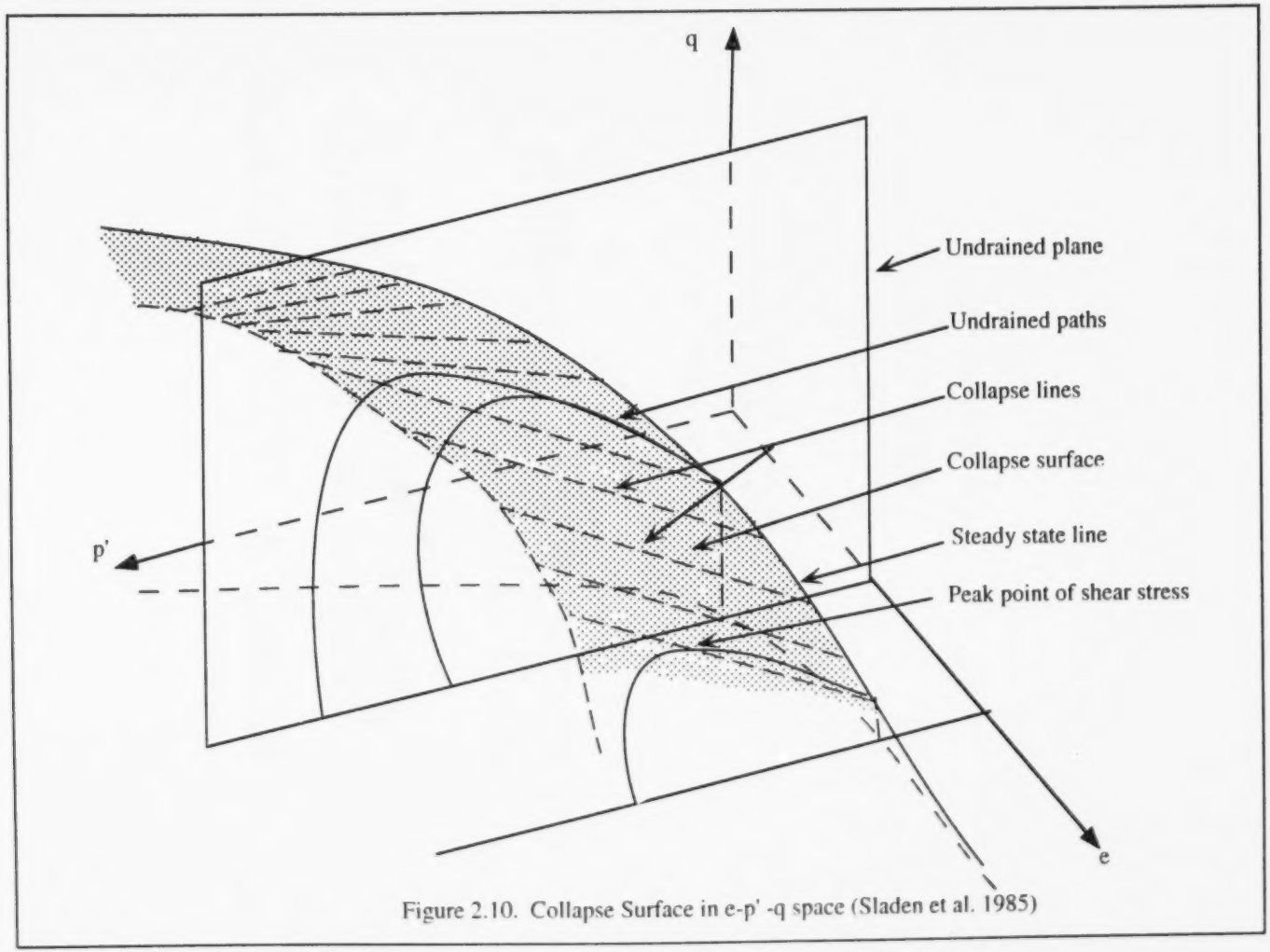

Figure 2.10. Collapse Surface in e-p' -q space (Sladen et al. 1985)

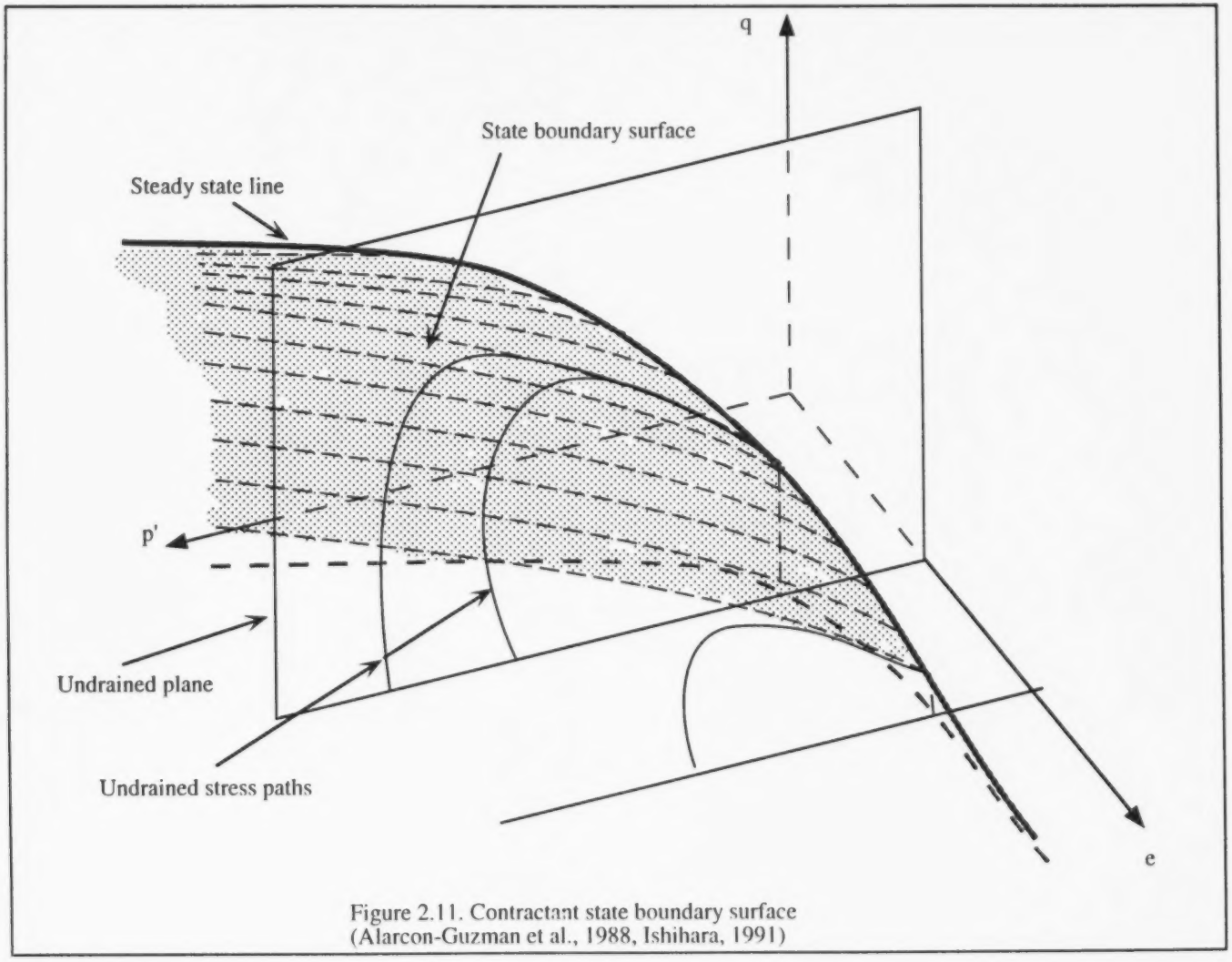

Figure 2.11. Contractant state boundary surface
(Alarcon-Guzman et al., 1988, Ishihara, 1991)

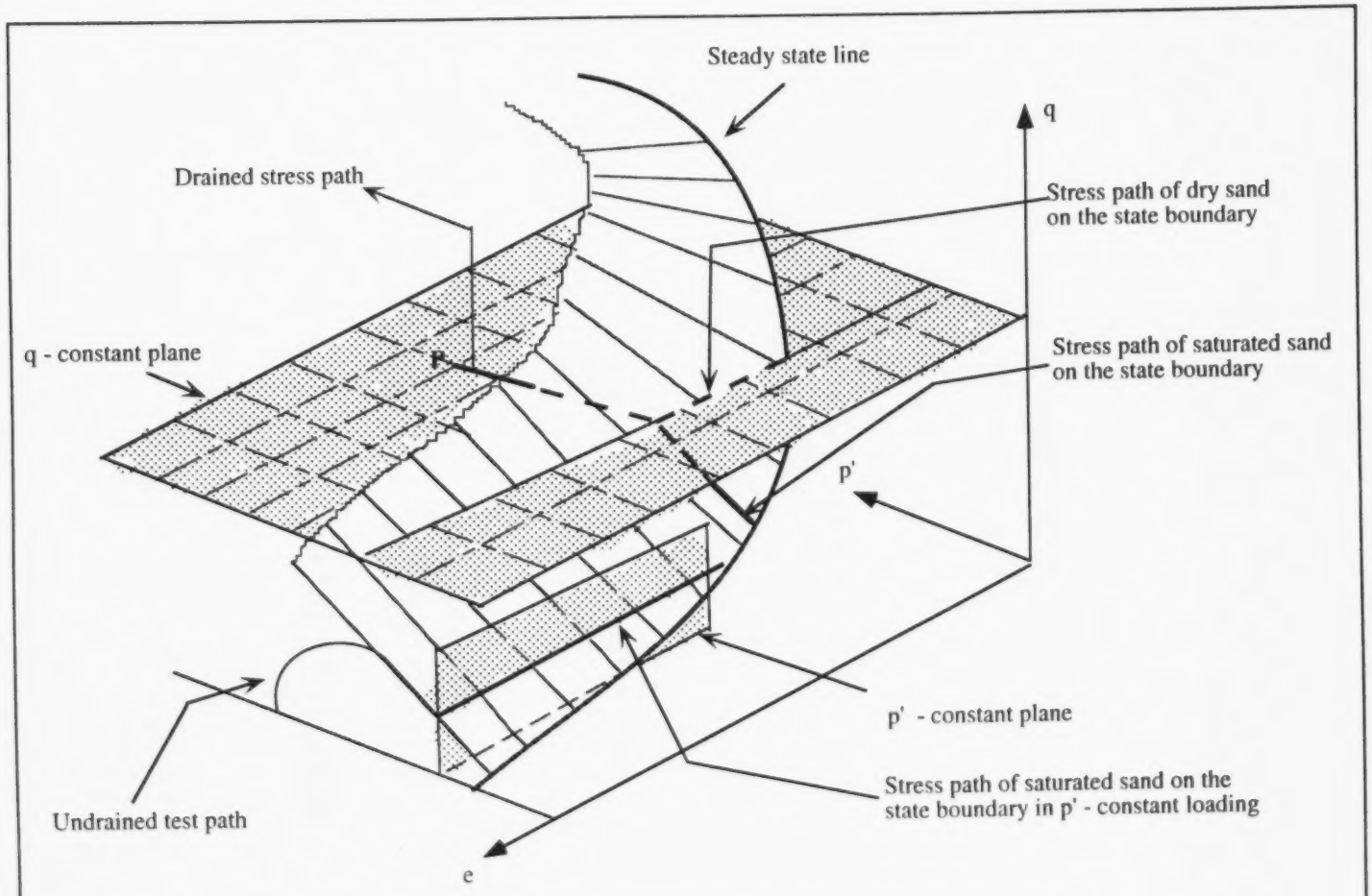

Figure 2. 12. Confirmation tests for Contractant state boundary surface

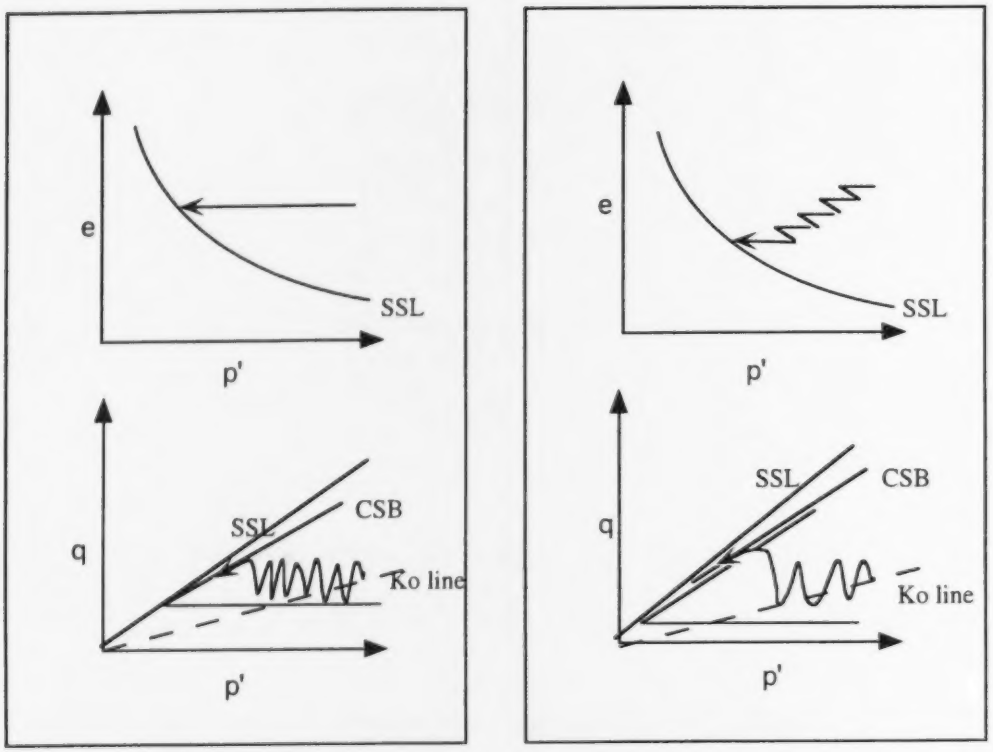

Case 1 Case 2

Figure 2. 13. Effect of cyclic loading on saturated liquefiable sands

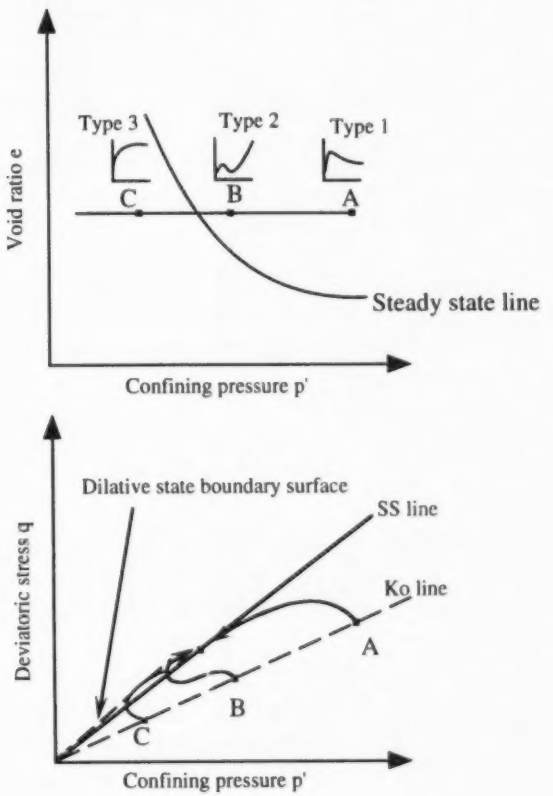

Figure 2.14. Dilative State Boundary Surface

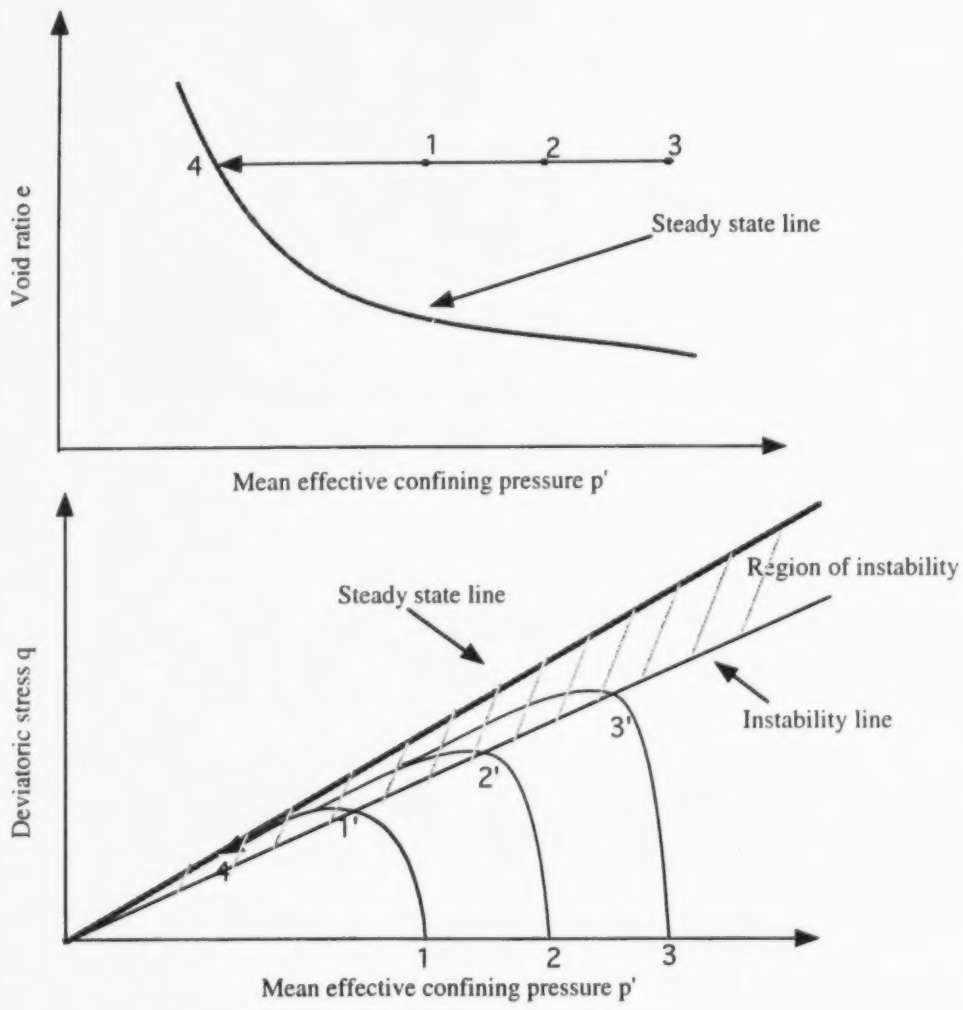

Figure 2.15. Instability line (Lade, 1993)

Undrained stress paths --- 1-1'-4, 2-2'-4, 3-3'-4

Peak points 1', 2', 3'

3.0 The Fraser River Delta

3.1 Introduction

The Fraser River delta is an actively prograding delta on the west coast of Canada. The delta builds thick sedimentary deposits in the Strait of Georgia from the clastic sediments supplied by the Fraser River. The deposits exhibit different characteristic facies resulting from interrelated fluvial and marine processes and environmental conditions. Fluvial processes include sediment discharged from the Fraser River, originating from the drainage basin of the river. River-mouth and tidal processes dominate the coastal environment. Nearshore wave power, tides and currents from the receiving basin control the deposition of the clastics. Winds and other forces such as Coriolis Force act upon the basin water and the river discharge influencing deposition. Among the other controlling factors, slope of the subaqueous platform and geometry of the depositional basin also contribute to shaping the delta. This chapter presents the physical setting of the delta and discusses different dynamic processes influencing the deposition and dispersion of the river-borne clastics.

3.2 Geographical and Geological Setting

The Fraser River delta plain extends 15-23 km west into the Strait of Georgia and south into Boundary Bay from a narrow gap in the Pleistocene uplands at New Westminster (Figure 3.1). It is bounded to the north by Burrard Peninsula, to the east by the Surrey uplands and to the south west by Point Roberts Peninsula (Luternauer, 1980). The Fraser River has multiple distributaries supplying water borne sediments to the coast. Two distributaries, called the North Arm and the Middle Arm, of the river lie to the north of the Main Channel and another distributary exists south of the Main Channel called the South Arm. The intertidal area between the North Arm and the Main Channel is Sturgeon Bank

and the area between the Main Channel and the South Arm is Roberts Bank. The region of the primary modern river mouth is Sand Heads. The most conspicuous feature of the delta front is a very gently sloping broad tidal flat extending up to 9 km from the dyked edge of the delta to the subtidal delta slope (Luternauer et al., 1994). Coleman (1976) states that deltas exposed to extreme tidal variations have tidal flats as their characteristic feature.

Burrard Peninsula consists of two pre-Pleistocene bedrock ridges trending east-west, overlain mainly by glacial and raised littoral deposits. Similar types of Pleistocene material is found in the Point Roberts Peninsula. Surrey uplands is evolved from glacio-marine gravelly clay deposits. Since the recession of the glaciers from the Fraser Canyon, the delta has built up deposits 90 - 200 m thick over Pleistocene sediments.

From earlier works Monahan et al. (1993) described the surficial environments of the delta extending from east to west (Figure 3.2).

(1). An upper delta plain that extends 23 km west from the gap in the Pleistocene uplands at New Westminster, is mantled by flood plain silt and peat, and is now protected by dykes.

(2). A lower delta plain consisting of dominantly sandy tidal flats

(3). A subaqeous delta plain, that is mantled by sand and is up to 2 km wide, and extends to the first major break in slope at a depth of up to 9 m below lowest low tide.

(4). A delta front and slope that descend at an average slope of 1.5 degrees to depths of up to 300 m in the Strait of Georgia and are dominantly silty to the north and sandy to the south of the Main Channel.

3.3 Morphological Setting

A network of several distributary channels of the Fraser River supplies sediments to the western delta front. The tidal flat has a gradient of approximately 0.05 degrees. Several

gullies dissect the delta front slope. The part of the delta foreslope which is not dissected by gullies has an average gradient of approximately 1.5 degrees (Mathews and Shepard, 1962), but may be inclined as steeply as 23 degrees along its upper reaches (Scotton, 1977). Recent geophysical surveys also revealed that the upper slopes of the gullies stand at angles of 23 degrees, but locally exceed 40 degrees along the flanks of submarine spurs. (Christain, H.A., pers. comm., 1994).

3.4 Fluvial Setting

The Fraser River has a drainage basin of 2.5 x 10^5 sq. km (Kostaschuk, et al., 1989). Many tributaries join the Main Channel of the river in the basin forming an alluvial valley. The Fraser River runs over a length of about 850 miles (Mathews and Shepard, 1962). The mean annual discharge through the river is 3400 m^3/sec (McKenna et al., 1992) and the average sediment yield through the river is 20 million tonnes annually (Luternauer, 1980). The River is characterized by low water and low sediment discharges during autumn and early spring, high water and high sediment during late spring and early summer, called the Freshet Period, and high water and low sediment in late summer (Milliman, 1980). The Main Channel of the Fraser River discharges 88% of the sediment-laden water into the Strait of Georgia. The snowmelt freshet carries about 80% of the sediment load. Over 50% of the sediment load is sand-sized particles. (Luternauer and Finn, 1983).

3.5 Progradation of the Delta

A delta plain starts to form at a point where the alluvial valley meets marine processes and the sediments from the river are disseminated. The delta plain can be subdivided into subaerial delta and subaqueous delta. The subaerial delta is that portion of the delta plain

above low tide limit. In the Fraser River delta, it is the area from the point of influence of the Straight of Georgia on the alluvial valley to the tidal flats. The subaqeous delta is that portion of the delta which lies below low-tide water level. It is the foundation on which progradation of the subaerial delta must proceed (Coleman, 1976). The main characteristic of the subaqeous delta plain is a seaward fining of the sediments carried in plumes. Sands and coarser sediments are deposited near the river mouth and finer grain sediments are transported farther from the shore. Figure 3.3 illustrates deposition of sediments at a river mouth. Rapid deposition of coarser sediments takes place close to the river mouth. A sand body deposited at a river mouth is called a distributary mouth bar deposit. Seaward of this point, the percentage of sand decreases and a zone of interfingering sands, silts and clays is commonly found. This zone is referred to as distal bar deposits. Farther away from this zone the deposition of suspended silts and clays take place on the lower slope, called prodelta deposits. As the delta progrades seawards, deposition of sand occurs on previously deposited delta front sediments and prodelta clays. Meandering of distributaries erodes and reworks the upper most delta deposit and produces well-sorted deposits overlying an unconfirmity.

In the Fraser River Delta near Sand Heads deposition of sand occurs with some amount of silt in tidal couplets. The deposition of silt size particles occurs at slack high water and leads to interbedding with sand during low tide periods. The sand deposits near Sand Heads form the distributary mouth bar of the Main Channel. The mouth bar extends to the break in slope of the tidal flats at about 9 m. The progradation rate of the delta at the depth of 9 m is approximately 9 m/year (Mathews and Shepard, 1962) and builds in thickness 12 cm/year (Barrie, Pers. Comm., 1994). The progradation of the delta occur essentially in parallel planes in time. The average sedimentation rate on the upper slope north of the main channel is 2.16 cm/year (Moslow et al. 1991).

3.6 Oceanographical Setting

In the estuary, a strong tidal effect is superimposed on the fluvial regime. The tides in the Strait of Georgia are mixed semi-diurnal tides (Thomson, 1981). The mean tidal range at Sand Heads is 2.6 m, but the extreme tidal range exceeds 5.4 m. The tides in concert with the river discharge control the intrusion of a salt-wedge which in turn affects the mechanisms and rates of sediment transport (Kostaschuk et al., 1989).

Once sediment is deposited on the delta front, wind generated waves and currents and strong tides rework the sediment. Strong winds cross the tidal flats from south, southeast and northwest (Luternauer, 1980). Northwest winds have the longest fetch of about 50 km and, consequently generate the highest waves (Thomson, 1981). The average wave height over the slope is about 0.6 m and the maximum significant wave height is 2.7 m, even during winter storms. The maximum probable waves arriving at the edge of tidal flats would be 2.9 m.

Over the delta slope tidal currents tend to parallel bathymetric contours and flood currents are somewhat stronger and of longer duration than ebb currents (Thomson, 1975). At the bottom, tidal currents reach speeds up to 50 cm/sec (Shepard and Milliman, 1978), and the currents are strong enough to transport sand sized particles (Luternauer and Finn, 1983). Flood tides dominate sediment transport along the delta front in a northeasterly direction.

3.7 Sediment Dynamics at the Mouth

River mouth sedimentary processes are controlled by tidal phase and river conditions. During the freshet periods, the sediment charged plume from the Main Channel extends far into the Strait of Georgia. At high tide the salt-wedge intrudes into the channel and the

flow at the river mouth is stratified. Fresh water outflow in the upper layer is strong and there is a moderate upstream flow in the lower saline layer, in response to entrainment of salt-water by the outflow. There is a seaward decrease in both the thickness and velocity of the surface layer and the strength of the return flow (Kostaschuk et al., 1989). Sediment concentrations are low at the mouth in response to the high tide and the landward intrusion of the salt-wedge in the channel. The rise of the tide in the Fraser results in deceleration of the outflow and deposition of suspended sediment. Silt sized particles can settle out of the suspension and are deposited at the mouth. During low tide, the salt-wedge recedes back out of the Channel and the velocity of the river flow increases. Sediment concentrations are high, and sands are deposited from bedload transport. Observations show only 10% of the sediment is deposited during high tide and 55% of the sediment is deposited during low tide (Kostaschuk et al., 1989). The buoyant plume with the suspended sediments from the river is acted upon by the Coriolis Force in association with the flood tide and deflects the plume towards the Sturgeon Bank slope resulting in the deposition of silt and clay. Even on ebbing tide more fine sediments tend to be directed to the north because the southeasterly ebb tidal drag on the plume can be balanced by the Coriolis effect (Luternauer, 1980).

The sediments deposited at the mouth of the Fraser River are reworked by currents. Turbulence associated with the storm wave action can maintain fine sediments such as silt in suspension at the river mouth. Currents also contribute to make the silt particles buoyant and carry these sediments away from the estuary and allow deposition as prodelta deposits. Furthermore, sediments in suspension in surface waters which reach the opposite side of the Strait may be carried back to the east by an intermittent clockwise eddy (Luternauer and Finn, 1983). Thus several processes contribute to northerly drift of the suspended sediments leaving primarily sand sized particles at the place of deposition.

3.8 Influence of Dredging on Sedimentation

Approximately 4 x 10^6 tons of sediment (consisting mainly of sand) are dredged annually from the Main Channel (Lutenauer, 1980). Dredging of sediment can suspend fine sediments and leave it in circulation. Dredging may also influence the intrusion of the salt wedge from the Strait of Georgia which could inhibit down channel movement of sand on a northward-flooding tide while permitting the silt and clay to be carried over the Sturgeon Bank Slope (Mathews and Shepard, 1962).

3.9 Influence of Mass Wasting Events

Middleton and Hampton (1976) proposed that flows consisting of sediment moving downslope under the action of gravity be called 'sediment gravity flows'. Major processes contributing to redistribution of sediment are sediment gravity flows. These flows are initiated following slumping or sliding of the deposits of a river mouth. Liquefaction flow slides are quite common in loose sandy soils in active river deltas. Varnes (1958) differentiates a variety of subaqeous mass movements. Slump is a kind of slide in which blocks of a failed mass rotate along curved slip planes. Slides are translational or rotational movements of essentially rigid, internally undeformed masses along discrete slip planes. When internal deformation is excessive, mass flows can result. Submarine slides can become mass flows as the sliding mass progressively disintegrates and as continued downslope movement occurs (Morgenstern, 1967).

Several researchers have attempted to identify between different sediment gravity flows in the submarine environment, such as turbidity currents, liquefied flows/fluidised flows, grain flows and debris flows (Middleton and Hamton, 1976; Postma, 1986 and Lee et al., 1993). The nature of sedimentary gravity flow depends on several characteristics of flows

including velocity, density, cohesive strength, flow thickness, apparent viscosity and the geometry of slope. Initiation of the flows occur due to excess pore pressures in the interstitial pore fluid. Hence, all the flows can be classified as liquefied flows. However, the support mechanisms of the flows differ from each other. Turbidity currents are observed as low density turbulent cohesionless sediment flows in which the sediments are supported by turbulence of the pore fluid. Debris flows occur when the sediment is heterogeneous and may include large clasts supported by a matrix of fine sediments. In grain flows, the sediment is supported by direct grain to grain interactions. When some sedimentary deposits fail, most commonly as a result of over steepening, they avalanche downslope as a thin grain flow. The factors that would deter a slump from transforming into a turbidity current are rapid decrease of slope inclination which decrease acceleration of the mass and the dissipation of pore pressures (Morgenstern, 1967).

Liquefaction failures are a recurrent phenomena in the distributary mouth of the Fraser River Delta. The failures displace silty sand from Sand Heads and spread the silty sand at the base of the slope. Scotton (1977) observed slump structures in the Fraser River Delta and believed that the structures were initiated by earthquakes. Hart et al. (1992) argued that the gas-charged silty sediments on the north of the main submarine channel did not show any evidence of disturbance due to any seismic activity. They believed that the transport mechanism of failed sediments through the main submarine channel of the Fraser River Delta is by debris flows. Turbidites are also observed in the deposits at the base of the slope (Moslow et al., 1991). These turbidites are believed to be derived either from turbidity currents associated with the debris flows or from river mouth suspensions (Hart et al., 1992). Heterogeneity of the sediments with supporting fine sediments is required in a debris flow. Liquefaction flow slides in the Fraser River Delta occur in silty sands. The presence of silty sands may support the initiation of turbidity currents. However, careful

examination of the depositional environments of the sediments at the base of the slope is needed to determine the nature of flow of the failed sediments.

3.10 Morphological Features on the Fraser Delta Slope

3.10.1 Sea Valleys

Sea valleys are observed on the Fraser River delta slope and are believed to be created and maintained by mass wasting events. The migration of the Main Channel over tidal flats during the last 100 years occurred prior to the construction of jetties (Luternauer and Finn, 1983; Clague et al, 1983). The short gullies at the head of the slope may be remnants of earlier features formed when the Main Channel disgorged sediments on this part of the slope in historical times (Luternauer and Finn, 1983). Geographical surveys show that the distributary mouth bar deposit at Sand Heads is incised by a series of deep gullies that coalesce downslope into a single large canyon (Kostaschuk et al., 1991). Heads of submarine canyons provide an extremely suitable environment for slumping because of their steeper inclination and their action as sediment traps (Morgenstern, 1967). The canyon at the mouth of the Fraser River has a meandering pattern with well defined cut-bank morphology and bedforms (debris flows) on the channel floor (Hart et al., 1992). The sea valley system has upslope tributary channels joining a single sinuous channel which splits into distributary channels at the base of the delta front (Kostaschuk et al., 1991). These distributary channels radiate over a submarine fan. The tributary channel gradients vary from 23 degrees locally in the upper reaches of the tributaries at the river mouth to 2 degrees at 45 m depth. The major gullies were formed as a result of mass wasting events transforming to turbidity currents and are maintained by the sliding of accumulated gully bottom sediments and flushing action of tidal currents (Mathews and

Shepard, 1962; Terzaghi, 1962; Scotton, 1977; Shepard and Milliman, 1978, Hart et al., 1992).

3.10.2 Sand Waves

These hydraulic bed forms are observed at depths of more than 100 m on the sandy southwestern Roberts Bank slope. They are subdued, straight-crested wave forms, oriented approximately north-south (Luternauer and Finn, 1983), which grade into higher waves with more sinuous crests. Towards the center of the zone, the features are disjointed and lobate and have heights of 2 - 3 m and wave lengths of 30 m or more. They appear to be generated by flood tidal currents. Local flood tide current velocities in these zones are high enough to permit general sediment motion in a northwest trending direction.

3.10.3 Foreslope Hills

On the basis of bathymetry, features consisting of rounded "hills" and troughs with over 10 m relief between hill and trough axes are observed (Hart et al., 1992). Mathews and Shepard (1962) observed them as large hummocks/ridges at the base of the slope off the Main Channel. These are the Fore Slope Hills (FSH). Mathews and Shepard (1962) and Terzaghi (1962) postulated that they were the evidence of a large slope failure. They may have been formed by the compressional folding of mass wasted material (Tiffin et al., 1971; Luternauer and Finn, 1983). Acoustic surveys have failed to clearly discern internal stratigraphy, but indicate in general that these are recent gas-charged fine grained deposits with high clay content and with moderate degree of plasticity (Hart et al., 1992). Hart (1993) reviewed the available seismic data and concluded that internal acoustic lineations might be shear planes. There could have been rotational displacements failures of sediments.

As indicated previously, as a delta progrades seawards, deposition of sand occurs on previously deposited delta front sediments and prodelta clays. The FSH in the Fraser River Delta may have originated from progressive deep-seated failures within these marine clays, arising in turn from stress imposed by the prograding delta rather than as rotational movements induced by overloading through upslope failures. (Christian et al., 1994). At places the sediment comprising the FSH could reach to its angle of repose. It appears that the FSH are still active (Christian et al., 1994).

3.11 Summary

The Fraser River delta on the western coast of Canada is an actively prograding delta. Sedimentation at the mouth of the river is very high during summer periods. Sand and silt sized particles are deposited at the river mouth and fine grained material is carried away in suspension to farther offshore. Additional agencies, such as the Coriolis Force act in association with tidal phases of the sea and deflect the sediment charged plume to the north of the Main Channel. Interacting fluvial and oceanographical processes influence the morphology of the delta slope. These processes contribute to the initiation of mass wasting events. Maintenance of features such as sea valleys and other suggest that mass wasting events of the distributary mouth bar deposits are recurrent phenomena. The contributions of different environmental processes are evaluated in the succeeding chapters.

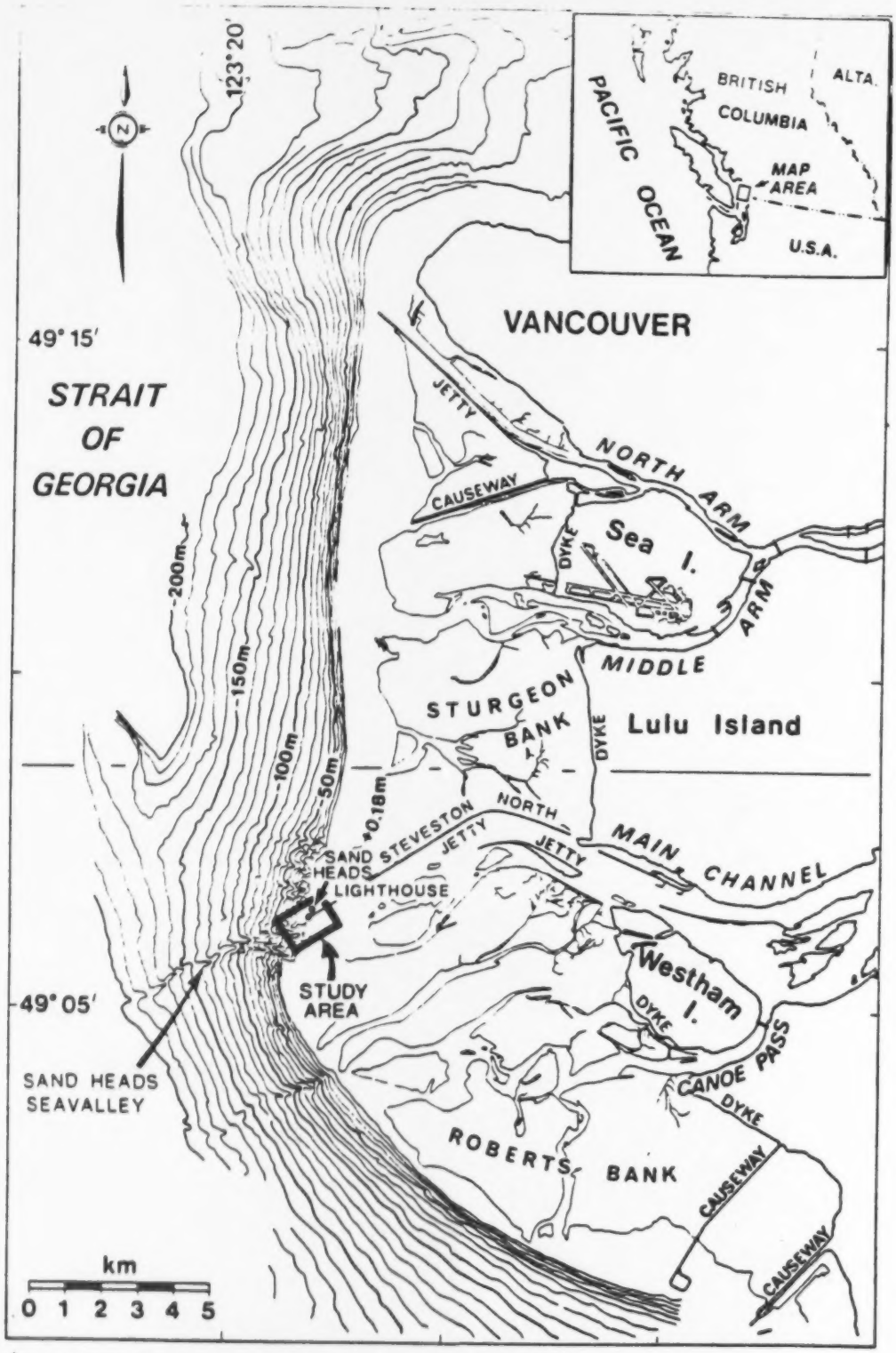

Figure 3.1. The Fraser River Delta front (after McKenna et al., 1992)

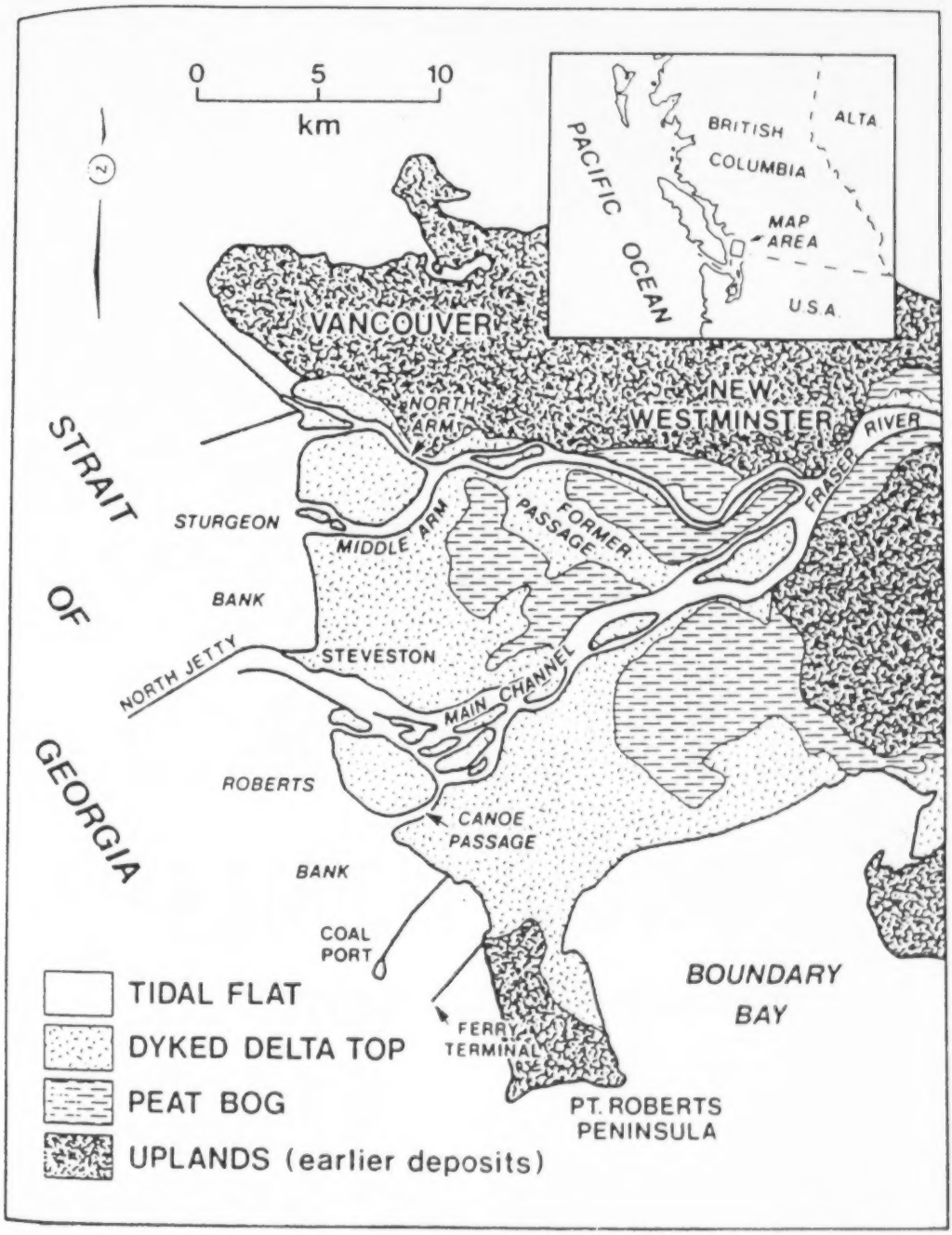

Figure 3.2. Surficial deposits in the Fraser River Delta (after Luternauer and Finn, 1983)

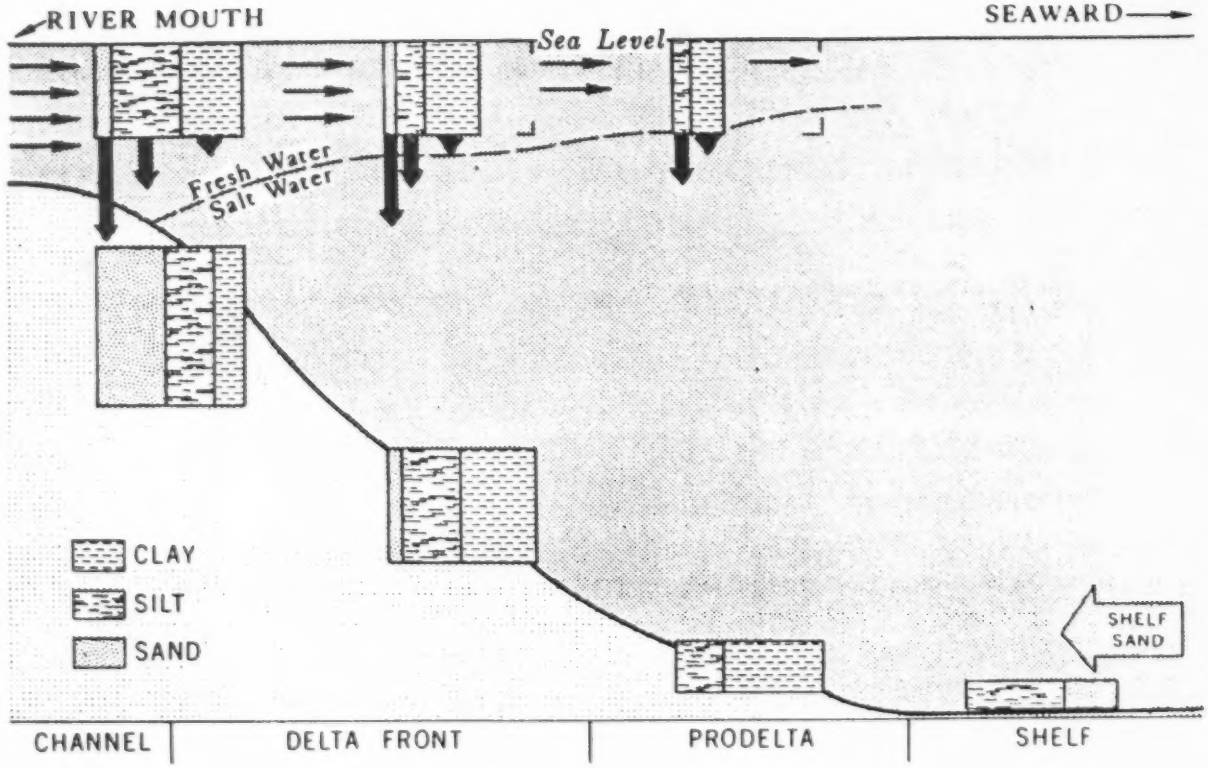

Figure 3.3. Deposition of sediments at a river mouth (in Coleman, 1976)

4.0 Characterization of the Fraser River Delta Sands near Sand Heads

4.1 Introduction

Robertson et al. (1992, a) suggested that the initial step in any liquefaction study should be to evaluate if the soil is contractant or dilatant at large strains. If the soil is contractant, it possesses a potential to liquefy. Steady state divides the two states of the soil. The investigation of contractant cohesionless soils for liquefaction susceptibility is often directed towards quantifying how loose the soil deposit is in-situ. Morgenstern (1967) indicated that the initiation of liquefaction failures was consistent with the mobilization of the undrained shear strength of the loose soils. Analyses based on laboratory testing as well as analyses based on *in-situ* testing are the currently available methodologies for the evaluation of liquefaction potential. Laboratory tests on undisturbed samples help determine undrained strengths as well as steady state parameters and provide a measure of available *in-situ* undrained shear strength of the loose soil deposits. Obtaining high quality undisturbed soils can be difficult and expensive. Ground freezing is one method to obtain the highest quality samples (Sego et al. 1994). In the subaqueous environment the method is rarely practical. Laboratory tests can be carried out on reconstituted samples. However, the preparation of sand samples requires careful handling and precision to obtain uniform samples and reliable laboratory data. Also there is often uncertainity with sample preparation techniques. *In-situ* testing provides a viable means of overcoming the uncertainties of the laboratory testing for evaluating liquefaction potential of a site. *In -situ* tests include cone penetration tests (CPT) and seismic cone penetration tests (SCPT). From a SCPT, a profile of shear wave velocity with depth as well as the penetration data from the CPT can be obtained. Empirical correlations exist to evaluate the *in -situ* state of the soils from the profiles of CPT and SCPT. The correlations are based on cone tip resistance and *in -situ* shear wave velocity measurements and provide an evaluation for

liquefaction potential of loose sandy soil deposits. This chapter presents laboratory test results on the reconstituted samples of Fraser River Delta (FRD) sand, results of *in-situ* testing performed in the delta and an assessment of the *in-situ* tests for liquefaction susceptibility.

4.2 Laboratory Testing on the Fraser River Delta Sand

4.2.1 Physical Properties of Material Tested

Triaxial tests have been conducted on the FRD sand sampled from a borehole (FD93S2 in Figure 4.1). Figure 4.1 also shows the locations of in-situ tests performed at Sand Heads. The details of the tests are discussed elsewhere in the Chapter. Monahan et al. (1993) presented an integration of CPT data in the FRD with the borehole data obtained by the Geological Survey of Canada and reported that distributary channel sand deposits form a continuous composite sand unit underlying most of the subaerial delta plain. The borehole (FD93S2) was drilled down to a depth of about 18 m below seabed and sampling was carried out using a hydraulically pushed Shelby tube wireline sampler. The soil stratigraphy encountered by the boring consists of clean fine sand interbedded with silty material with small quantities of organics. The natural moisture content of the stratum ranged from 24 to 40%. The grain size distribution of the fine sand is shown in Figure 4.2. The average particle size D_{50} is 0.25 mm and the uniformity coefficient is 1.7. The average mineral composition of the FRD sand is approximately 40% quartz, 11% feldspar, 45% unaltered (unweathered) rock fragments and 4% other minerals (Vaid and Thomas, 1995). Maximum and minimum void ratios in accordance with ASTM D2049 are 1.00 and 0.6 respectively. The specific gravity is determined as 2.75. Atterberg limits could not be determined on the silty material and hence it is non-plastic.

4.2.2 Testing Apparatus

Triaxial tests were performed on very loose samples of the FRD sand. Usually in triaxial tests the major principal stress σ_1' is applied in the vertical direction and the other two principal stresses σ_2' and σ_3' ($\sigma_2'=\sigma_3'$) are applied horizontally by fluid pressure surrounding a soil specimen. The vertical stress can be increased in either a stress controlled or a strain controlled manner.

A modified Wykeham Farrance strain controlled loading machine was used in this testing program. In the modified machine, dead load can be applied to the top of the sample. The triaxial cell is also modified accordingly. An internal load cell was used to measure the magnitudes of axial load application. The use of an internal load cell eliminates friction corrections between the loading ram and the top of the triaxial cell. The loading frame had a variable gearing system to shear the sample in the triaxial cell at a constant strain rate. A schematic diagram of the test set up is shown in Figure 4.3. Electronic pressure transducers were used for the measurement of cell pressure, back pressure and pore pressure and a linear voltage displacement transducer (LVDT) was used for measurement of axial displacement. Volume change measurements were carried out using another LVDT during consolidation and drained shear tests. During a test the data were recorded on an IBM 80286 AT computer through an interface board DAS 16.

4.2.3 Sample Preparation

Samples were prepared by the moist tamping technique. The triaxial specimens were approximately 63 mm in diameter and 127 mm in height. However, accurate measurements of samples were performed on each sample before testing. A small error of 0.1 mm in height measurements reflects in a change of void ratio by 1%. Moist tamping

yields a very loose structure for reconstituted soil samples (Ishihara, 1993). Sample uniformity is maintained in moist tamped specimens (Sasitharan et al, 1993). Some samples were also prepared by water pluviation. Methods of preparation of samples are described in the Appendix. It was observed that water pluviation inhibited the formation of a loose structure by maintaining fine particles in suspension and resulted in slightly dense samples. The fine particles formed thin lenses in the water pluviated sand specimens resulting in non uniform samples.

4.2.4 Testing Program and Results

Isotropically consolidated monotonic undrained and drained triaxial compression tests were performed on the samples. During shearing in the undrained tests, the drainage valve was closed. The volume of the sample did not change in the undrained tests, that is, void ratio of the sample remained constant. The samples were sheared undrained at a constant strain rate of 0.15 mm/minute after consolidation to a specific confining stress. Figure 4.4 shows the stress-strain curves for undrained tests and the corresponding pore pressure variations. It can be seen that samples prepared by moist tamping reached a peak deviatoric stress within 0.5% axial strain and the change in the pore pressures shows a continued increase to about 4 to 6% axial strain before reaching a constant value. The tests (UDFR3,UDFR5,UDFR10) exhibited a strain softening response to their steady states of low stress values at large strains.

Monotonic drained triaxial compression tests were performed after consolidating the samples to a specific confining stress. Samples were sheared at a constant strain rate of 0.15 mm/min under fully drained conditions. Volume changes occur during drained loading and the corresponding void ratio can be calculated from the volume measurements. The stress-strain curves for drained tests (DFR1, DFR2) and the corresponding volume

changes are presented in Figure 4.5. As the deviatoric stress approaches the steady state, the corresponding volume change reaches a constant value. Decrease in volume change for an applied deviatoric stress indicates contractant behavior.

Figure 4.6 presents normalized stress paths in terms of q/p'_{ss} against p'/p'_{ss}, where p'_{ss} is mean normal confining stress at the steady state. Due to the normalization, all tests will terminate at (1,M), where $p'/p'ss = 1$ and $q/p'ss = M$.

A typical undrained stress path and a drained stress path are plotted in Figure 4.7. The undrained path in the e-p' plane remained horizontal without any changes in void ratio. It can also be seen that void ratio changed during the drained loading. The undrained stress path in the p'-q plane represents very brittle behavior and strain softening response of the sample to its steady state value at low stresses. The slope of the drained stress path in the p'-q plane is a straight line with a slope of 3:1. The slope of the contractant boundary surface (CSB), 's', can be determined as the slope of tangent drawn to the post peak portion of undrained stress path at steady state in the p'-q plane. Table 4.1 summarizes test data obtained during consolidation and steady state values for all the tests.

The steady state line is established from the steady state points obtained from all the tests on the FRD sand as shown in Figure 4.8. In the e-p' plane, it can be seen that the steady state line is bilinear with a break occurring at a stress level of about 800 kPa. This observation is consistent with a break in steady state line for Erksak Sand at 1000 kPa (Been et al., 1991). The change in shearing mechanism at this stress level is due to the crushing or the breaking of material grains. Beyond the break, the slope of steady state line is very much steeper. However, for the surficial sand deposits at the FRD the typical engineering stress levels vary between 0-700 kPa. The steady state line for the FRD sand can be approximated as a straight line in the stress range 0-800 kPa. The steady state line in the

p'-q plane is a straight line passing through the origin. From the laboratory test results, the steady state parameters are determined, following Sasitharan (1994), as

Γ = 1.11 (Ordinate of the steady state line at p = 1kPa)

λ_{ln} = 0.029 (Slope of the steady state line in e-ln p' plane)

M = 1.4 (Angle of shearing resistance at steady state $\Phi' = 35^{o}$)

t = 0.8 (Slope of collapse surface)

s = 1.00 (Slope of contractant state boundary)

4.3 Shear Wave Velocity Measurement

Shear wave velocity , Vs, is a parameter that can be measured both in the field and in the laboratory. Shear wave velocity measurements can be used to analyze foundations subjected to dynamic loading as well as defining in-situ state of soil. Robertson et al. (1994) state that shear wave velocity is controlled primarily by void ratio, effective confining stresses, the intrinsic characteristics of soil (grain size distribution, grain shape, angularity, surface roughness and mineralogical composition) and its structure (fabric, aging and cementation). Grain crushing induces significant changes in the intrinsic characteristics. Structure of the soil is changed with changes in void ratio and effective confining stresses. Flow liquefaction occurs in loose, relatively fresh and uncemented sands. Hence, well cemented and aged sands are not a concern in flow liquefaction studies. Fabric can influence shear wave velocity, Vs. However, tests have shown that fabric has little effect in very loose sands (Robertson, et al., 1994). Hence, for these materials, shear wave velocity is primarily a function of void ratio and effective confining stresses.

The shear wave is a body wave which has particles in motion perpendicular to the direction of wave propagation. In the field, Vs can be measured by intrusive methods such as SCPT

(Robertson et al, 1992) or non intrusive methods such as spectral analysis of surface wave (SASW) methods (Christian et al., 1994). In SCPT, the cone is equipped with a geophone to record seismic wave arrivals triggered by a source at the surface. The travel time of a wave through a known distance measures the shear wave velocity of the deposit.

4.3.1 Laboratory Measurements of Shear Wave Velocity

Measurements of shear wave velocity in the laboratory have been carried out successfully using bender elements (Sasitharan et al., 1993, Cunning, 1994). Fabrication of bender elements is well described by Dyvik and Madshus, (1985). A bender element is composed of two thin plates of piezoceramic material rigidly bonded along their lengths with conducting surfaces between them and on the outside to function as an electro-mechanical transducer. The transducer is capable of converting mechanical energy either to or from electrical energy. The polarization of the ceramic material in each plate and the electrical connections are such that when a driving voltage is applied to the element, one plate elongates and the other shortens. The net result is a bending of the element, inducing tension in one plate and the compression in the other. This results in a back and forth motion of the element.

Bender elements can act as a source which converts electrical signals to mechanical signals as well as a receiver which converts mechanical signals to electrical signals. Mounting two bender elements, one at the top and the other at the bottom pedestals of triaxial testing apparatus, enables the creation of a very small strain shear wave through a soil sample. The arrangement of bender elements in a triaxial cell is shown in the Figure 4.3. In order to avoid electrical shorting of the bender element due to moisture, the element is coated with a water proof material. The gap between the bender element and the porous stone is filled with silicon to prevent soil protrusion.

The bender element protrudes into the specimen as a cantilever as shown in the Figure 4.3. The vibration of the tip of the bender element results in propagation of shear wave through the specimen in a direction parallel to the length of the unagitated bender element. A shear wave generated by electrical pulses through a transmitter bender element travels through the soil sample and is received by the other bender element. With the use of an oscilloscope, a wave generator and an amplifier for the received signals, the input electrical wave can be compared to the received electrical wave. Using the first pulse arrival method the shear wave travel time can be obtained from the oscilloscope. A typical oscilloscope output of generated electrical pulse and received electrical pulse is shown in Figure 4.9. Knowing the distance of separation of the bender elements along with the travel time of the shear wave, the shear wave velocity can be calculated.

4.3.2 Shear Wave Velocity Measurements in the Present Study

The equipment used in this study consisted of piezoceramic bender elements, a Wavetek 148 A - 20 MHz AM/FM/PM generator, a Kistler 5004 Dual Mode Amplifier, A Phillips PM 3365A 100 MHz, 1000 MS/s oscilloscope and a Hewlett Packer HP Color ProPen Plotter. Each bender element was 31.8 mm long x 12.5 mm wide x 0.05 mm thick. Protrusion of the bender element was 5 mm from each pedestal. The bender element placed in the bottom pedestal was used as a transmitter and the element in the top pedestal was used as a receiver. After each stage of isotropic consolidation of a soil sample for an applied confining stress, the bottom bender element was excited with a $\pm$ 15 volt dc, 20 Hz square wave by the Wavetek generator. Velocity of the generated shear wave was determined as the ratio of the known height of soil sample to the time taken for the wave to travel through the sample. All test data for shear waves were recorded on hardcopy plots of the Hewlett Packer plotter. Measured shear wave velocities for all the tests on the FRD sand are included in table 4.1.

4.4 Coupling of V_S Measurements to the Steady State Line

A relationship between void ratio - effective mean confining stress - shear wave velocity (e -p_c' - V_S) was developed by Cunning (1994). V_S is mainly a function of both void ratio and mean normal effective consolidation stress (p_c') for istropic consolidation state. Hence for a sand of constant void ratio the Vs will increase with increasing stress. Robertson et al. (1992,a) suggested normalization of the shear wave velocity to the effective overburden pressure as

$$V_{s1} = V_S\left(\frac{p_a}{p_o'}\right)^n \tag{4.1}$$

where

V_{S1} = nomalized shear wave velocity

V_S = measured shear wave velocity

p_a = Reference stress (typically, 100 kPa)

p_o' = Effective overburden stress (kPa)

n = an exponent, (usually 0.25)

Cunning (1994) suggested the normalization to the effective confining stress (p_c').

The relationship between Vs1 and void ratio (e) over a wide range fits a linear regression for isotropic conditions as

$$V_{S1} = A - Be \tag{4.2}$$

where

A = intercept of the Vs1 - e relationship at e = 0

B = slope of the Vs1 - e relationship

e = void ratio

Equations (4.1) and (4.2) result in a relationship of e - p_c' - Vs as

$$Vs = (A - Be)(\frac{p_{c'}}{100})^n \qquad (4.3)$$

The constants A and B and the exponent n constitute shear wave velocity parameters for a particular sandy soil.

A steady state line can be represented by a straight line in the e-log p' plane within the range of engineering stresses (10 -700 kPa). Contours of shear wave velocity can be superposed on the laboratory derived steady state line of a sand in the e- log p' plane using Equation 4.3. This diagram serves as a chart for evaluating in-situ state of soil in the field. Field void ratio can be estimated, when the field measured shear wave velocities and the effective stress conditions are known. These estimates position the in-situ state of soil on the chart relative to the steady state line, which determine the possible behavior of the soil as contractive or dilative.

4.4.1 e - p' - V_S Relationship for Fraser River Delta Sand

Normalized shear wave velocities, Vs1, are determined from the measured shear wave velocities during consolidation of samples of the FRD sand and the effective confining stresses, and are included in the Table 4.1. Linear regression of the limited Vs1 - e data (Figure 4.10) would result in an average equation as follows;

$$V_{S1} = 295 - 143\ e \qquad (4.4,a)$$

The upper and lower bounds are computed to fit most of the data which is scattered slightly and the relationships can be expressed as

$$V_{s1}\ (\text{upper}) = 307 - 143\ e \qquad (4.4,b)$$

$$V_{s1}\ (\text{lower}) = 283 - 143\ e \qquad (4.4,c)$$

The e - p_c'- V_s relation of the FRD sand can be expressed as

$$Vs = (295 - 143e)(\frac{p_{c'}}{100})^{0.26} \qquad (4.5)$$

The measured shear wave velocity parameters for the FRD sand are

A = 295

B = 143

n = 0.26

Figure 4.11 presents a chart showing the contours of shear wave velocity on the steady state line in e-p' plane and shear wave velocities during consolidation of the FRD sand samples in the laboratory. The consolidation data for moist tamped samples fell on the contractive side of the steady state line. The data for the water pluviated samples lie on the dilative side and demonstrate that water pluviation techniques result in dilative sand samples. Observations from other laboratory results also showed that the water pluviation techniques for sample preparation resulted in dilative samples (Sasitharan, 1993; Cunning, 1994). During the preparation of samples using water pluviation, segregation was observed in the present study and upward turbulence of water left fine particles in suspension. Fine particles formed thin lenses in the sand samples. Hence, the water pluviation technique may not simulate the contractive state of in-situ deposits. The isotropic consolidation curve of the loose samples has a flat slope on the contractive side indicating that the sand has low to moderate compressibility.

4.5 *In-situ* Tests in the Fraser River delta

In-situ tests such as CPT and SCPT were carried out on the FRD front in water depths ranging from 5 to 10 m at Sand Heads. The field work was performed under the supervision of the Geological Survey of Canada by ConeTec Investigations Ltd. The test sites are close to the heads of the submarine channels and are located as shown in Figure 4.1. The depth of investigation was targeted at 30 m for all sites. Different in-situ tests and results for characterization of the sediments in the Robert Banks of the Fraser River Delta are discussed by Christian et al (1994).

The CPT data were obtained using a standard 10 sq. cm electric cone with 60 degree apex cone angle and a friction sleeve area of 150 sq. cm. Pore pressures were measured immediately behind the cone tip using a 5 mm thick porous plastic filter. The pore pressure filters were saturated in glycerin under vacuum prior to penetration. The porous filter allows water pressure communication between soil and a pore pressure transducer located inside the cone. The cones were equipped with a geophone to record seismic wave arrivals. Data were collected every 5 cm and stored in a data acquisition system. Seismic shear wave velocity measurements were made every one meter during brief pauses in the cone penetration.

Figures 4.12 and 4.13 show the soil profiles of FD93CPT2 (refered as CPT2) and FD94CPT1 (refered as CPT5), in terms of CPT penetration resistance, sleeve friction, friction ratio (ratio of the sleeve friction to the cone bearing resistance) expressed as percentage, and penetration pore pressures. These two sites are over a distance of about 100 m. The profiles consist of sands interbedded with normally consolidated silts. These formations are mouth bar deposits and are consistent with the geological observations as described in Chapter 3. The cone penetration resistance profile of CPT2 shows that the

deposits are loose sands with silt layers over its depth. It can also be observed from CPT5 profile that loose deposits of sands with silts seams are underlain by dense deposits beyond 20 m of depth. Comparison of the two profiles shows that the deposits of sands with silt seams in the upper 20 m depths are very loose.

4.6 Evaluation of Liquefaction Susceptibility of the Deposits at Sand Heads

Assessment of liquefaction potential of the sand deposits at Sand Heads can be carried out based on in-situ tests such as CPT and SCPT. Empirical evaluations, based on cone penetration resistance from CPT and shear wave velocity measurements from SCPT, are discussed. These evaluations differentiate contractive states from dilative states for a given sand.

4.6.1 Evaluation based on Cone Penetration Tests

Robertson et al (1992,a) suggested a criterion using normalized cone resistance values for differentiating contractant and dilatant responses of sand during shearing as

$$q_{c1} \leq 50 - 75 \quad \text{(bars)} \tag{4.6}$$

and

$$q_{c1} = q_c\left(\frac{p_a}{\sigma_{vo}'}\right)^{0.5} \quad \text{(bars)} \tag{4.7}$$

where

q_{c1} = normalized cone penetration resistance (kPa)

q_c = cone penetration resistance

p_a = atmospheric pressure (100 kPa)

σ_{vo}' = effective vertical overburden stress (kPa)

Equation (4.6) indicates that there exists a potential for the sand to undergo flow liquefaction when the q_{c1} values are less than 50 - 75 bars.

From the experiences of liquefaction flow slides in the Beaufort Sea, Sladen and Hewitt (1989) proposed another relation as

$$q_c / (\sigma_{vo}')^{0.65} = 70 \quad \text{(bars)} \tag{4.8}$$

Figure 4.14 includes the evaluation of CPT2 for flow liquefaction susceptibility. Both criteria suggest that sand deposits at the crest of the foreslope at Sand Heads are susceptible to flow liquefaction. However, the relationships may not indicate the response of silt deposits interbedded in the sand deposits.

4.6.2 Evaluation from Seismic Cone Penetration Test (SCPT)

Robertson et al. (1992,a) suggested that a range of normalized shear wave velocity, V_{s1}, (Equation 4. 1) between 140 m/sec to 160 m/sec divides contractant and dilatant boundaries.

SCPT were carried out close to the crest of the foreslope (Figure 4.1). The soil profile was interpreted from the SCPT and it consisted of loose sand to a depth of 20 m. The average shear wave velocity ranged from 50 m/sec to about 190 m/sec in compact sands at a depth of 25 m. Shear wave velocity measurements appear to be insensitive to fines content and therefore can be used to evaluate liquefaction potential in silty sands without the need for large corrections (Christian et al, 1994). Fear and Robertson (1994) suggested that Vs1 = 160 m/sec is the dividing line for contractant and dilatant behavior for incompressible quartz sand. For more compressible sands, V_{s1} tends to decrease to 140 m/sec. From the laboratory tests carried out as part of this study, it is observed that the FRD sand appears to

be moderately compressible. Hence, the value Vs1 = 160 m/sec can be used to estimate liquefaction potential of the sand deposits at Sand Heads. Figure 4.15 illustrates that the sand at the location of the testing appears to be contractive in the upper depths and therefore, susceptible to flow liquefaction.

4.6.3 Evaluation Based on State Parameter Approach

Been and Jeffries (1985) introduced the concept of a state parameter to describe the relationship between in-situ void ratio and effective stress level and their relation to the steady state void ratio at the same stress level. The state parameter, Ψ, is defined as the void ratio difference between the current state and steady state at the same stress level. A positive and a negative state parameter would mean strain softening and strain hardening undrained responses at large strains, respectively. A state parameter of $\Psi = 0$ is on the steady state line delineating the boundary between the contractive state and the dilative state.

Cunning (1994) developed a relationship between V_{S1} at $\Psi = 0$ and effective vertical stress using the e -p'-V_S relation as

$$(Vs1)_{\psi=0} = \mathrm{B} \times (K_0)^{n/2} \times \{(\frac{A}{B} - \Gamma) + \lambda_{\ln} \ln[\sigma_v' \times (1 + 2K_o)/3]\} \qquad (4.9)$$

where A, B, n are the shear wave velocity parameters, Γ, $\lambda_{\ln}$ are the steady state parameters and Ko is the coefficient of lateral earth pressure. Equation 4.9 defines the V_{S1} value for $\Psi = 0$ for a given $\sigma v'$ and can be converted to Vs values using Equation 4.1. It can be plotted in a V_S against σ_V' plot with the $(V_S)\Psi = 0$ boundary to divide the contractant state to the dilatant. However, a knowledge of Ko is required for the in-situ deposits. Comparison of in-situ shear wave velocity profile with the steady state boundary evaluates the in-situ state of the soil deposits.

The shear wave velocity profile obtained from SCPT in the Fraser River Delta is compared with the $(Vs)\Psi = 0$ boundary derived from the laboratory data in the Figure 4.15. A K_O of 0.43 was used in Equation 4.9. The in situ state is close to the boundary between contractant and dilatant behaviour. It also illustrates that the surficial sand deposits at the location of the testing appear to be contractive. However, it may be prudent to predict the soil behaviour at selected depths of the profile using Figure 4.11. The derived boundary, $\Psi = 0$, is based on limited laboratory data on the FRD sand. Additional laboratory study may provide sufficient data for the prediction of the sediment behaviour .

Robertson et al (1992,b) proposed a correlation between normalized cone penetration resistance and normalized shear wave velocity as

$$q_{c1} = (\frac{V_{s1}}{102})^4 \text{ MPa} \qquad (4.10)$$

where V_{s1} is in m/sec. The denominator in the equation increases for highly compressible soils (Fear and Robertson, 1994).

The values of Vs1 derived from Equation 4.9 for $\Psi = 0$ can be correlated to q_{c1} to determine a boundary on a cone penetration resistance profile of a CPT. Figure 4.14 shows the $(qc)\Psi = 0$ boundary on the CPT2 profile. The field data plots below the boundary in the surficial depths indicating the possibility of liquefaction of sand. Denser deposits may be encountered below the evaluated depths.

4.7 Summary

Laboratory tests and in-situ tests were carried out to characterize the Fraser River Delta sand. Moist tamping techniques for sample preparation resulted in very loose sand samples, whereas water pluviation techniques resulted in dilative samples. The usefulness of the methods is discussed in the next chapter. The steady state line was established for the sand and the flatness of the slope of the steady state line indicates that the sand is moderately compressible. Application of the steady state characteristics of FRD sand is presented in the succeeding chapters. A chart has been developed to characterize in situ state of the sediments of the delta in the e-p' plane by coupling the steady state line with the shear wave velocity measurements of soil samples during consolidation in triaxial tests. Using the chart, an evaluation of the state of sediments in the FRD is presented in the following chapter. Based on empirical correlations, the results of the in-situ tests have been evaluated for the liquefaction susceptibility of sand deposits in the delta and they indicate that the fresh deposits of the sand are prone to liquefaction.

Test #	Mean pressure p' (kPa)	e during consolidation	Vs (m/sec)	p' at steady state (kPa)	q at steady state (kPa)
	148.43	1.06	150		
UDFR3	164.63	1.047	151		
	214.42	1.033	165		
	265.4	1.03	179		
				13.24	17.73
	126.63	1.07	142		
	152.73	1.06	158		
UDFr5	203.12	1.05	173		
	303.29	1.03	203		
	427.46	1	226		
				34.53	46.72
	194.3	0.8			
UDFR7	244.1	0.79			
	293.87	0.79			
				1024	1530
	202.47	1.012	183		
	224.95	1.009	189		
UDFr10	273.68	1	200		
	325.12	0.99	213		
				49.65	64.47
	162.2	1.1	156		
	186.79	1	165		
DFr1	236.57	1.09	180		
	289.96	1.08	196		
				535.61	743.2
	204.49	1.11	164		
	230.13	1.11	180		
DFR3	279.47	1.1	192		
	328.2	1.09	205		
	427.77	1.07	228		
				806.62	1138.94
	307.83	0.89	201		
	357.63	0.882	213		
DFr5	408.03	0.879	227		
	457.83	0.875	232		

Table 4.1. Shear wave velocity measurements during consolidation and stresses at steady state

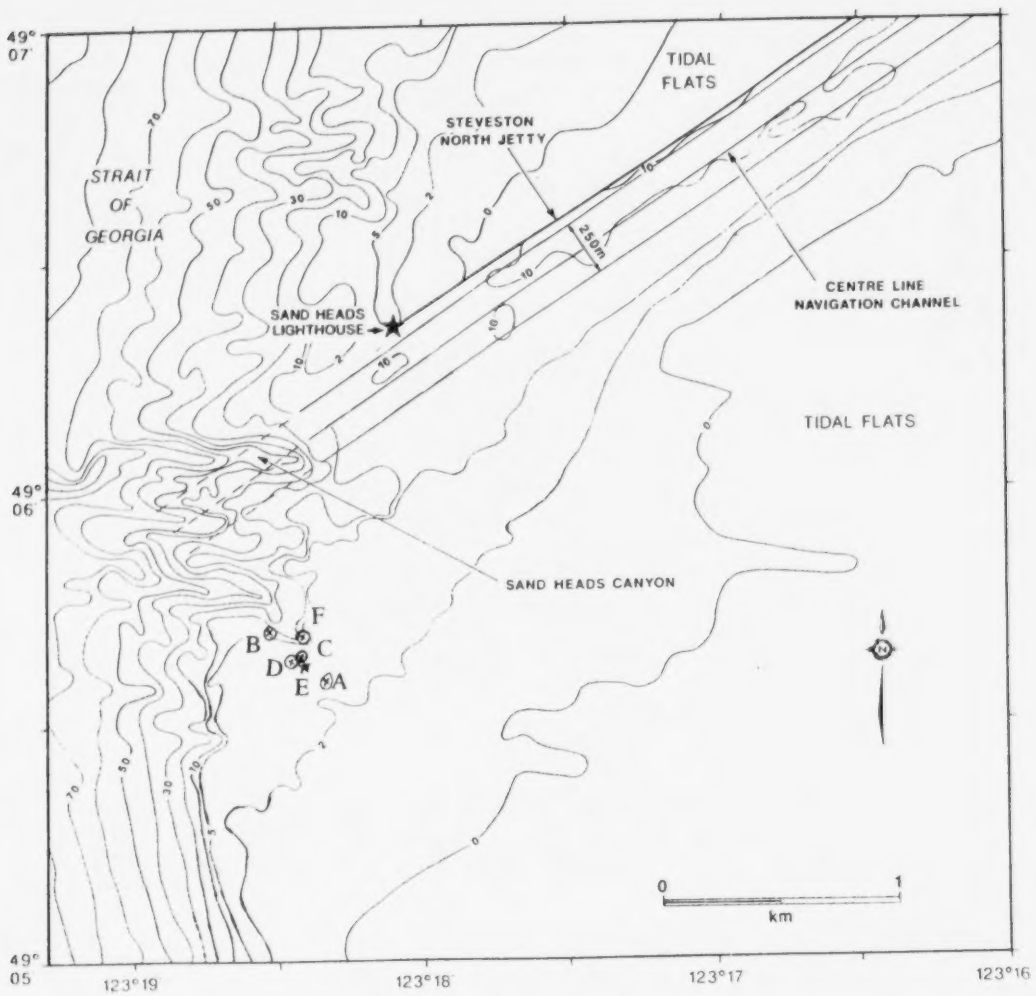

Figure 4.1 Morphology of the Fraser River delta foreslope off the Main channel. Contours are in meters (after Mckenna and Luternauer, 1987). A,B,C,D,E,F indicate in situ tests locations

A: FD93CPT1

B: FD93CPT2

C: FD93RCPT3

D: FD93SCPT4

E: FD93S2 (BOREHOLE)

F: FD94CPT1

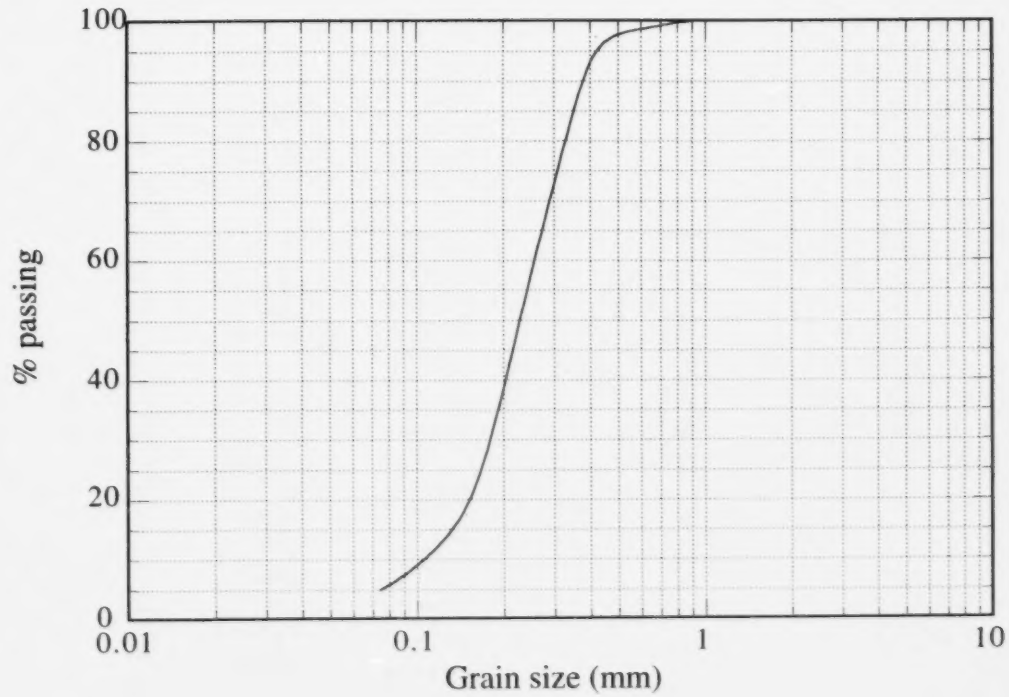

Figure 4.2. Grain size distribution curve of Fraser River delta sand

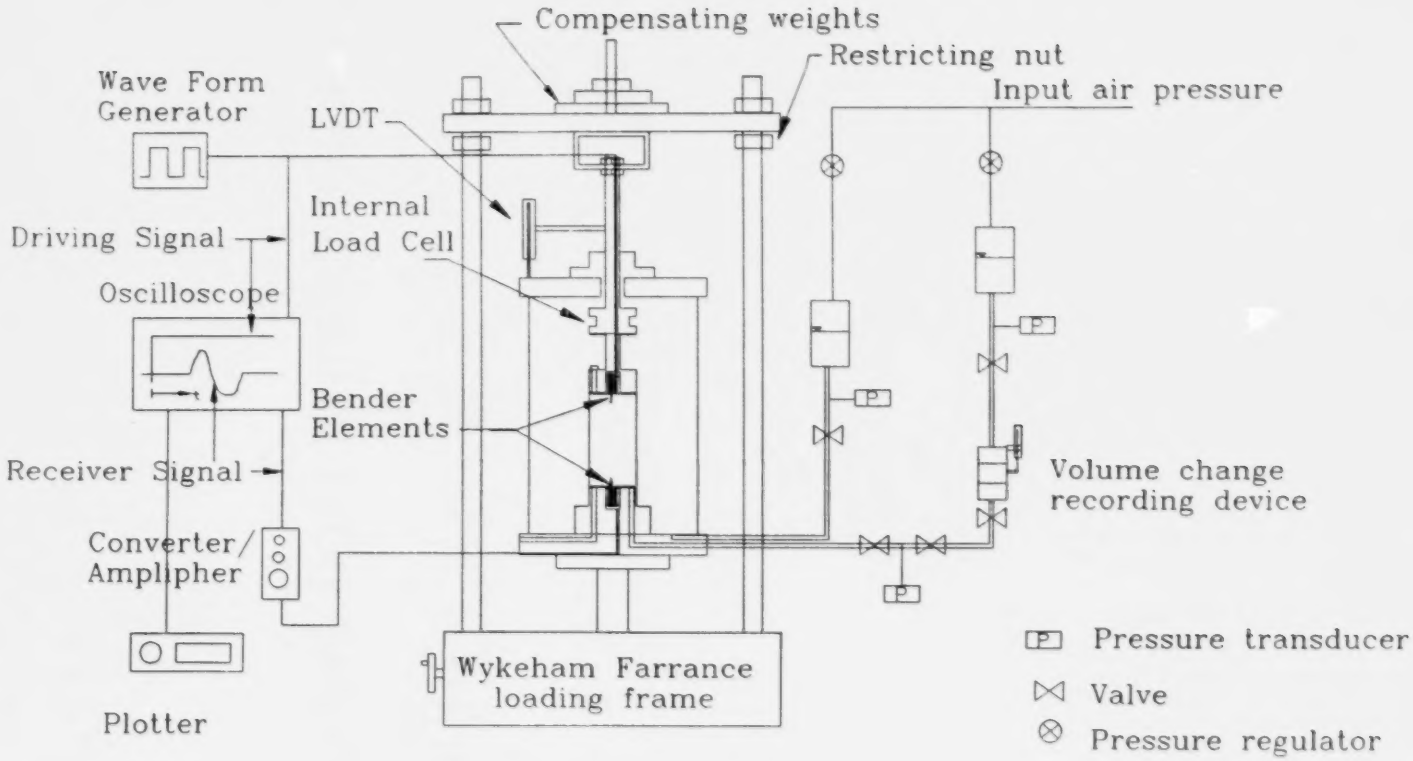

Figure 4.3. Triaxial test set-up (after Cunning, 1994)

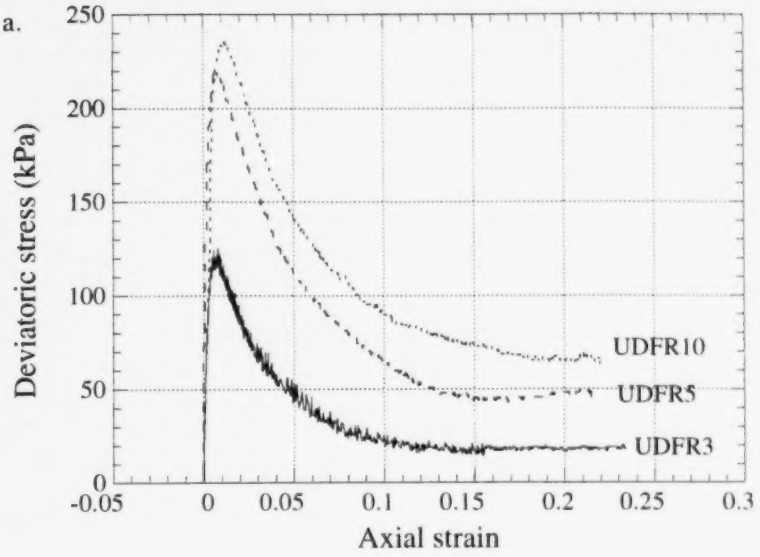

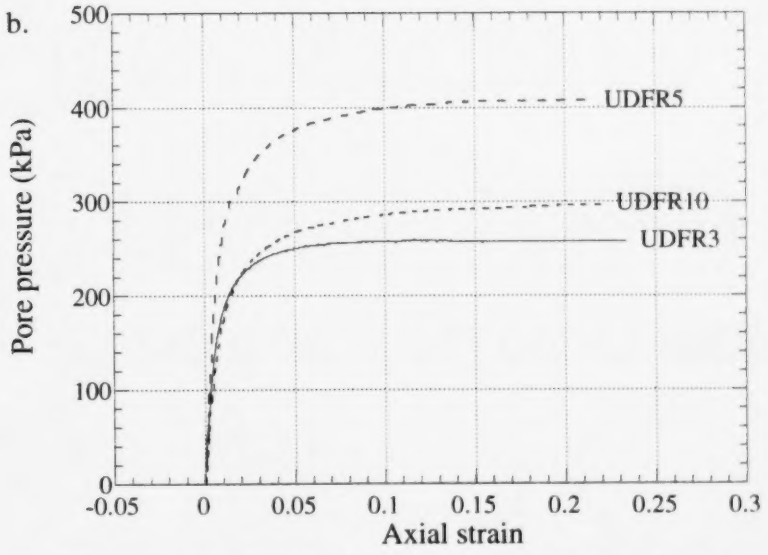

Figure 4.4 - Results of consolidated undrained triaxial tests
a). Stress -strain curves b). Pore pressure variation

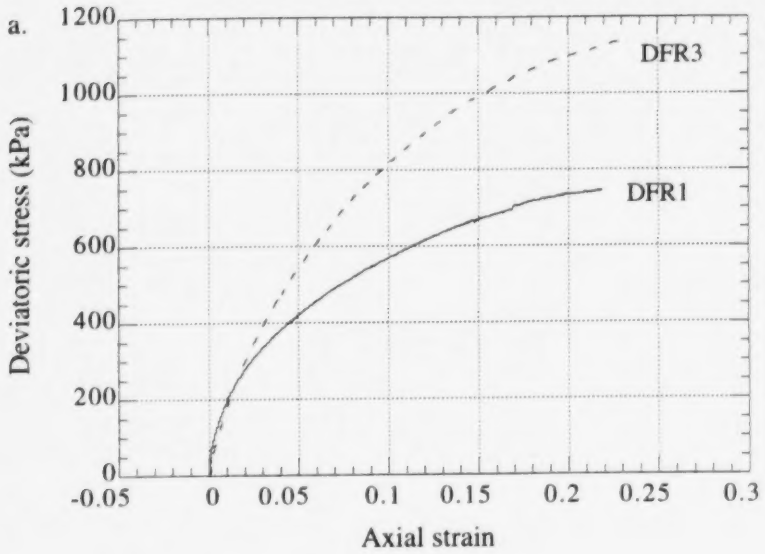

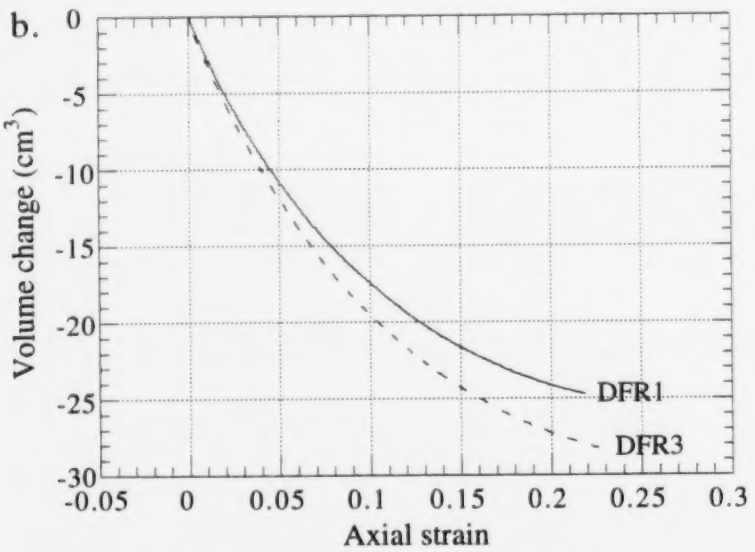

Figure 4.5. Results of consolidated drained triaxial tests
a). Stress - strain curves b). Volume change

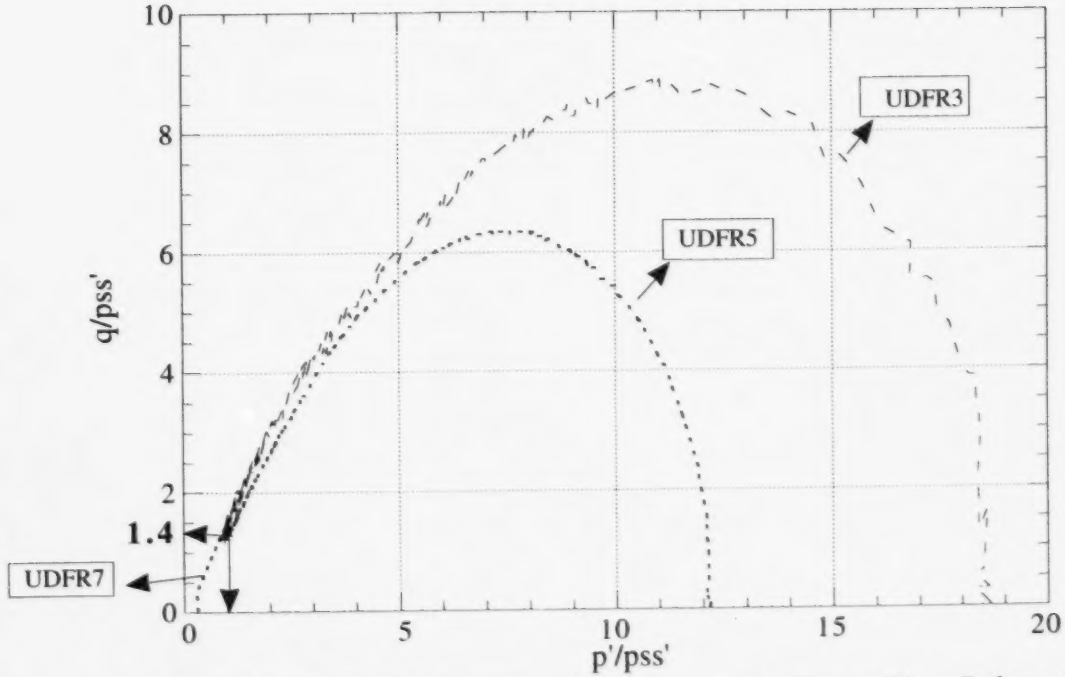

Figure 4.6. Normalised stress paths of tests on the Fraser River Delta sand

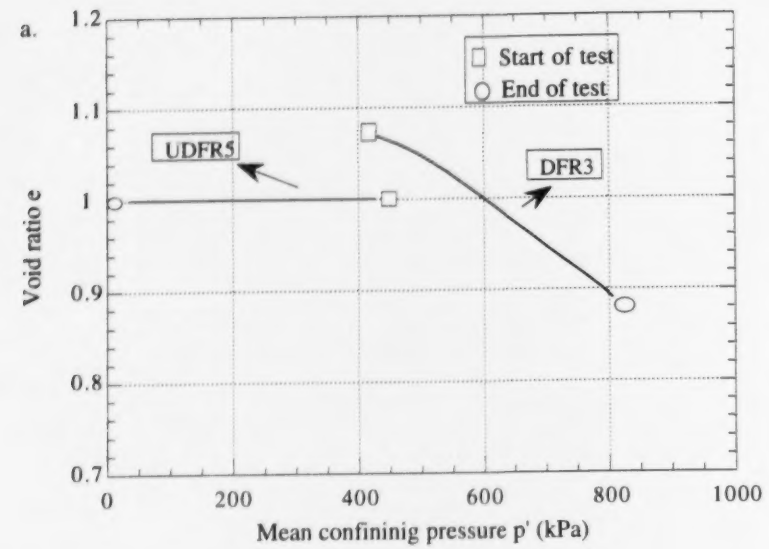

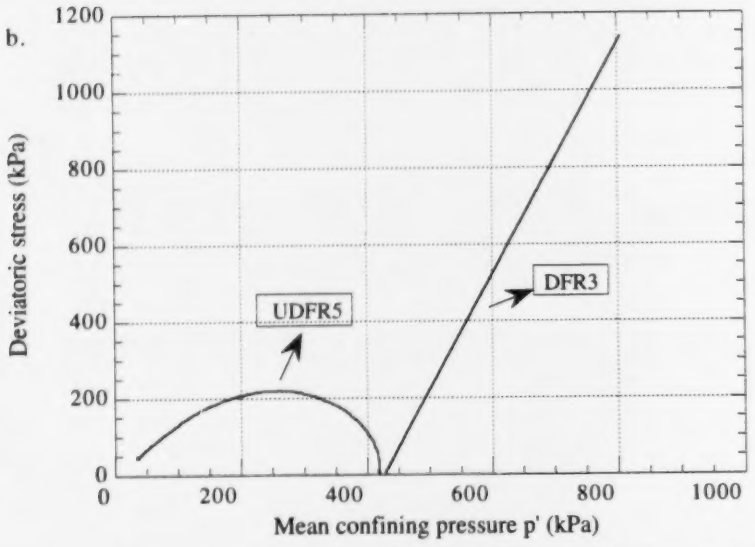

Figure 4.7 Typical undrained and drained stress paths

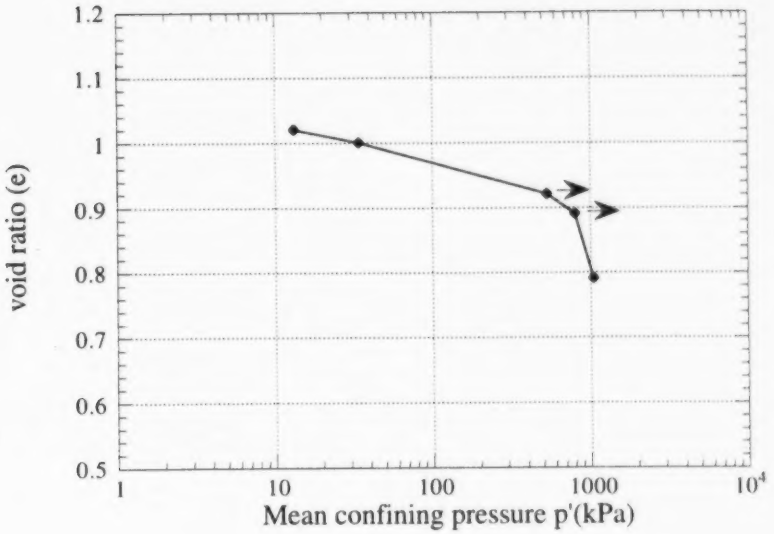

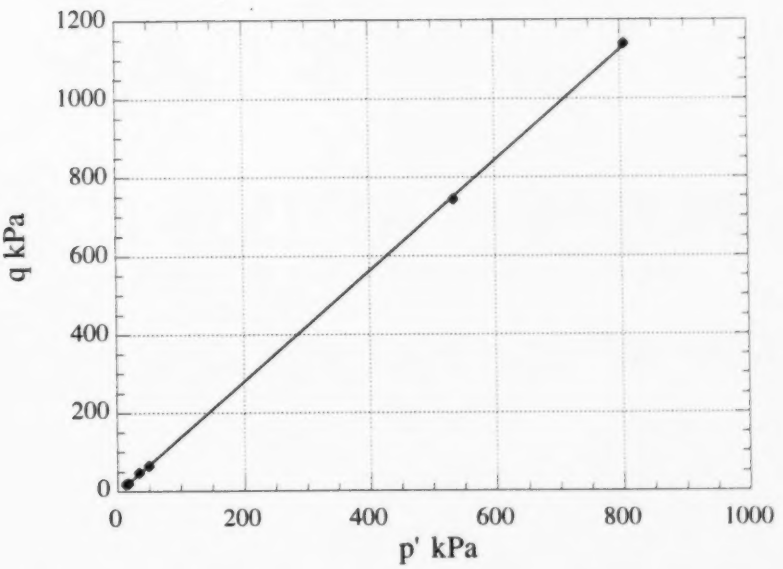

Figure 4.8. Steady State Line - Fraser River delta sand

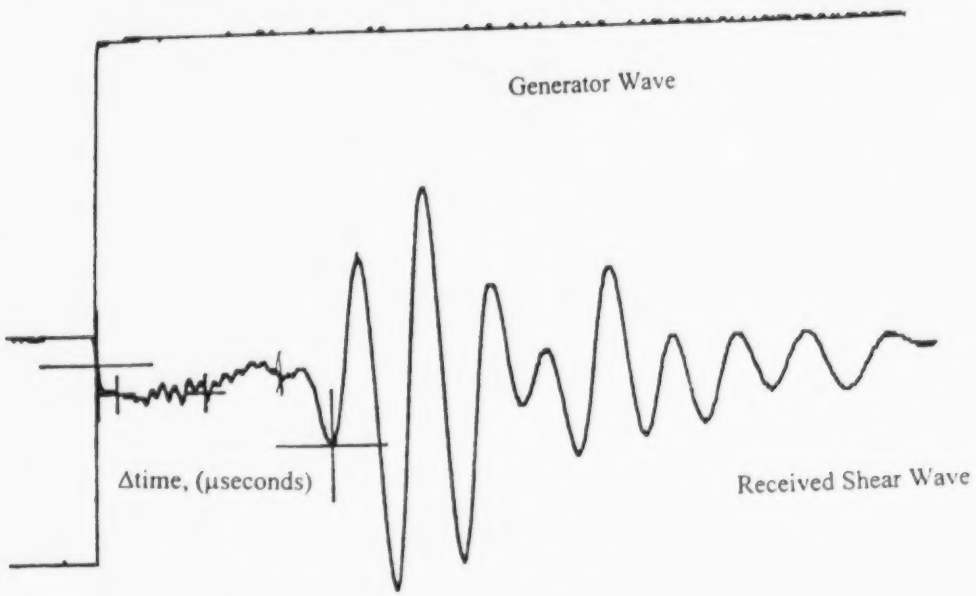

Figure 4.9. Typical oscilloscope output

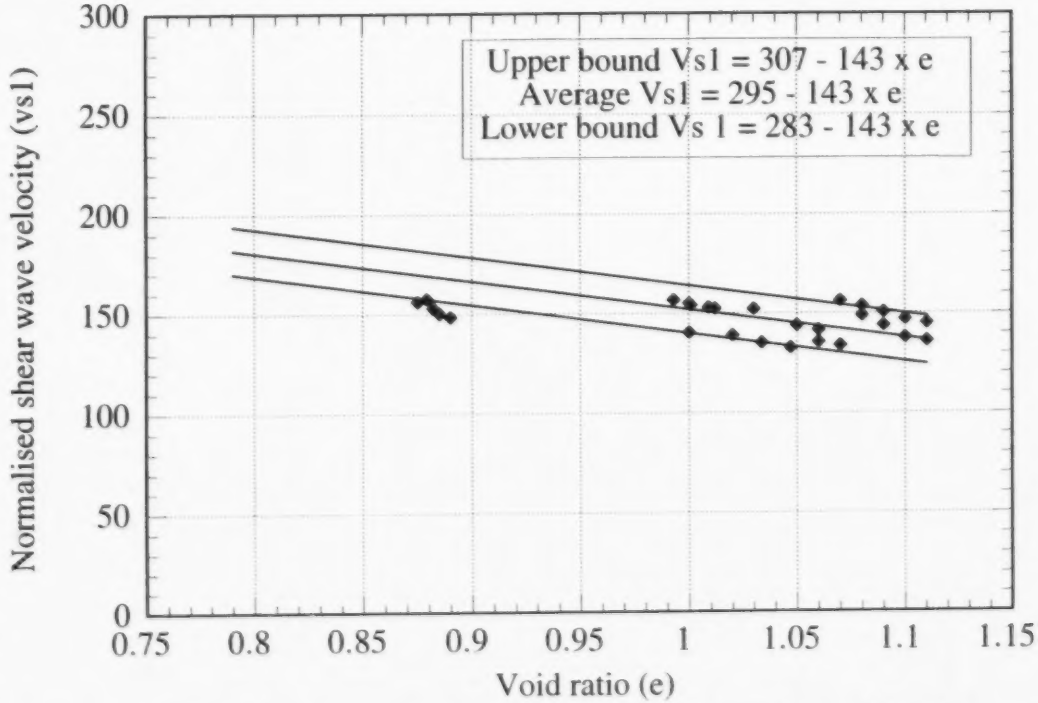

Fig.4.10 Normalised shear wave velocity against void ratio during consolidation of the Fraser River delta sand samples

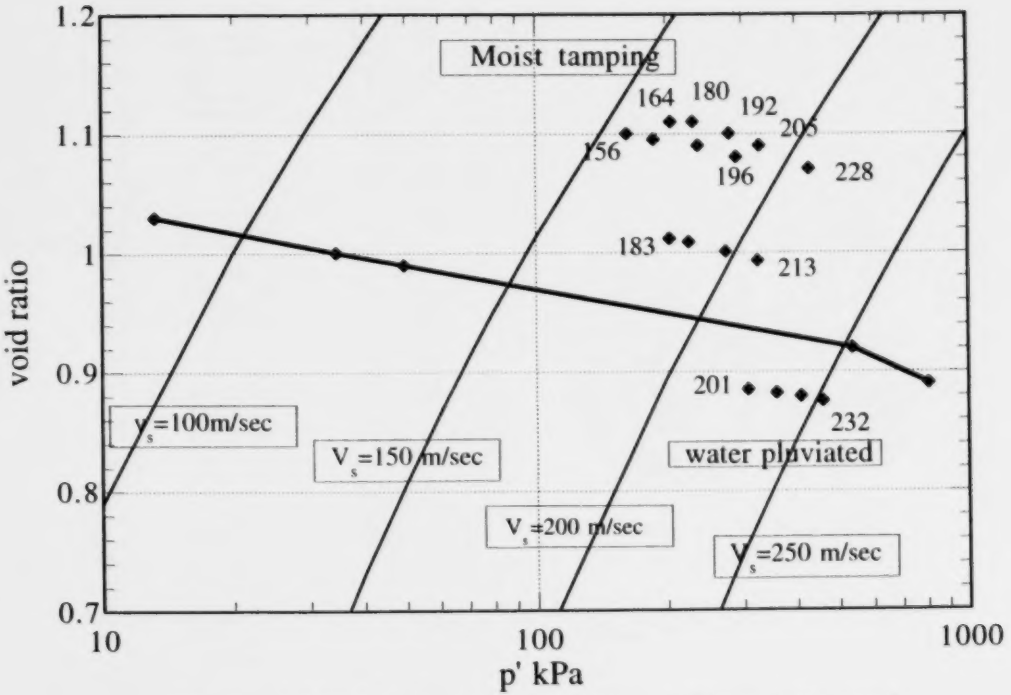

Figure 4.11. Steady state line- Fraser River delta sand
Measured shear wave velocities during consolidation
Contours of shear wave velocities

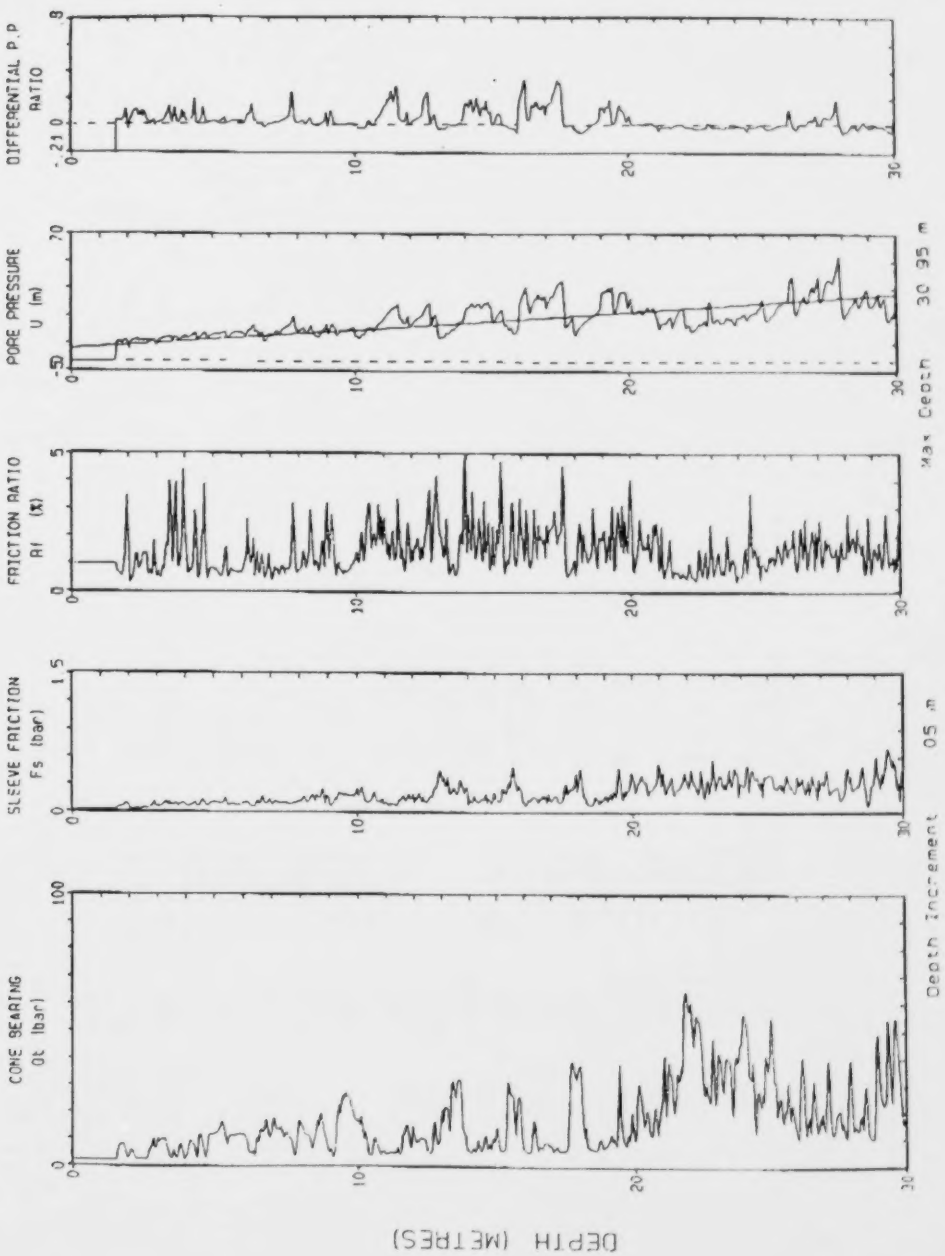

Figure 4.12. CPT profile at Site B (Figure 4.1) in the Fraser River Delta

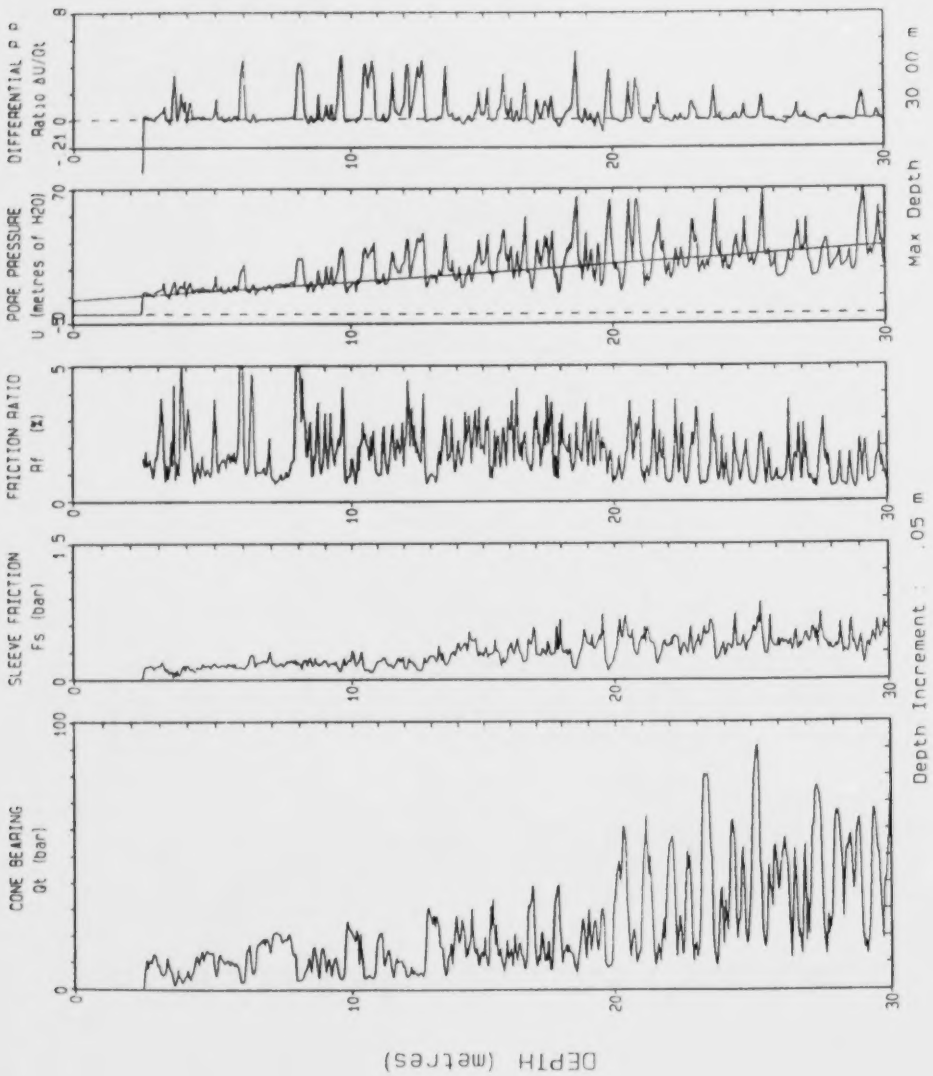

Figure 4.13. CPT profile at Site D (Figure 4.1) in the Fraser River Delta

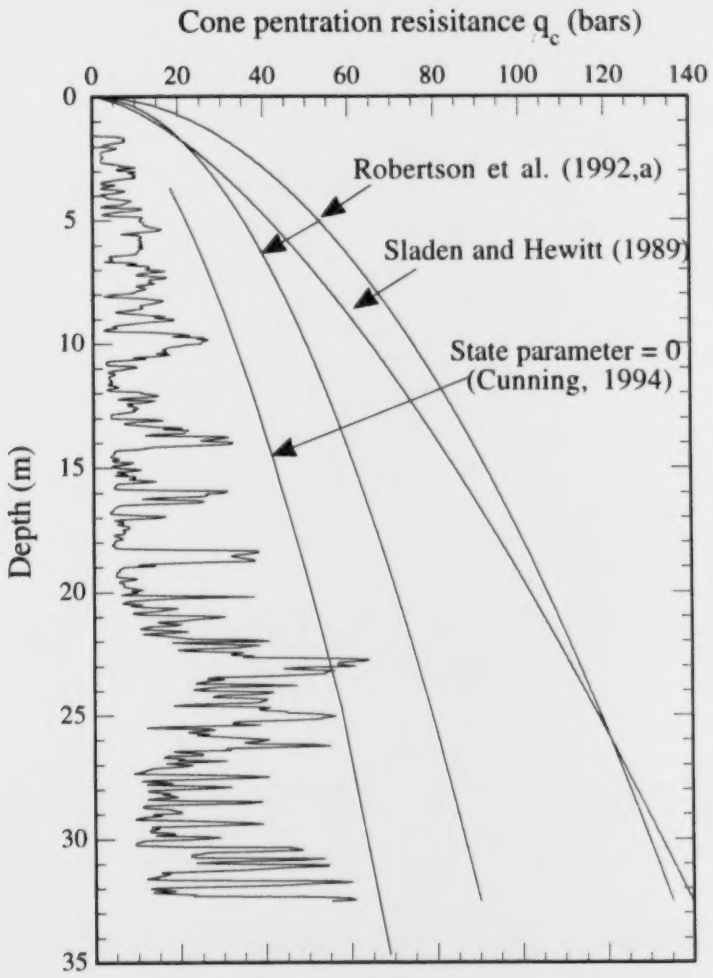

Figure 4.14. Assessment of liquefaction potential of sand deposits from CPT2 profile at Sand Heads

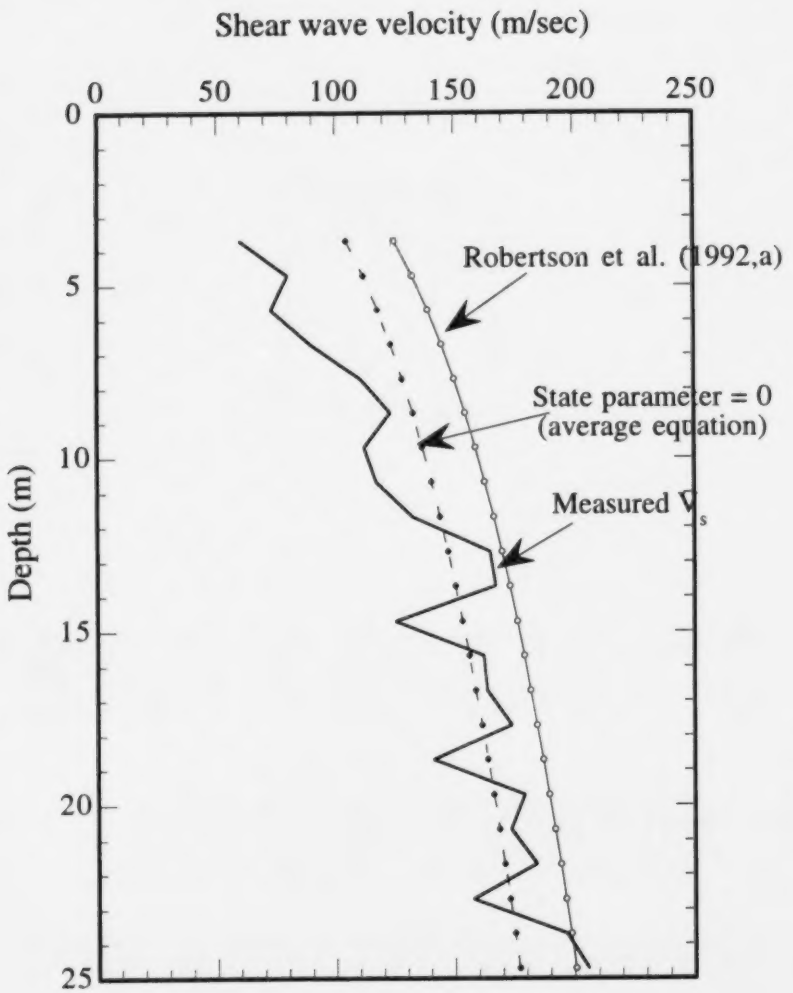

Figure 4.15. Assessment of liquefaction potential from shear wave velocity measurements

5.0 Evaluation of Influence of Sedimentation

5.1 Introduction

Rapid deposition of sediments in the estuaries of rivers is believed to be one of the triggering mechanisms of liquefaction flow slides in subaqueous slopes. The sand and silty materials of river-borne clastics are deposited at the mouth of the river building up mouthbar deposits. Retrogressive liquefaction flow slides are common phenomena in the mouthbar deposits of the Fraser River. McKenna and Luternauer (1987) believed that rapid sedimentation at the mouth of the Fraser River was one of the causes of a major liquefaction flow slide in 1985. The deposition rate of sediments in the Fraser River Delta (FRD) is very high during the periods of late spring and early summer. However, the history of flow slides in the FRD suggests that the occurrence of slides spreads over the whole year. An analysis investigating the causes of the 1985 failure is required to quantify the influence of sedimentation in triggering the failure. This chapter discusses the evaluation of the effect of sedimentation in initiating a liquefaction flow slide in the FRD.

5.2 Configuration of the slope in the FRD

Five known major mass wasting events have occurred between 1970 - 1985 on the upper delta slopes at the mouth of the Fraser River. The shift in the position of the delta-front crest (10 m contour) was used as a base for reporting the liquefaction failures of the sediments in the FRD (McKenna et al., 1992). Figure 5.1 presents the bathymetric contours of the foreslope of the FRD and also shows the areal extent of the flowslide that occurred at 10 m depth between 27 June and 11 July 1985 (McKenna and Luternauer, 1987). The volume of the sediment involved in the flow slide is very extensive (one million cubic meters). Bathymetric soundings at the area of the failure provided the post-

event changes of the contours clearly. Figure 5.2 shows the configuration of the slope (Section 1-1 in Figure 5.1) obtained from the contours of the foreslope. The break in the slope occurs at about 10 m depth of water. The foreslope had an angle of inclination of 23 degrees before the failure. The post-event head scarp had a relatively steep slope with a vertical relief of about 15 m and intersects basal planes which are subparallel to the original seafloor. The foreslope constitutes the extreme configuration of the slope before a liquefaction failure could occur. When flow liquefaction is initiated in the slope, the failure retrogresses towards its upper reaches, developing a flow slide. The retrogression continues until a stable or dense head scarp is encountered. The state of stress in the slope before a failure brings the state of the sediments in the slope to the verge of collapse. To determine whether the slope becomes unstable, it is necessary to establish the state of stress in the slope and locate it relative to the collapse surface/contractant state boundary in stress space.

5.3 State of Stress in the Slope

The limiting stress state of the soil in a slope can be established by conventional slope stability analyses assuming the failure plane as either an infinite slope or circular failure surface. Submarine slopes typically stretch over large areas. Hence, an infinite slope stability analysis may provide the limiting stress state on a plane parallel to the slope. A drained infinite slope analysis of the FRD slope results in high factors of safety. The horizontal stresses acting in the soil deposit have been ignored in the conventional limit equilibrium analysis. However, the analysis produces reliable stress states on potential sliding surfaces. A correct stress analysis should be performed by finite element calculations incorporating a realistic constitutive model to describe the stress-strain behaviour of the soil.

In the FRD, when slope failures occur in the fresh deposits of silty sands, the scar is replenished by the sediments of the Fraser River. Thus, in reality, the slope in the FRD is built up in parallel layers by the sediments from the backscarp of a previous failure to the extreme configuration for further failure. It is realistic to use a model simulating the sequential construction of the slope for estimating the stress state in the slope. The deposition of sediments occur with thin lenses of silty material in sands. It can be precluded that no excess pore pressures exist in the thin lenses of silt. An incremental finite element stress analysis, duplicating the building of the slope while incorporating drained linear elastic effective stress parameters, would be useful in simulating deposition in the delta. A finite element based program SIGMA/W handles such analysis very well and has been used.

5.3.1 Modeling the Slope Using SIGMA/W Program

The slope was discretized into a number of finite elements. Figure 5.3 shows the finite element mesh exaggerated vertically by 10. The boundary conditions are such that the displacements at the base were constrained in either direction and the displacement behind the backscarp of the failure line was laterally constrained. Robertson and Campanella (1983) presented a method of interpretation of CPT results for sands for estimating stiffness properties. Based on the CPT results of the fresh deposits in the FRD, the Young's Modulus has been estimated as 15 MPa. A Poisson's ratio of 0.3 and a K_O value of 0.43 are additional parameters used in the analysis.

SIGMA/W simulates the process of accretion of the slope by the addition of finite elements in parallel layers having the same properties. In the analysis, the stress file obtained from the preceding layer becomes the initial conditions for the succeeding layer.

5.3.2. Stress path Evaluation

The state of stress in an element of soil in a slope can usually be described in plane strain condition by two normal stresses (X-stress and Y-stress in the present case) and one shear stress component (X-Y stress) on the element of soil in the slope. For the system of stresses, there exists two principal stresses and the associated maximum shear stress. However, the stress state can also be represented by the mean confining stress $p' = J_1'/3$ and deviatoric stress $q = \sqrt{(3J_2)}$; where J_1' is the first stress invariant, $(\sigma_1'+\sigma_2'+\sigma_3')$, and J_2 is the second stress invariant, $\frac{1}{\sqrt{6}}\sqrt{(\sigma_1-\sigma_2)^2+(\sigma_2-\sigma_3)^2+(\sigma_3-\sigma_1)^2}$.

The stress state in the slope of the FRD before failure can be obtained from the extreme configuration of the slope, that is, after the addition of finite elements in the final layer. Figure 5.4 (a) to Figure 5.4 (f) show the contours of effective stresses including X stress, Y-stress, X-Y stress, maximum shear stress, mean confining stress (p') and deviatoric stress (q) for the extreme configuration of the slope. From all the plots, it can be seen that the maximum values of the stresses occur for the elements which are at a depth of about 36 m.

The stress path of the elements in p'-q space can be evaluated due to sediment deposition (accretion of the finite elements) by plotting the calculated effective confining stresses (p') and the corresponding deviatoric stresses (q) at Gaussian points of the finite element mesh. Figure 5.5 illustrates the stress path of the elements due to the sediment deposition. Small magnitudes of tensile stresses are observed at the surface of slope. All the stresses are determined for a K_o value of 0.43 and they appear to follow the K_o line in stress space. Also shown in Figure 5.5 is the steady state line which has been established from the laboratory tests. It can be observed that the effect of sedimentation is to build up the shear stresses.

The stress state has to be brought on to the collapse surface (CS) and the Contractant State Boundary Surface (CSB) for triggering of flow liquefaction of the sediments. Hence, it is necessary to study the implication of the stress path on the CS and the CSB for triggering of flow liquefaction of the sediments due to sedimentation. The stress path (Figure 5.5) represents the state of stress of the sediments from the back scarp (having a depth of 15 m) of the failure in 1985 to the extreme configuration of the slope (about 36 m depth). It may be difficult to denote the CS and the CSB by a straight line in p'-q space for the stress state, because the steady state strength (undrained shear strength) of the sediments increases with depth. Alternately, the path of maximum shear stress for each increment of a layer can be drawn in stress space and can be assessed for the initiation of instability.

In each increment of a parallel layer of sediments, there exists a maximum shear stress value in the freshly deposited sediments in the slope. The maximum shear stress for each layer occurs at a node. SIGMA/W can estimate the stress state of each node in the finite element mesh in the form of Mohr's circle. Using the Mohr's circle plots, the magnitude of maximum shear stress for each layer is estimated. The path of maximum shear stress is drawn in p'-q space in Figure 5.6, as the slope is built up in parallel layers.

The addition of one layer of sediments influences the maximum shear stress of previous layers. Figure 5.6 also presents the shift of the maximum shear stress path due to subsequent additions of sediments in parallel layers. For the addition of the first layer of sediments, node 1800 (Figure 5.4,a) experiences maximum shear stress. The stress state of the node 1800 can be estimated from the Mohr's circle. As the slope is built up in subsequent layers, the layers will induce changes in stress state of the node 1800, corresponding to the first layer and moves the stress state as shown in Figure 5.6. Similarly, all the nodes of maximum shear stress corresponding to different layers will experience a shift from their initial positions. The stress state of node 616 (see Figure

5.4,a) corresponds to the maximum shear stress state in the fresh deposits in the slope. The maximum shear stress state of the node 616 is at a depth of 36 m (see Figure 5.4,a). The stress state of the node 616 is shown in the form a Mohr's circle in Figure 5.7.

The state of stresses represents the stress state in the slope due to the sedimentation (Figure 5.6). The steady state line is also shown in the Figure 5.6. The stress state of the sediments can be evaluated for triggering of flow liquefaction by comparing its position relative to the CS or the CSB in stress space. This evaluation requires a knowledge of the undrained shear strength of the sediments. However, the chart (Figure 4.11) that was developed in Chapter 4 for the characterization of the in-situ state of sediments can be used to evaluate the stress state of the sediments (Figure 5.6).

5.3.3 Characterization of the Stress State of the Soil in the Slope

In Chapter 4.0, it has been established from in-situ tests that fresh deposits of silty sands are susceptible to flow liquefaction. However, the available undrained shear strength of the sediments has to be determined for assessing the possibility of flow liquefaction due to sedimentation. Figure 4.11 presents a chart to characterize the in-situ state of the sediments in the e-p' plane by coupling the steady state line with the shear wave velocity measurements. The stress state of the slope (in Figure 5.6 - from node 1800 to node 616) can be located in the Figure 4.11 for evaluating the effect of sedimentation. The positioning requires the knowledge of the in-situ void ratio. It is difficult to estimate the in-situ void ratio of underwater sandy deposits accurately. Hence, the shear wave velocity has been used as a parameter for evaluating the stress state in the e-p' plane.

Figure 4.15 presents the profile of in-situ shear wave velocity from a SCPT. The shear wave velocities corresponding to the stress state can be estimated from the profile. The

stress state at node 1800 corresponds to an average shear wave velocity of 155 m/sec. For the stress state at node 616 (depth of 36 m), the average shear wave velocity can be extrapolated to about 190 m/sec. The relative positioning of the stress state of all the nodes is shown in Figure 5.8(a) with respect to the steady state line. The state indicates that the soil is contractant and the corresponding steady state strength is at a void ratio of about 0.98 and mean confining pressure of about 77.5 kPa.

As discussed previously, the stress state in Figure 5.6 represents the stress state of fresh deposits in the FRD. Since the stress state (Figure 5.6) falls in the contractant region of Figure 5.8(a), it can also be anticipated that the state of fresh deposits in the slope remain in the contractant region. However, this observation alone does not confirm the susceptibility of the fresh deposits for flow liquefaction unless the in-situ shear stresses are higher than the steady state strength of the deposits. The steady state strength at the mean confining stress of 77.5 kPa (Figure 5.8,b) controls the behaviour of the stress state. The steady state strength corresponding to the void ratio of 0.98 and the mean confining stress of 77.5 kPa can be estimated to be about 108 kPa (Figure 5.8,b).

From undrained triaxial compression tests on the samples of FRD sand, the slopes of CS and CSB were established in Chapter 4. Using the slopes, the CS and the CSB corresponding to the steady state strength (108 kPa) are also plotted in Figure 5.8(b). The stress states do not reach the CS or the CSB indicating that sediment deposition alone may not initiate flow liquefaction of the deposits. However, the stress state of node 616 is very close to the CS indicating that the state is close to collapse. It can be also observed that the stress state of the deposits is higher than the steady state strength, implying that the fresh deposits of the FRD have the potential for flow liquefaction. However, the stress state at node 1800 is lower than the steady state strength and indicates that the stress state may not be prone to flow liquefaction. The mean confining stress of 77.5 kPa is obtained on a

logarithmic abscissa from the Figure 5.8(a). Moreover, the stress state of node 1800 experienced a liquefaction flow slide in 1985. Hence, within the constraints, it can be concluded that the fresh deposits have a potential for flow liquefaction.

Progression of liquefaction from one node to another leads to a retrogressive flow slide. The stress state of node 616 happens to be in a critical state because of its proximity to the CS. Certain other mechanisms could trigger flow liquefaction at node 616 and progressive softening of the other nodes would be followed because of their liquefaction susceptibility. If node 616 is triggered to collapse leading to flow liquefaction, the progression of liquefaction does not cease until a dilative stress state is encountered beyond node 1800.

Figure 4.11 was derived from the consideration that the shear wave velocity is a function of void ratio and effective confining stress. It was also discussed in Chapter 4 that flow liquefaction could occur in loose, fresh and uncemented sands. Laboratory prepared samples are very fresh samples. The sand deposits at the delta front of the FRD are also relatively fresh deposits. Hence, the framework (Figure 4.11) is very powerful in establishing the characteristics of in-situ state of fresh deposits of the FRD. However, certain corrections due to ageing may be necessary while using Figure 4.11 for the evaluation of aged sands.

5.3.4 Characteristics of the Sediments in the Slope

The liquefaction characteristics of the sediments in the upper 36 m can be estimated using Figure 4.11 and the shear wave velocity profile (Figure 4.15). Figure 5.9 presents the evaluation of the state of sediments in the upper 36 m. The mean confining stress for the deposits is estimated as $\sigma_1'(1+2*K_O)/3$, where K_O is 0.43. The state appears to follow a steep line indicating the influence of K_O. Also shown in Figure 5.9 is the isotropic

consolidation states (ICS) from laboratory testing on very loose samples. During the ICS, the samples have moderate consolidation. Along the K_O consolidation line, the shear stresses induce additional consolidation and cause densification of the soil. In sandy slopes, rotation of principal stresses results in further densification. Hence, the state of the recently deposited sands in the FRD follows the steep line in Figure 5.9.

The void ratios of the upper 36 m of sediments are compared to the ASTM derived e_{max} and e_{min} in Figure 5.9. The in situ state has higher void ratios than e_{max} indicating the relative density of soil in the delta is less than 0% at shallow depths, and is about 5% at 36 m depth. This infers that undisturbed soils can exist with a relative density of less than 0%. ASTM values should only be used as guides rather than taken to be absolute limits.

5.4 Summary

An incremental linear elastic drained stress analysis has been carried out using a finite element program SIGMA/W, simulating the building of the slope in the FRD. The stress state appears to follow the Ko - line and builds up shear stresses in the slope. The characterization of the state of stress has been carried out using a chart (Figure 4.11), developed from laboratory tests. The stress state falls on the contractive side of the chart. The estimation of in situ state of the sand deposits shows that the deposits have void ratios comparable to those obtained from moist tamping techniques. Samples prepared by the water pluviation technique are on the dilative side and may not represent the state of the recently deposited sediments in the FRD. The in-situ shear stress state has been compared with the steady state strength. It is observed that the stress state of the fresh deposits in the FRD has a potential for flow liquefaction. The point of maximum shear stress (node 616) is a critical point in initiating flow liquefaction because its magnitude is close to the CS.

The relative density of the fresh deposits in the Delta is less than 10%. It is concluded that sedimentation in the Fraser River Delta may not initiate flow liquefaction failure. However, it builds up the state of stresses in the soil close to the collapse boundary. Other mechanisms are necessary to bring the state of the soil on to the collapse surface and the collapse state boundary surface. Evaluations of the other mechanisms are discussed in the following chapters.

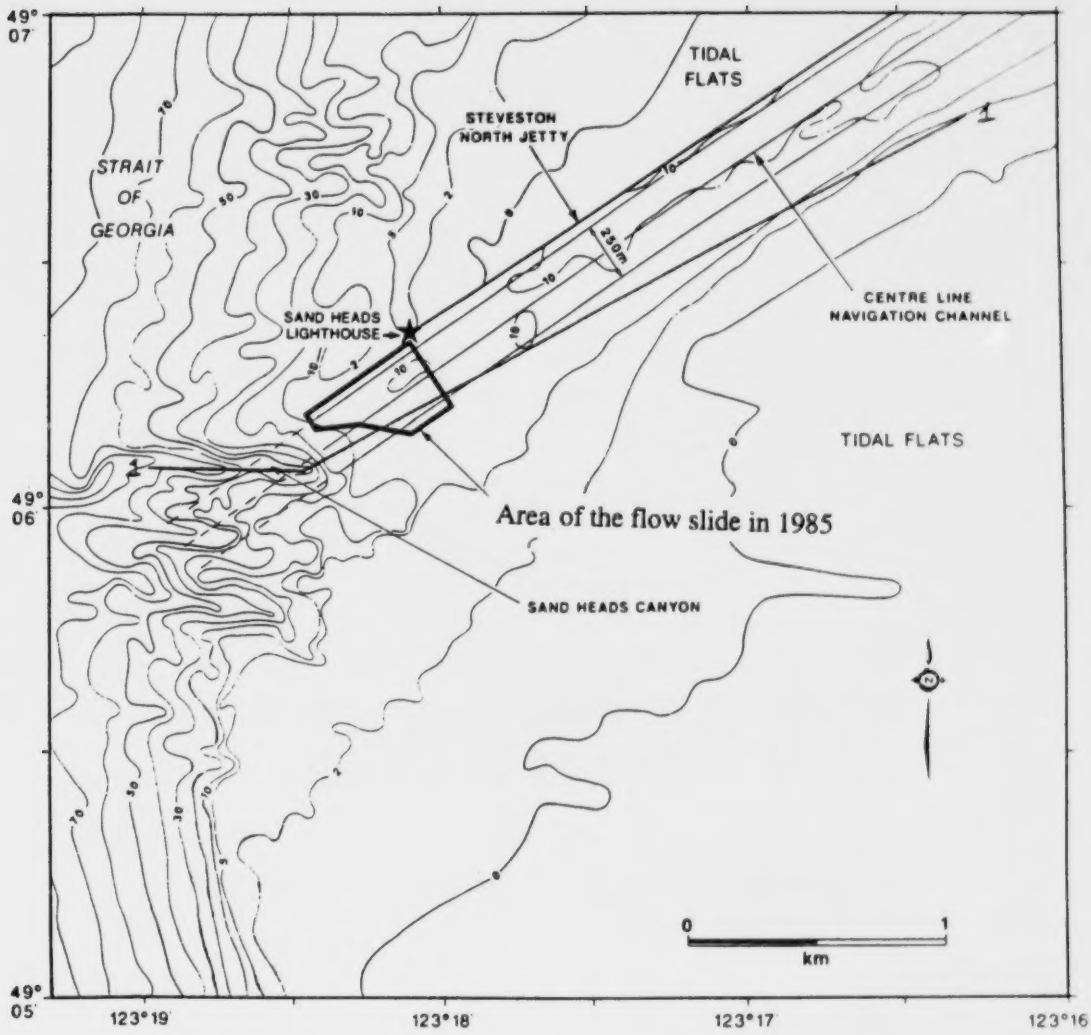

Figure 5.1. Areal extent of the flow slide in 1985 (after McKenna and Luternauer, 1987)

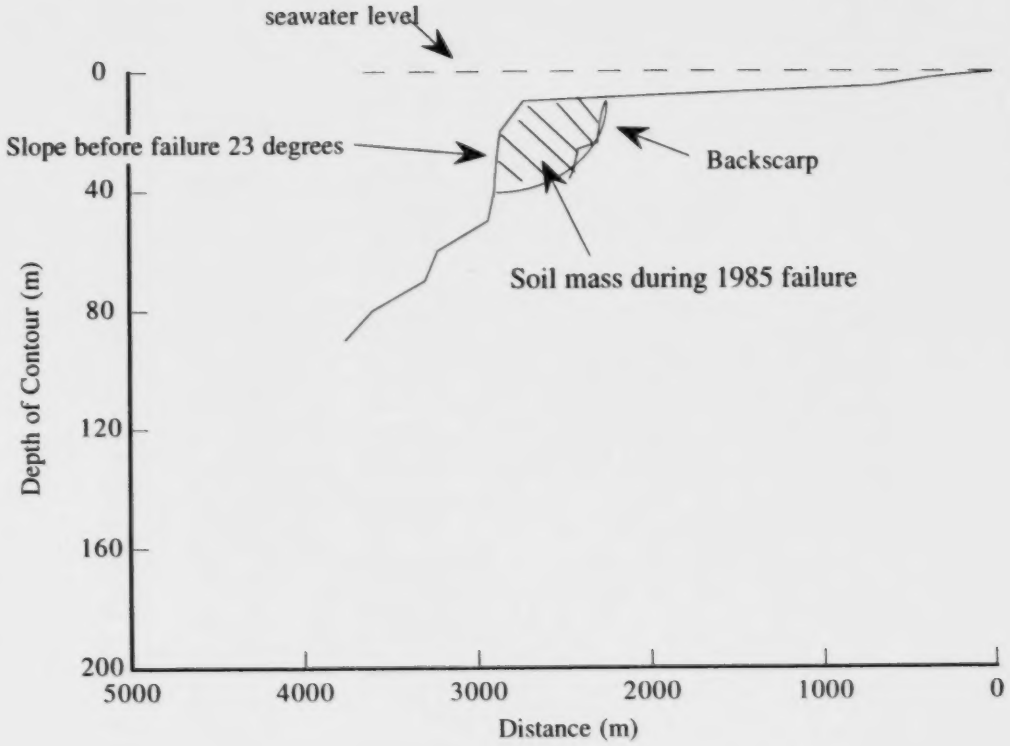

Figure 5.2. Slope along section 1-1

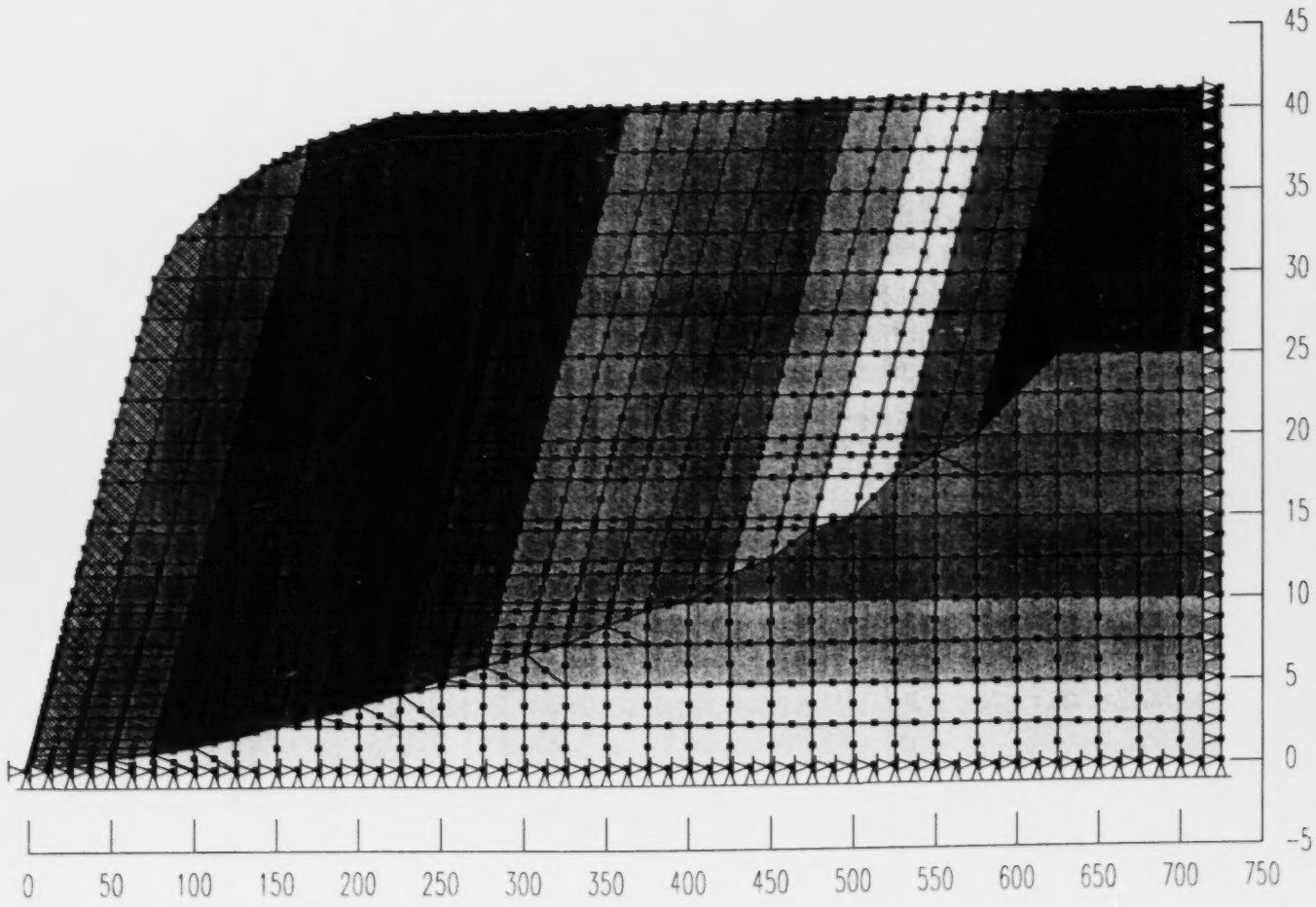

Figure 5.3. Finite element mesh (vertical exaggeration 10)

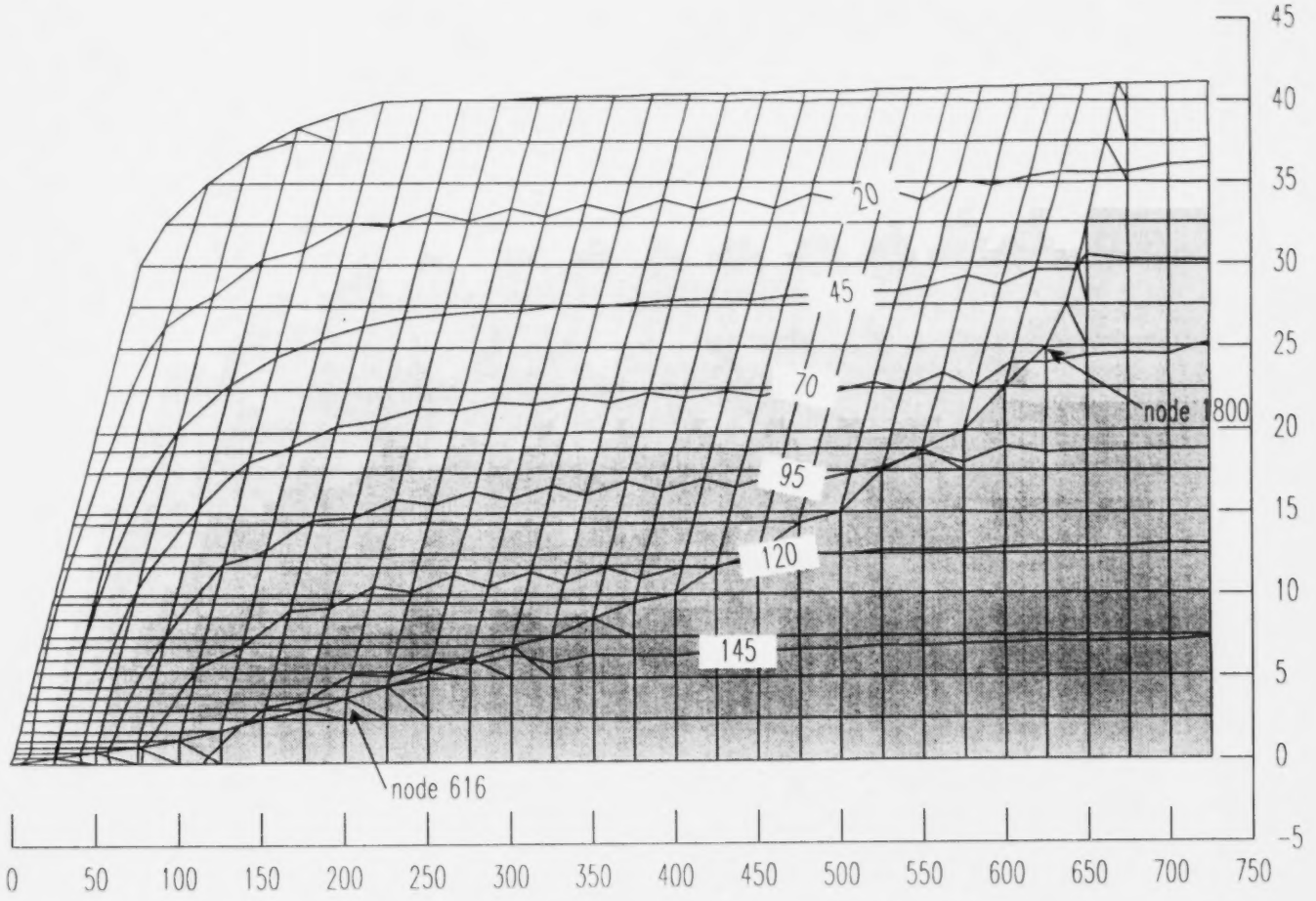

Figure 5.4(a). Contours of the effective X - stress state of elements

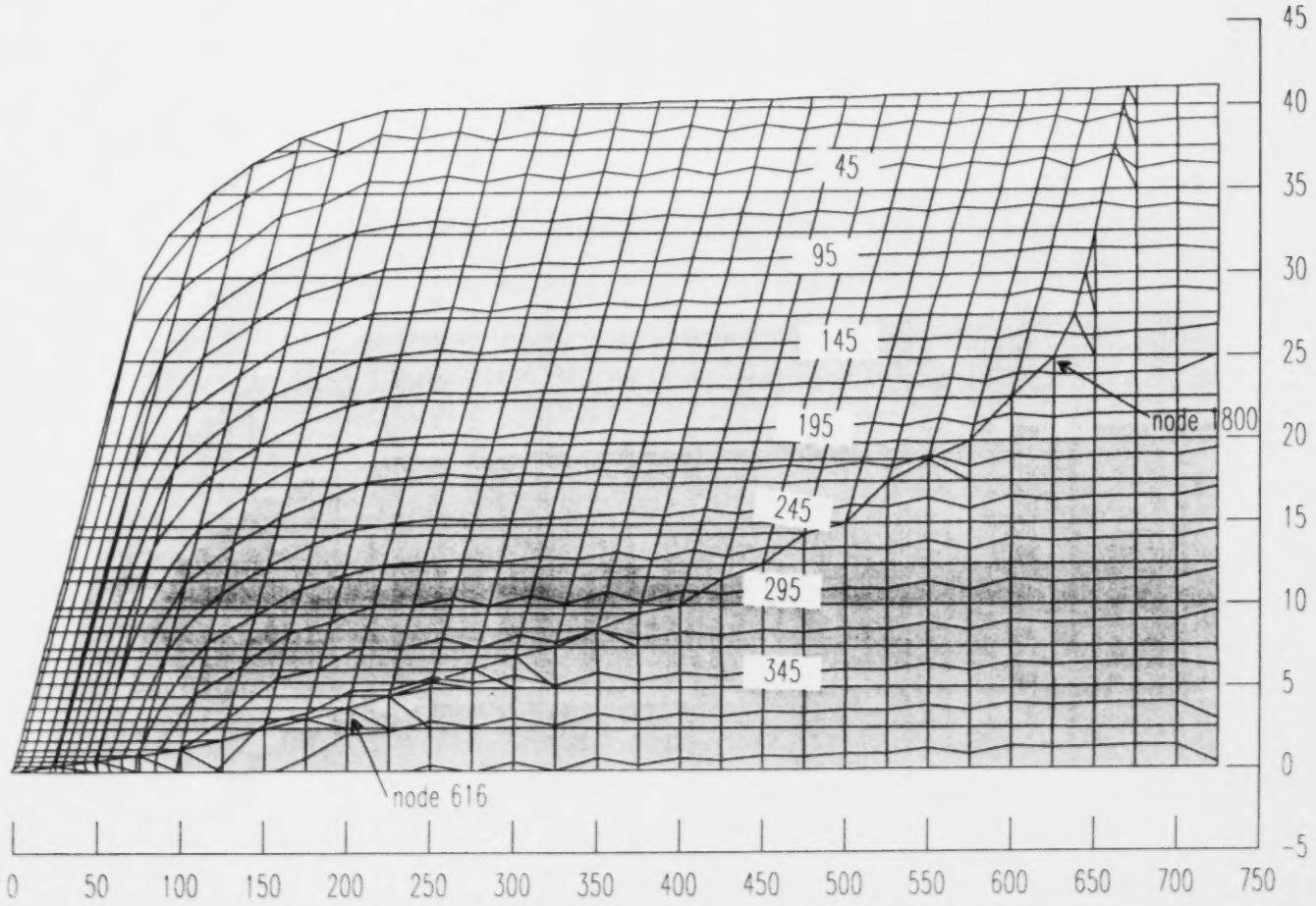

Figure 5.4(b). Contours of the effective Y - stress state of elements

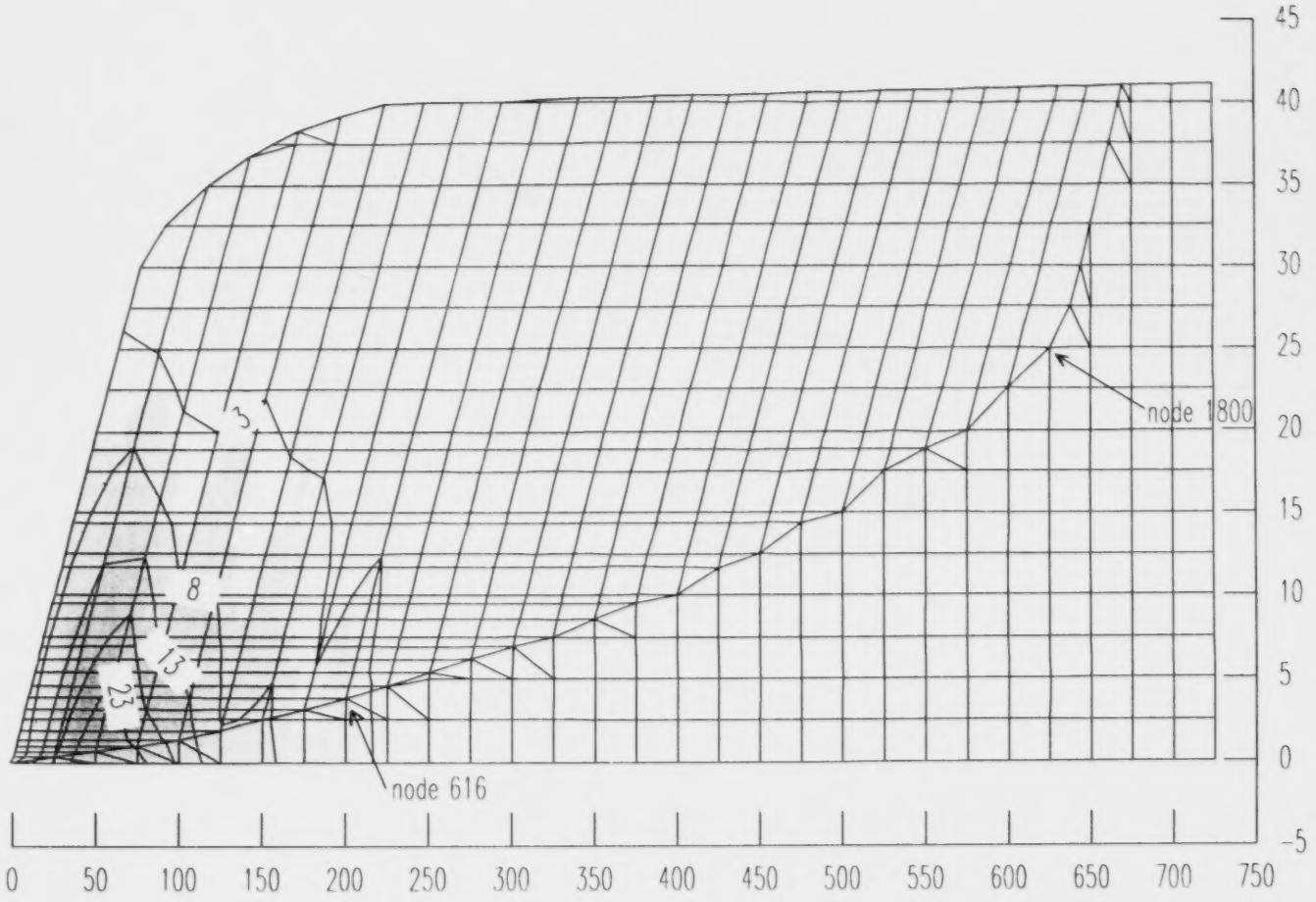

Figure 5.4(c). Contours of the effective X-Y stress state of elements

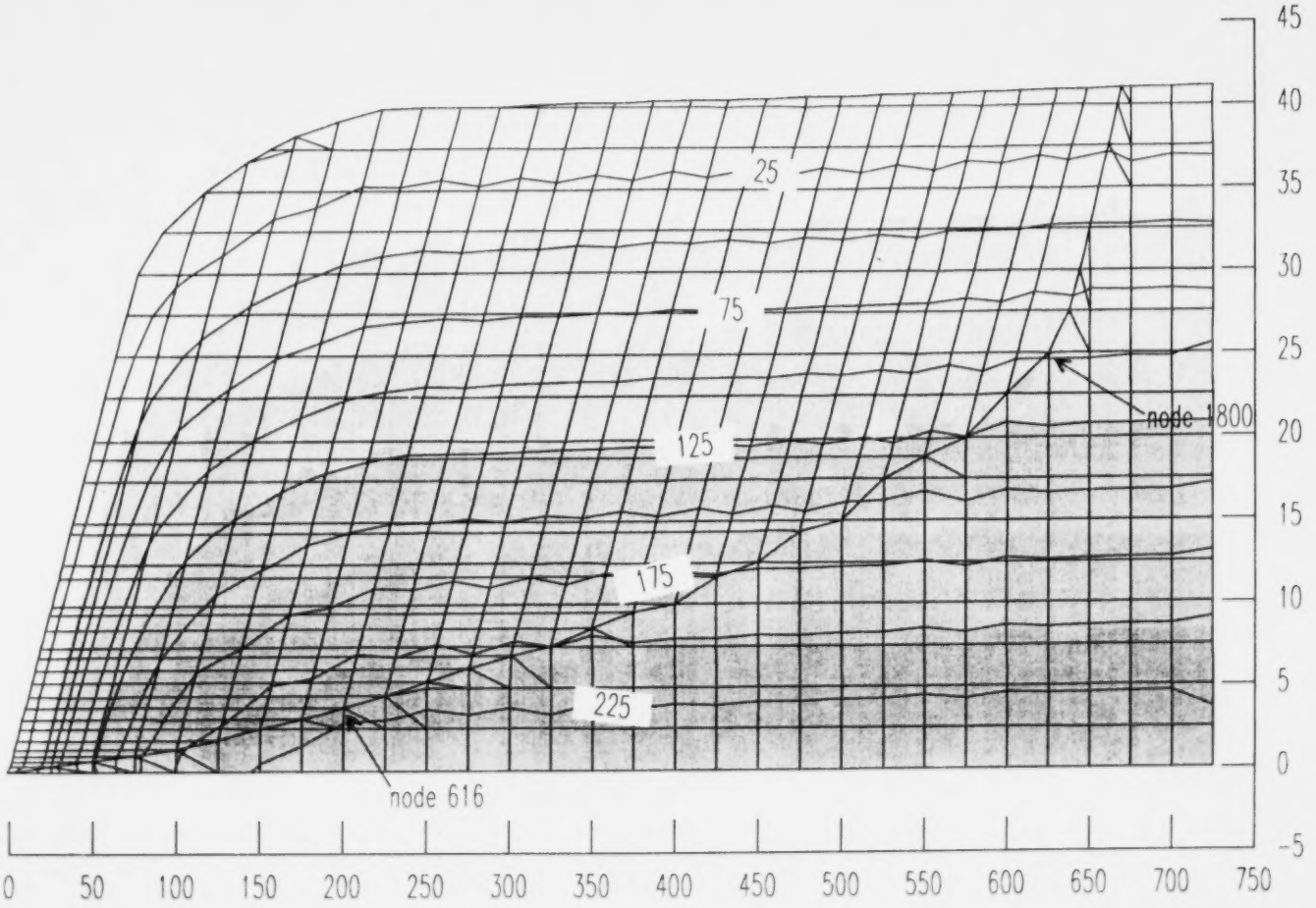

Figure 5.4(d). Contours of mean confining stress (p') state of elements

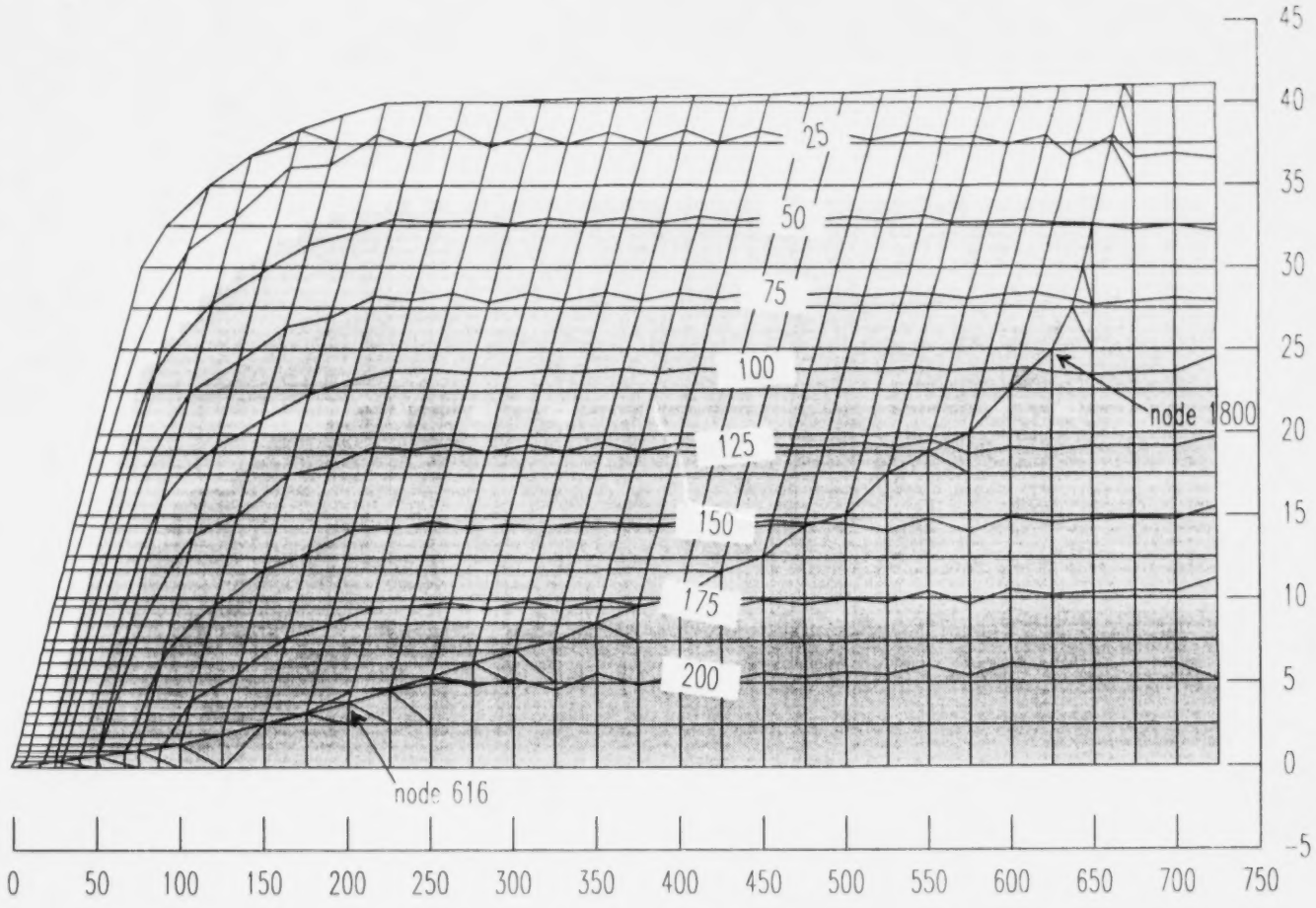

Figure 5.4(e). Contours of deviatoric stress (q) state of elements

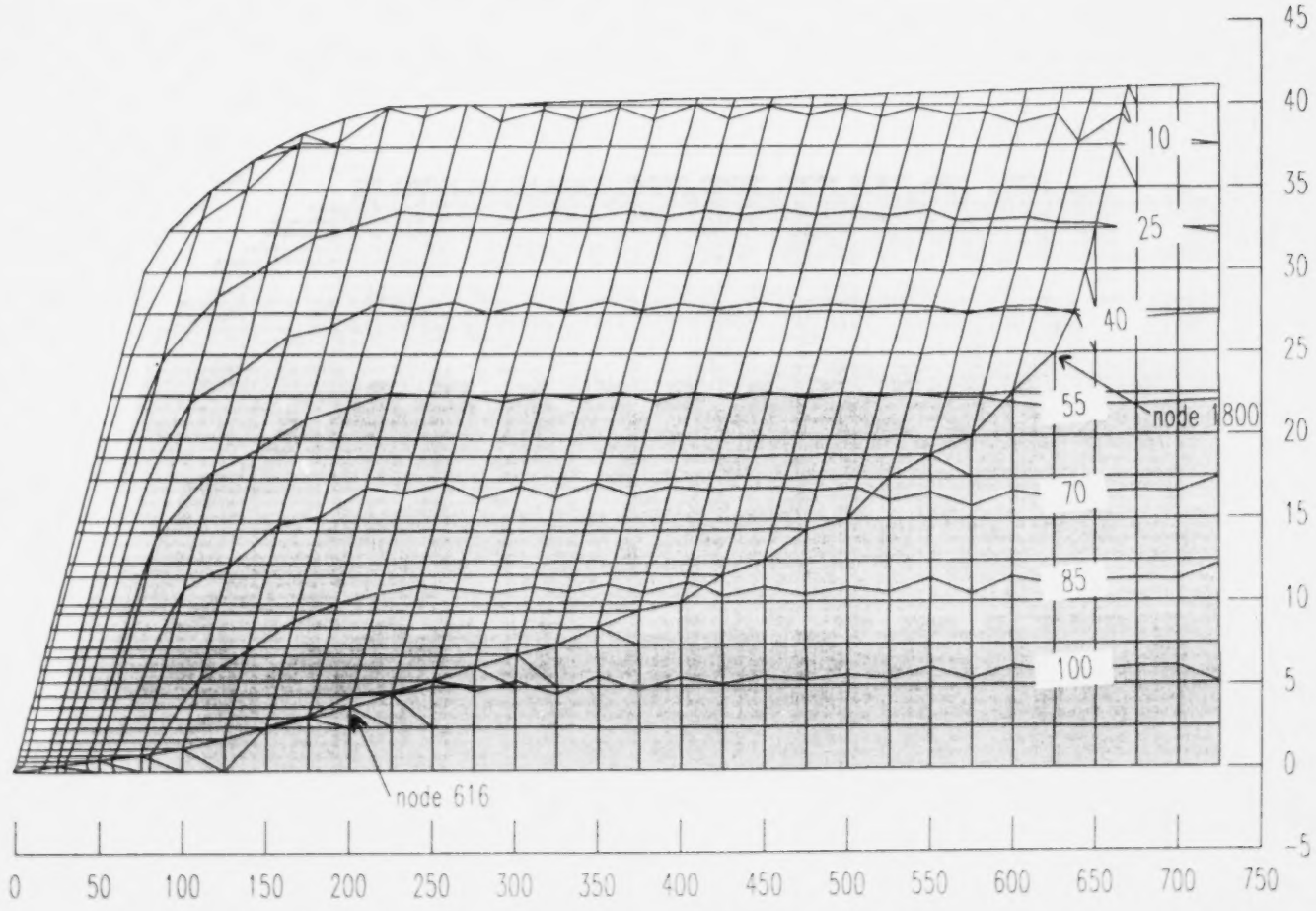

Figure 5.4(f). Contours of maximum shear stress state of elements

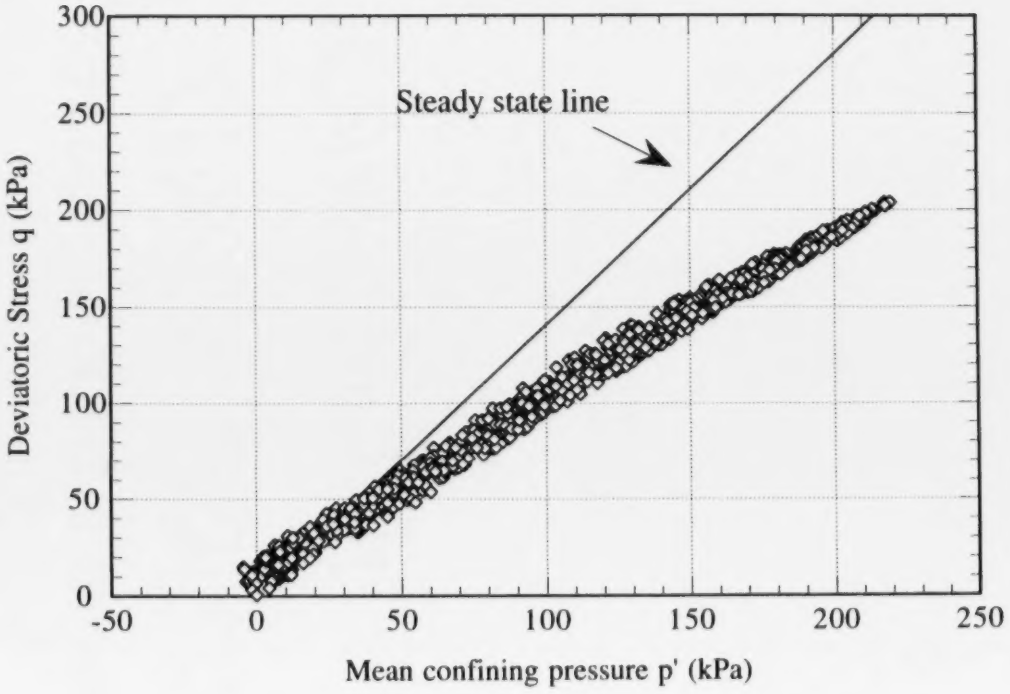

Fig. 5.5. Effective stress state of elements in the slope

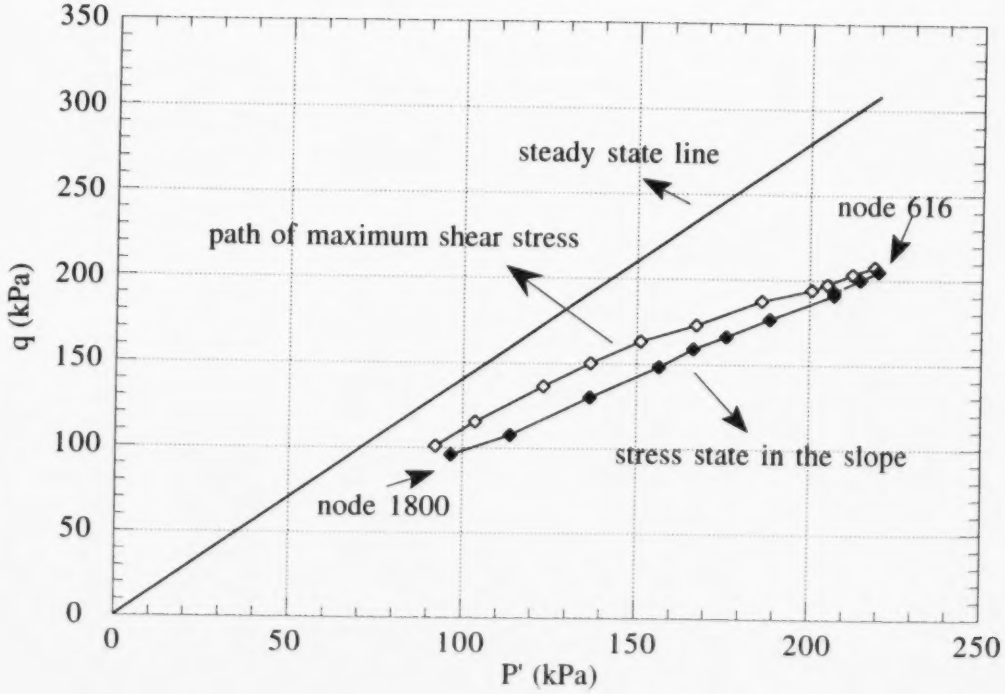

Figure 5.6. Path of maximum shear stress due to sedimentation

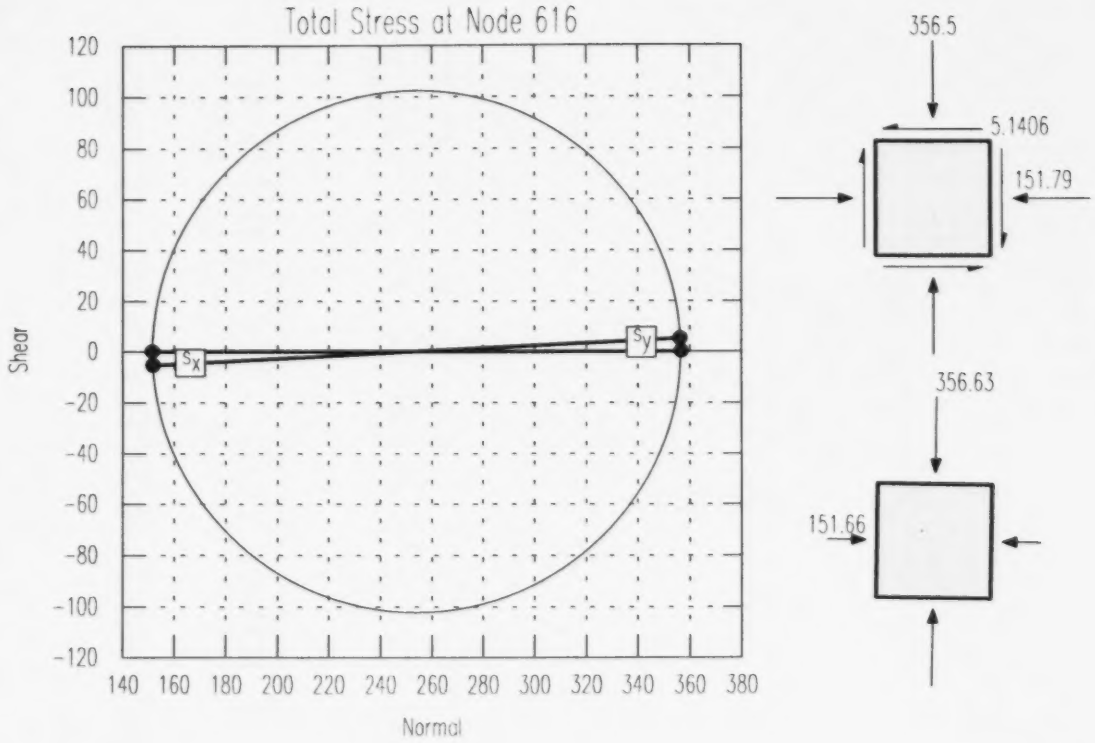

Figure 5.7. Stress state of the node 616

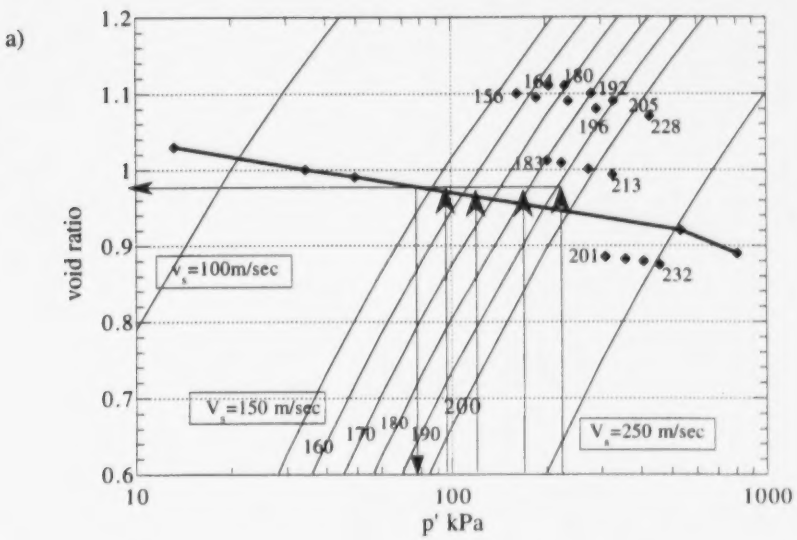

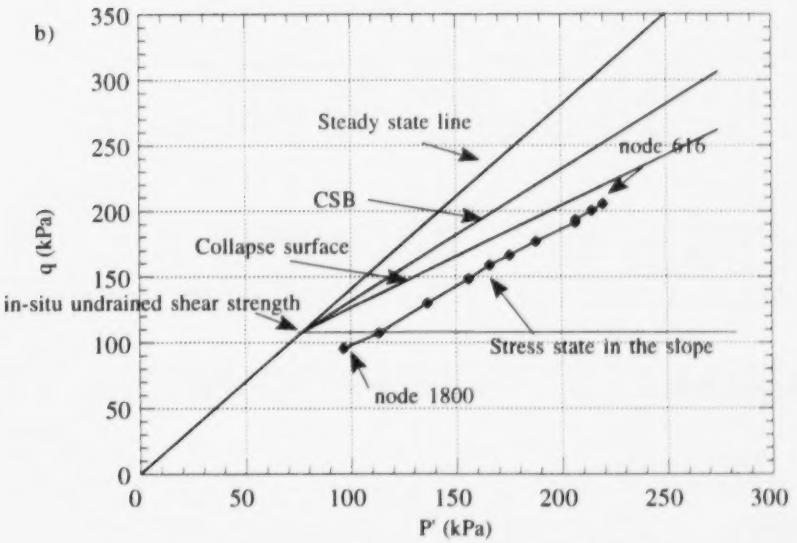

Figure 5.8 Characterization of the stress state in the fresh deposits of the FRD (SIGMA/W)

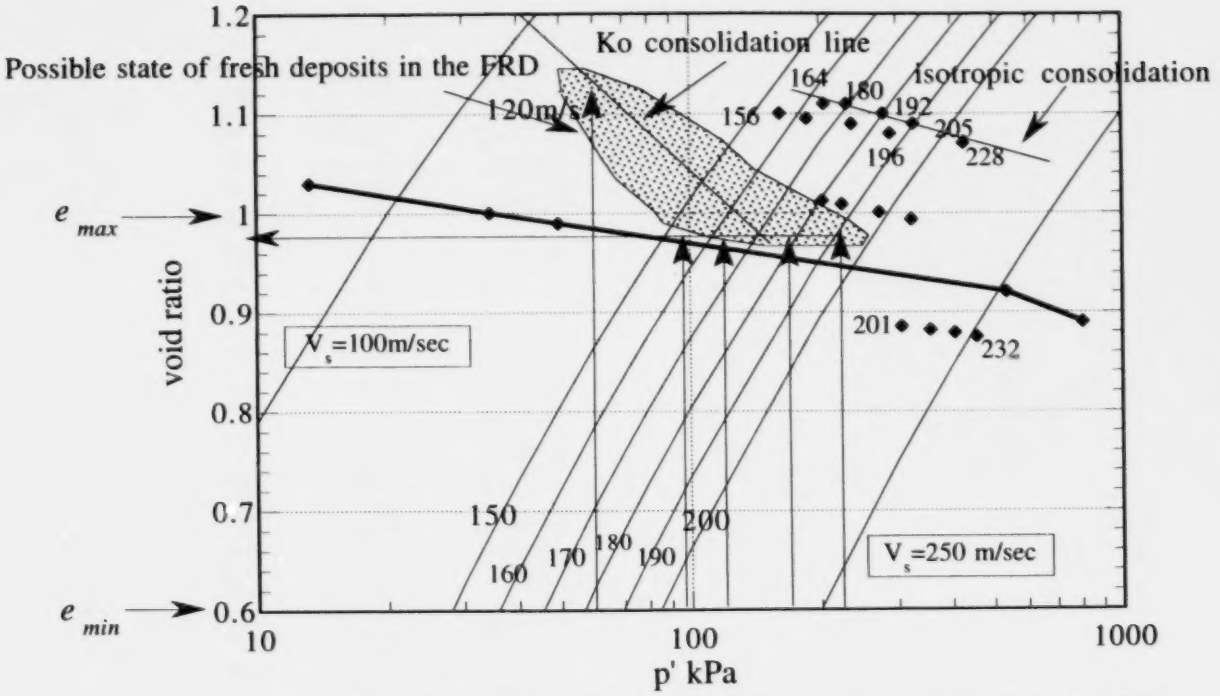

Figure 5.9. Evaluation of the stress state of fresh deposits in the FRD

6.0 Evaluation of Surface Wave Effects

6.1 Introduction

Surface gravity waves in the marine environment are well recognized in causing seabed instability. During Hurricane 'Camille' in 1969, surface waves triggered mudslides in the Gulf of Mexico. These slides applied lateral forces to two offshore platforms causing structural damage (Bea et al., 1983). Storm wave induced liquefaction of sands was thought to have resulted in the floatation of a pipeline in Lake Ontario (Christian et al, 1974). Surface waves are believed to be one of the potential triggering mechanisms of liquefaction flow slides in the FRD (McKenna et al., 1992). Ever since the observation of seabed failure, much attention has been drawn towards the evaluation of surface wave effects in causing liquefaction of sands and seabed instability. This chapter discusses previous research studies into the influence of surface waves on the stability of marine deposits. It also presents the results of in-situ measurement of wave induced porewater pressures using pore pressure probes near Sand Heads. The evaluation of wave effects on the liquefaction-induced instability of the sand deposits in the FRD will also be presented.

6.2 Wave-induced Bottom Pressures on the Ocean Floor

The interaction of ocean surface waves with the seafloor has been studied under simplified assumptions. The wave loading is assumed to be a series of harmonic waves, creating dynamic pressure waves on the ocean floor, increasing the pressure under the crest and reducing it under the trough. A wave form of sinusoidal variation is illustrated in Figure. 6.1.

The dynamic pressure, p, for the harmonic component of a wave using Airy's linear wave theory, is

$$p = p_o \cos (kx - \omega t) \qquad (6.1)$$

where k = wave number $(2 \pi / L)$, L = wave length, ω = circular frequency $(2 \pi / T)$, T = Time period of the wave

The wave length, L, is given by

$$L = \frac{gT^2}{2 \pi \tanh kd} \qquad (6.2)$$

The amplitude of the pressure wave p_o is given by

$$p_o = \frac{\gamma_w H}{2 \cosh kd} \qquad (6.3)$$

in which, γ_w = unit weight of sea-water, H = wave height and d = depth of still water. The bottom pressure is based on the assumptions that the amplitude of the wave is small relative to the water depth and that the seafloor is rigid and impermeable.

The effects of a deformable sea floor for the dynamic pressure amplitudes have been analyzed by Mallard and Darlymple (1977) and the analysis indicated that the pressures on a deformable impermeable seafloor are higher than those on a rigid base. The increase may be significant for very soft cohesive sediments (increases up to 15%), but may be ignored for most sands (Finn et al., 1983). Measurements on laboratory wave tank studies have generally confirmed that the linear wave theory predicts the bottom pressures adequately (Demars and Vanover, 1985).

Simple charts for evaluating the wave length, L, for different wave periods and water depths and the corresponding values of the pressures, p_o, were developed by Weigel (1964) and Seed and Rahman (1978), respectively and are illustrated in Figures 6.2 and 6.3.

6.2.1 Wave induced Stresses within the Seabed

If the seabed deposit is assumed to consist of a homogeneous elastic material extending to an infinite depth, the stresses can be determined for a sinusoidal wave form loading by using Boussinesq's elastic solution for a two dimensional plane strain problem. For the sinusoidal harmonic load on the sea bed as given by equation (6.1), the vertical stress, σ_v, horizontal stress, σ_h, and shear stress, τ_{vh}, at any depth z in the elastic half space are given by Poulos (1988)

$$\sigma_v = p_o (1+ kz) \exp(-kz) \cos (kx - \omega t) \qquad (6.4,a)$$

$$\sigma_h = p_o (1- kz) \exp(-kz) \cos (kx - \omega t) \qquad (6.4,b)$$

$$\tau_{vh} = p_o (kz) \exp(-kz) \sin (kx - \omega t) \qquad (6.4,c)$$

6.3 Wave induced Porewater Pressures

Both transient and residual porewater pressures are generated in seafloor soils for wave loading. The transient fluctuations of the pore pressures are caused by the cyclic normal stresses, when the time for drainage is very small compared to the period of the waves. Residual pore pressures are caused by the cyclic shear stresses associated with the wave loading varying harmonically in space and time.

6.3.1 Transient pore pressures

Several theoretical studies have focused on the generation of transient pore pressures due to surface waves. Models were developed assuming the sand skeleton to be incompressible and hydraulically isotropic and the sea water to be incompressible (Liu, 1973; Putnam, 1949; Sleath, 1970). These assumptions permitted the use of Darcy's law for the flow equation. In these models, the coupling of the sand skeleton and the pore water in resisting the waves is ignored. Consequently, these methods of analysis are called uncoupled analyses of the pore water pressure response. Another type of solution, called coupled solutions, was developed on the basis of Biot's general theory of consolidation (Madsen, 1978; Yamamoto et al., 1978). Biot's theory of behavior of poroelastic solids considers the elastic deformation of the porous medium, the compressibility of the pore fluid and Darcy's law. For an infinite homogeneous seabed, both the uncoupled analyses and the coupled analyses result in the same magnitudes of pore pressures and effective stresses (Finn et al., 1983). For a sandy bottom, the poroelastic theories are well suited for the determination of bottom sediment response (Dawson *et al.*, 1981).

6.3.2 Residual Porewater Pressures

A proper analysis of the effects of cyclic pore pressures on the stability of the seafloor requires consideration of the simultaneous generation and dissipation of the residual pore pressures (Seed and Rahman, 1978). The wave induced cyclic shear stresses may cause cumulative development of residual pore pressures. However, they depend on the intensity and duration of the loading and the drainage characteristics of the seafloor. Seed and Rahman (1978) presented an analysis of the wave -induced generation and dissipation of residual pore pressures in sandy soils.

6.3.3. Distinction Between Transient and Residual Porewater Pressures

When the time for the drainage of pore pressures due to waves exceeds the period of the waves, cumulative development of pore pressures occur, that is, residual pore pressures start building up in the soil. It is important to identify the levels of shear strain required to develop residual pore pressures. Figure 6.4 illustrates results of cyclic loading tests on saturated sands by Stokoe et al. (1987) and shows that the residual pore pressures start building up when the shear strain exceeds about 1 x 10^{-2}%. Stokoe *et al.* (1987) suggested that this value of the shear strain was a threshold shear strain above which a progressive build up of residual pore pressures will occur for cyclic loading conditions on saturated sands. An investigation into the relationship between shear strain and wave loading provides a check on the possible cumulative build-up of pore water pressures.

6.4 Additional Studies on the Effect of Surface Waves on Seabed Instability

Laboratory studies have been carried out in wave tanks to draw comparisons of measured pore pressures with the analytical solutions of transient pore pressures due to surface waves (Chari et al, 1986; Demars and Vanover, 1985; Sleath, 1970; Tsui andd Helfrich, 1983). It appears that the theory can give reasonable predictions of the pore pressures and the effective stresses in sand layers for wave loading.

Field studies have concentrated on the measurement of wave-induced pore pressures (Bennet et al, 1980; Okusa, 1984) and have shown essentially the same findings as those in the laboratory tests. The measured pore pressures have also been used in stability analyses of seabed slopes (Bennet et al, 1980).

Henkel (1970) provided an analytical framework using limit equilibrium considerations to assess the stability of the seafloor under wave loading for an assumed circular slip surface and for undrained conditions. Finn et al. (1983) presented a stability analysis of seabed deposits on the basis of the effective stress principle incorporating transient and residual pore pressures on an assumed failure surface.

6.5 Wave-induced Liquefaction Studies

Wave-induced liquefaction of loose saturated sands has also been the focus of several studies where liquefaction has been identified as the state of zero effective stress (Seed and Rahman, 1978; Zen and Yamazaki, 1990). Two simplified approaches were developed to evaluate the possibility of wave-induced liquefaction of granular seabed deposits. One approach makes use of the Standard Penetration Test (SPT) data (Nataraja and Gill, 1983) and the other uses the relative density of the sand to evaluate liquefaction resistance (Ishihara and Yamazaki, 1984). Both methods are similar in principle and compare wave-induced shear stresses with the values required to cause liquefaction.

6.6 Measurement of Wave-induced Pore Pressures in the FRD

6.6.1 Design of Probes

Two identical probes for measuring in-situ pore pressures for surface waves were designed and constructed by Adara Systems Ltd., Vancouver. The two probes were installed in the Fraser River Delta front by ConeTec Investigations Ltd., Vancouver with cables connected to a data acquisition system placed in the nearby Sand Heads Lighthouse. The installation work was supervised by the Geological Survey of Canada. The probes were designed to measure mudline water pressures and pore water pressures at a depth of about 2 m A

sketch of the probes is provided in Figure 6.5. For measuring the pressures, each probe was equipped with two pore pressure transducers - one at the top of the probe operating at the mudline and the other at the tip of the probe, which was about 2 m below the mudline. Each probe had a large 30 cm x 30 cm square steel plate at the top to prevent settlement of the probe into the sediment. Each pressure transducer had a calibrated range of 0-413 kPa absolute giving a system resolution of about 0.1 kPa. The signal conditioning electronics were incorporated into an anodized aluminum cylinder on top of the settlement plate. This cylinder also housed the mudline pressure transducer. A protective plate was added above the settlement plate to protect the signal conditioning electronics and its associated cables. A 3 mm diameter pipe was attached along the side of the each probe for jetting water under pressure to assist during the installation of the probe. The jetting system was operated by divers and was powered by a pressure pump located at the surface. A coupling attachment was made on the top of the protective plate for disconnecting the pressure hose to the jetting pipe. Each probe weighed about 100 kg to offer enough rigidity for installation. Lifting rings were provided at the top of the protective plate to attach lifting cables for installation and retrieval. The connecting cables were run along the seabed to the data acquisition system.

6.6.2 Data Acquisition

The data acquisition system consisted of an interface unit, a IBM PC compatible computer and a data translation card with 12 bit resolution. This system was designed such that it would acquire data from the probes at a fixed rate when the mudline pressure exceeded a user entered trigger threshold. This data would be saved in a data file on the hard disk of the computer. The data acquisition would continue at the specified rate for a given period of time. The data file would then be closed and the computer would enter a post trigger phase. This feature was added to prevent the hard disk capacity from being exceeded.

Each time a data file was opened or closed the item would be recorded in a log file giving the time and type of operation. Statistical information such as peak mudline and differential pore pressures would be recorded in this file to help to identify significant pore pressure events. Once identified, a system user could more closely check the file for useful information.

6.6.3 Probe Installation

The probes were labeled as No.1 and No.2. Probe No.1 was installed in a water depth of about 10 m at a distance of 400 m from the Sand Heads Lighthouse on 7 December 1992. The location of the probe was close to the northern margin of the ship navigation channel as shown in Figure 6.6. Installation was carried out by jetting water under pressure through the pipe attached along the length of the probe. Lateral forces from underwater currents made the installation of the probe difficult. Verticality of the probe could not be maintained which resulted in a slight inclination of the probe in the seabed. Bad weather added further complications when connecting the cable from the probe to the data acquisition system. The probe was connected to the data acquisition system on 12 December 1992. The data system was set to trigger datalog when either transducer recorded 12 m of water. The sampling rate was set at 20 Hz for a duration of 1 minute.

Installation of probe No. 2 was delayed due to poor weather conditions and was completed on 29 January 1993. It was deployed in about 9 m of water and 18 m from the Sand Heads Lighthouse as shown in Figure 6.6. The data system for probe No.2 was set to trigger when either transducer recorded a pressure of 11 m of water. The sampling rate was set at 20 Hz for a duration of 2 minutes.

6.6.4 Results from the Pore Pressure Probe Study

Three events were recorded by probe No.1 between 3:55 p.m to 4:17 p.m. on 12 December 1992. Predicted tides at the Sand Heads indicated that there would be an increase of tide levels between 1:30 p.m. to 6:00 p.m. on 12 December 1992. No other events were recorded by the probe. A diver was sent to retrieve the probe and observed that the probe had been displaced and that the cable was heading in a direction approximately 90 degrees to the south of where it had been placed. The cable was completely buried under sediments and the probe could not be retrieved. A bathymetric survey showed no significant changes in the contours on the same scale of the 1985 movement. However, there was evidence of a depression in the seafloor. Turbidity current meters placed inside the sea valley (debris flow canyon) detected a gravity flow during the same time period (Barrie, pers. Comm., 1993). It appears that a shallow slide may have occurred and carried the probe into deeper water.

The data recorded by probe No.1 at 4:17 p.m.on 12 December 1992 are shown in Figure 6.7 (a,b). The signal from the mudline transducer at the top of the probe appears to contain a large amount of noise. The cause of this noise is unclear. However, there appears to be a difference of approximately 1.5 m of water pressure between the mudline and tip pressures, indicating that the tip of the probe was at a depth of 1.5 m below mudline.

The data recorded by probe No.2 at 3:49 a.m. and 9:07 a.m. on 19 February 1993 are shown in Figure 6.8 (a,.b). The records also show a differential pore pressure between the transducers of about 1.5 m. The recording of the pressures at the mudline appears to be approximately sinusoidal over a time period of each wave. For both events no significant excess pore pressures were recorded by the tip pressure transducer indicating that at the

burial depth of 1.5 m, wave-induced pressure fluctuations were filtered out or attenuated. The pressure data do indicate close tracking of tidal variation suggesting that the surficial sediments were free draining.

6.7 Wave Effects on the Seabed Instability at the FRD

McKenna et al. (1992) speculate that the surface waves contributed to the triggering of the liquefaction induced flow slide that occurred between 27 June 1985 and 11 July 1985. To study the wave effects in causing the flow slide, the magnitude of wave heights and wave periods are required in the analysis. Hindcasting methods were used for predicting the wave history at the site using Bretschneider's theory (Shore Protection Manual, 1984). The theory requires wind speed and fetch at the site for predicting signficant wave heights (average of the highest one-third). Figure 6.9 presents the predicted significant wave heights (SWH) from the wind data supplied by the Atmospheric Environment Service, Canada. A maximum SWH of 2.7 m with a period of 5.32 sec is calculated, which coincides with the value suggested by Thomson (1981).

The waves affect the foreslope of the Delta either by transient pore pressures or by residual pore pressures. However, a comparison between the shear strain associated with the maximum SWH and the threshold shear strain provides a check on the possible cumulative build up of residual pore pressures.

6.7.1. Verification of Threshold Shear strain

Using the relationships in Equations 6.2 and 6.3, the wave length, L, for the maximum SWH of 2.7 m and the amplitude of the wave pressure near mudline are determined as

40 m and 5.5 m respectively. Hardin and Drnevich (1972) suggested a relation between cyclic shear strain and cyclic shear modulus as follows;

$$\frac{G}{G_o} = \frac{1}{(1+ \gamma_a / \gamma_r)} \qquad (6.5)$$

Where γ_a is the shear strain induced for the cyclic loading conditions, γ_r is the reference strain and equals τ_f / G_o (in which τ_f is the shear stress at failure) and G_o is the initial small strain shear modulus. A reference strain of 2.4×10^{-3} was recommended for cohesionless soils (Poulos, 1988). G can be calculated using Equation 6.4,c for the calculated shear stress τ_{vh}.

The small strain shear modulus G_o is related to the shear wave velocity through the basic expression

$$G_o = \rho \ Vs^2 \qquad (6.6)$$

where ρ is the mass density of the soil and V_s is the *in-situ* shear wave velocity. Using these relationships, the calculated maximum shear strain for the 2.7 m wave is only 10^{-4}% and occurs at a depth of about 3 m. Hence, the shear strains induced by 2.7 m wave are not expected to exceed a threshold strain of 10^{-2}%. Therefore, the waves at the Fraser River Delta front were of insufficient amplitude to cause cumulative build up of residual pore pressures at the time of failure in 1985. However, transient pore pressures are created in the soils due to these waves.

6.7.2 Influence of Transient Pore pressures

Transient pore pressures are determined for 2.7 m wave using the coupled solution of Yamamoto et al. (1978) and are presented in Figure 6.10. Pore pressure fluctuations are at a maximum near the mudline and attenuate rapidly with depth. It has been established in Chapter 5 that the in-situ stress state of the near surface fresh deposits are susceptible to liquefaction and in-situ shear stresses of the deposits are greater than their undrained shear strength, indicating that the deposits have a potential for flow liquefaction. From the observed magnitudes of the transient pore pressures, the pressures may be sufficient to trigger shallow undrained instability within the upper 2 to 3 m in the loose sands at the Delta front. However, the pressures do not extend to a sufficient depth to cause deep seated failures.

6.8 Summary

The effect of surface waves in causing deep seated liquefaction flow slides in the FRD has been investigated. The work has been aided by the field measurement of wave-induced pore water pressures. Two probes were designed, constructed and installed to monitor pore pressures at shallow depths due to wave loading. Results from these probes suggest that pore pressure development due to wave loading near the Sand Heads Lighthouse is insignificant. A brief review of the theory related to wave induced pore pressures has confirmed the observations from the probes. Wave induced pore pressures at the Fraser River Delta front are expected to be very small. In very loose cohesionless sediments these pore pressures may be sufficient to trigger shallow instability within the upper 2 to 3 m. However, wave induced pore pressures are unlikely to be a major contributing factor in triggering a large scale deep seated instability.

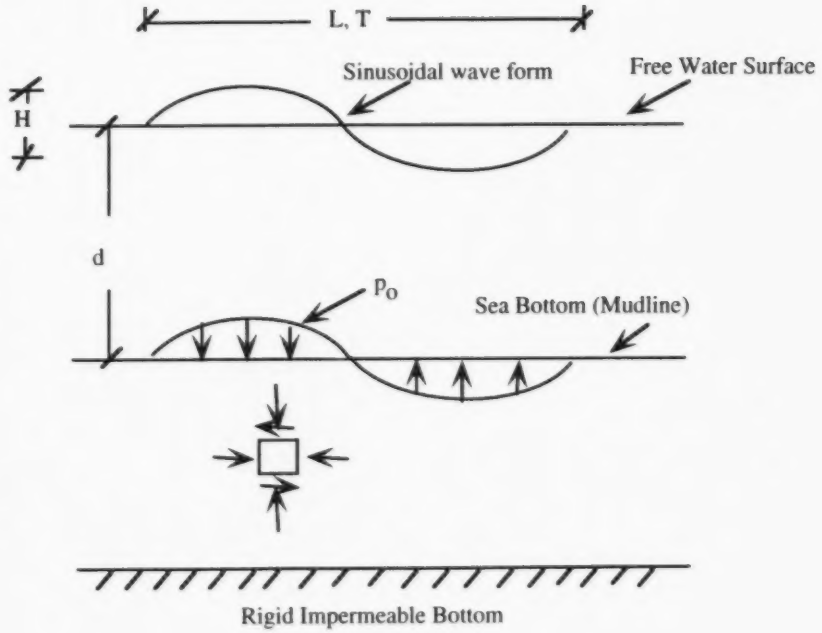

Figure 6.1. Bottom pressures and stress changes from wave loads

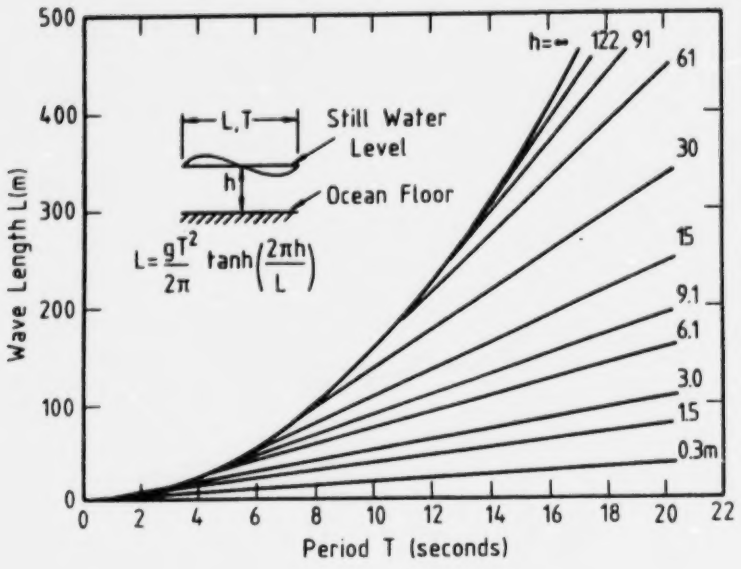

Figure 6.2. The relationship between wave period, wave length and water depth (after Wiegel, 1964)

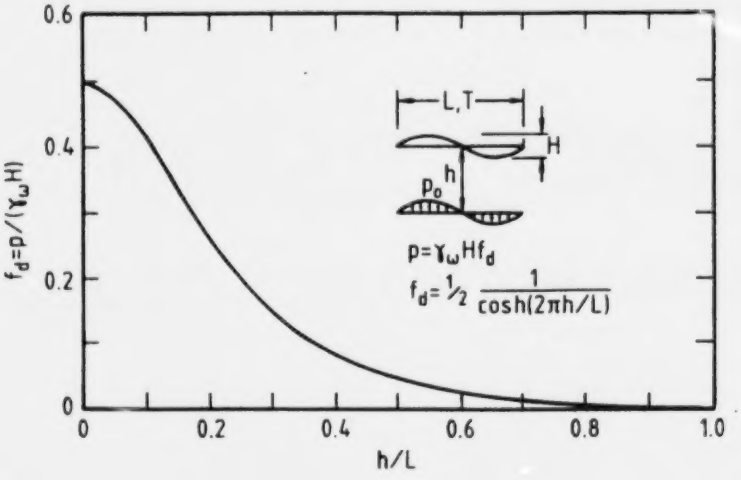

Figure 6.3 The Wave-induced pressure on ocean floor (Seed and Rahman, 1978)

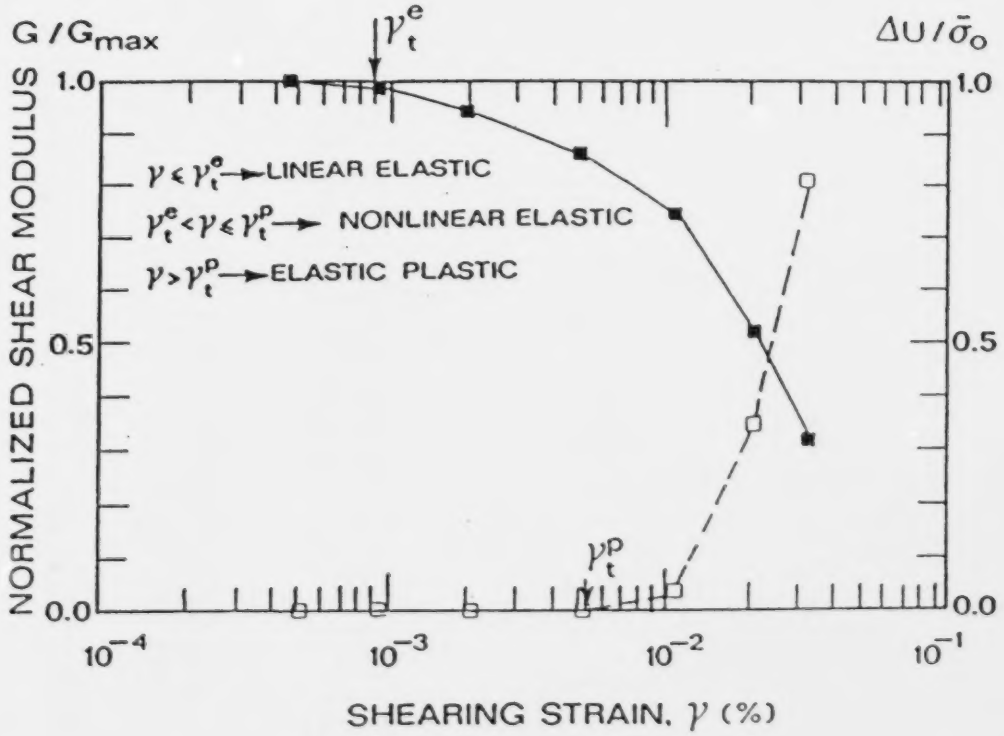

Figure 6.4. Results of cyclic loading tests on saturated sands (Stokoe et al., 1987)

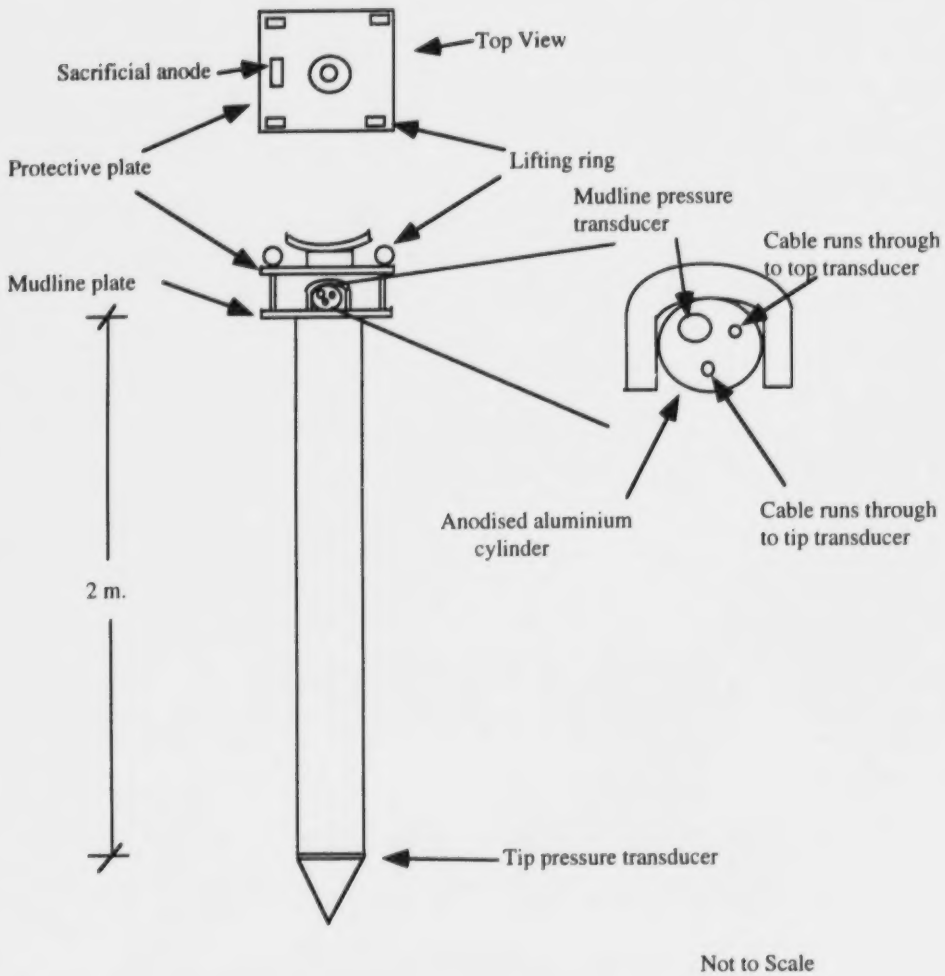

Figure 6.5. Pore pressure probe

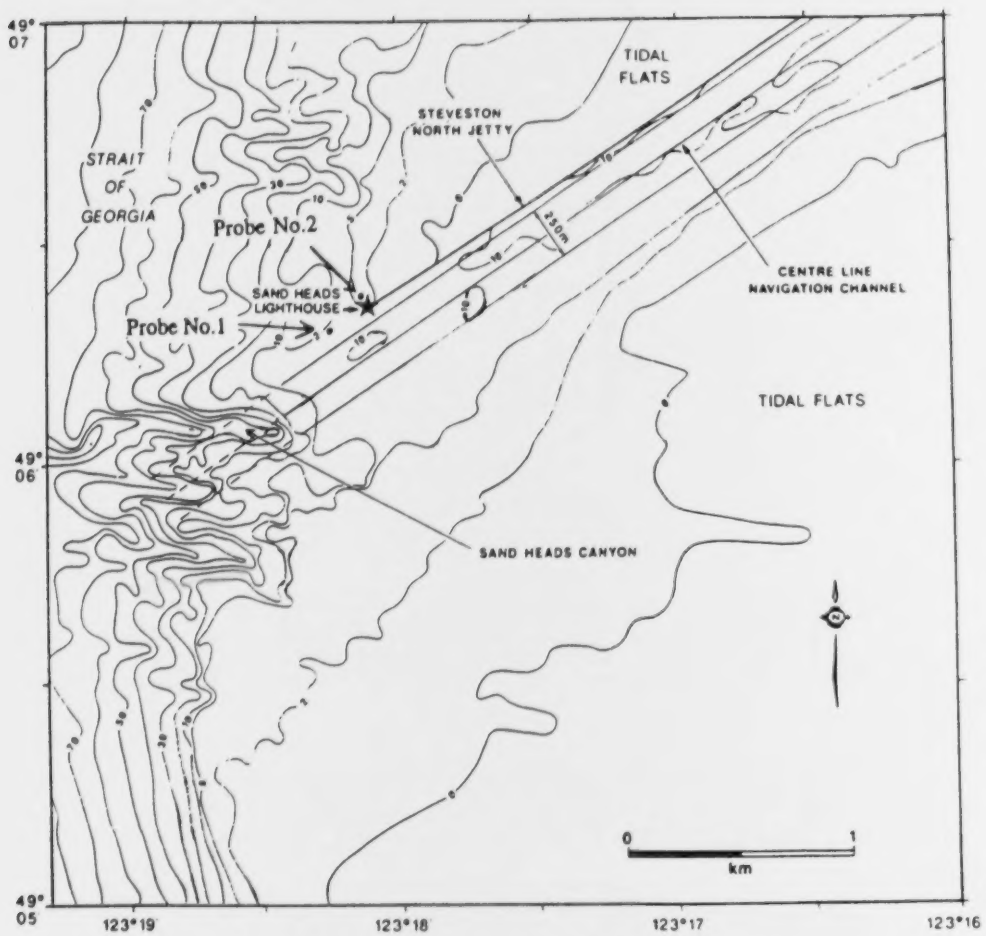

Figure 6.6. Location of probes in the FRD (after McKenna and Luternauer, 1987)

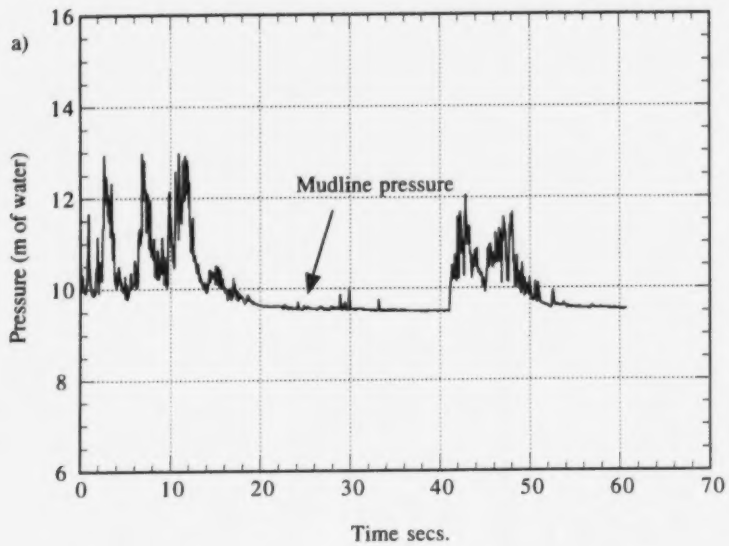

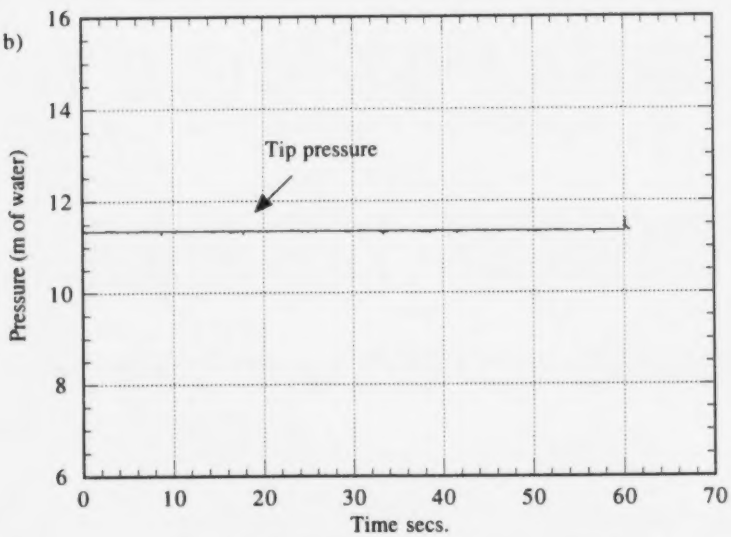

Figure 6.7. Pressures @ 4.17 p.m. - Probe No.1
a) Mudline pressure
b) Tip pressure

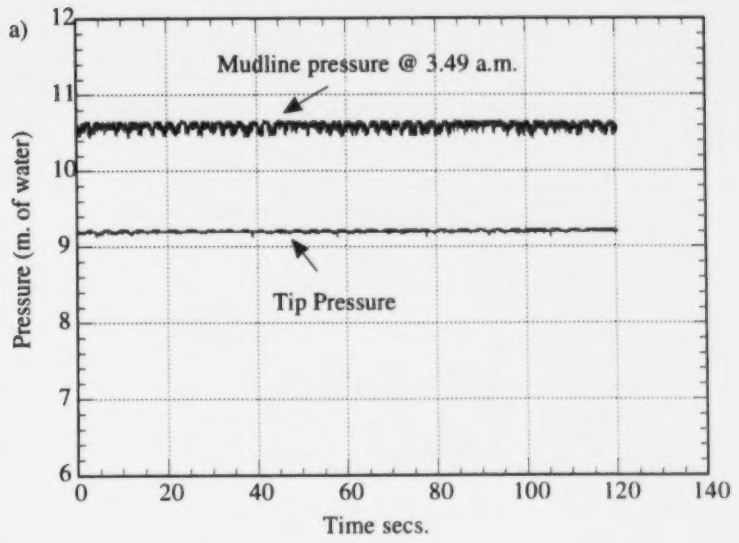

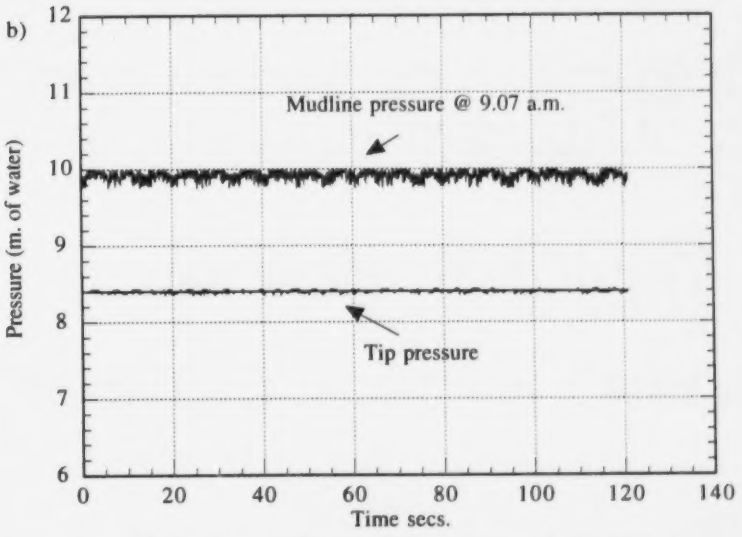

Figure 6.8. Mudline and tip pressures - Probe No.2
a) pressures at 3.49 a.m.
b) pressures at 9.07 a.m.

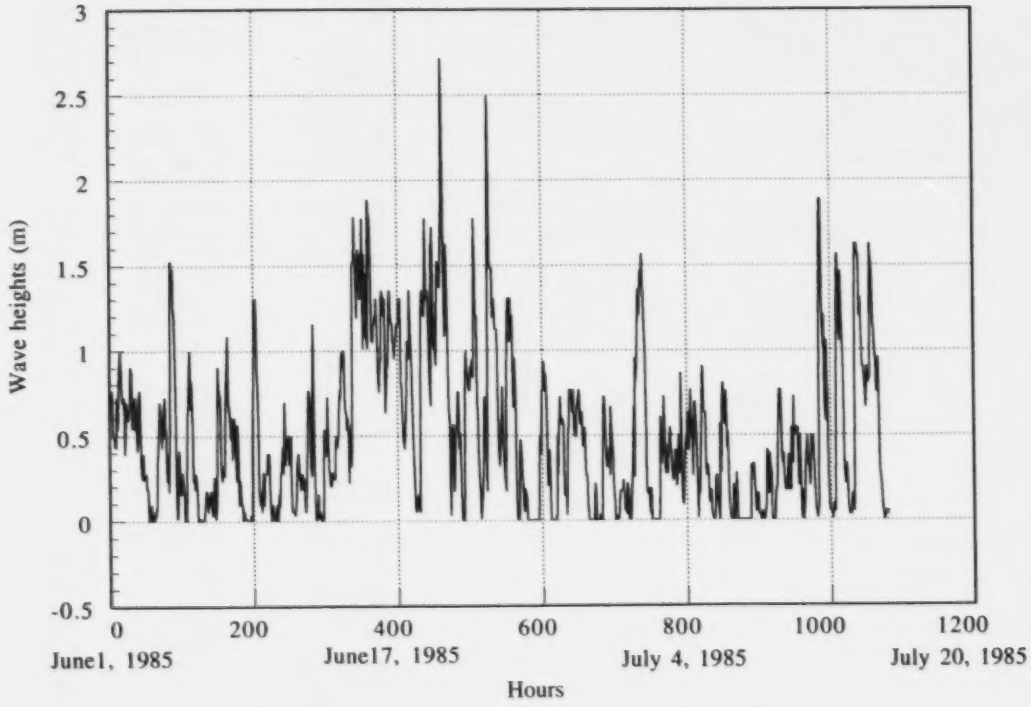

Figure 6.9. Significant wave heights (Bretscneider's theory)

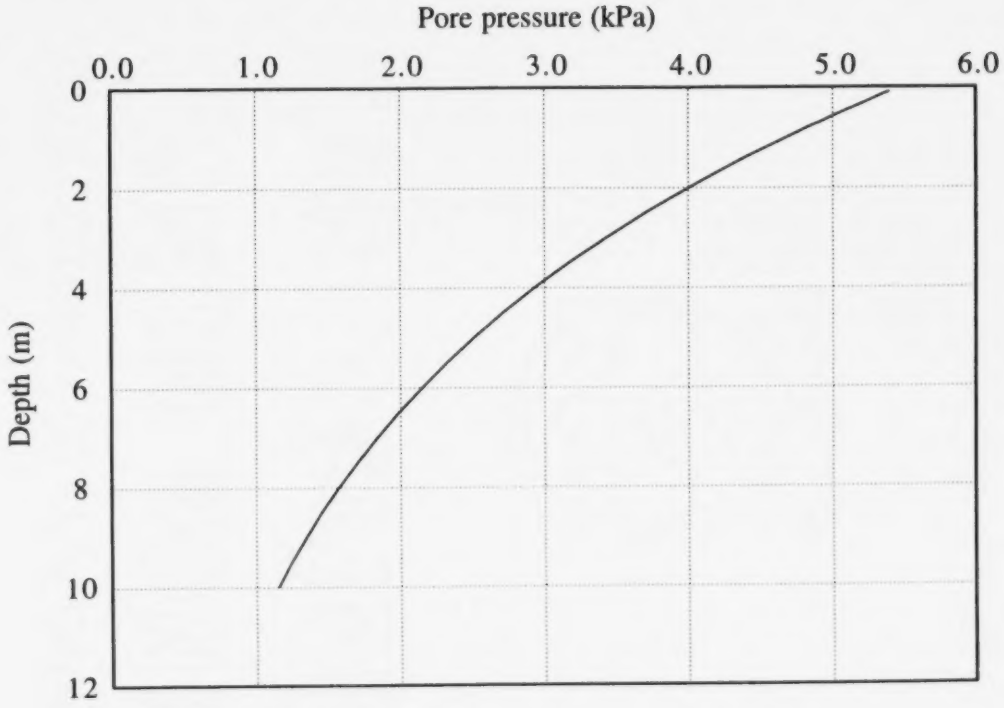

Figure 6.10 Variation of pore pressure due to a wave of 2.7 m and wave length of 40 m

7.0 Evaluation of the Effect of Tides

7.1. Introduction

From a review of statically triggered liquefaction flow slides in the marine environment, it may be observed that almost all the slides occurred during extreme low tide conditions. The flow slides are the consequences of spontaneous liquefaction of sand deposits (Terzaghi, 1956). It was believed that excess pore pressures in low permeability materials during low tides triggered liquefaction flow slides in Kitimat Fjord, Canada in 1975 (Johns et al., 1986). However, the influence of tidal drawdown on the stability of the sand deposits has not been quantified. Koppejan et al. (1948) and Terzaghi (1956) speculated that seepage pressures during low tides were triggering the flow liquefaction in these submarine deposits. However, an explanation for the initiation of flow slides due to the seepage pressures has not been established in the literature. Seepage pressures are created during low tides due to the storage of pore water in the aquifers. Kramer (1988) assumed that flow liquefaction may be triggered in shoreline sand deposits for very small changes in shear stress under undrained conditions during low tides. He also identified that if the sand is in equilibrium initially under shear stresses higher than the steady state strength of the soil, the triggering of flow liquefaction may lead to flow sliding. However, this explanation lacks sufficient evidence since deep deposits will not experience shear stress changes due to tidal drawdown. Hence, the theory does not explain the initiation of flow liquefaction in deep deposits.

Gas generation is a natural phenomenon in river deltas. The presence of methane gas is common in the Mississippi River Delta (MRD). It has been reported that the gas influences the wave induced pore pressures in the MRD (Dunlop et al., 1978). Gas has also been found in the borehole samples of the Fraser River Delta (Christian, 1994; personal

communication). Organic material is deposited along with the river borne clastics in estuaries. Burial of some marine organisms may also occur during deposition. Consequent decay of the organics results in gas generation. Gas generation in occluded form in the pore water desaturates the sediments. It is also known that the effective stress state of sediments is very much influenced by the presence of gas in the sediments. The effect of tidal drawdown on gaseous sediments and its consequences on the liquefaction stability of sediments has never been studied.

This chapter investigates the effect of tidal drawdown on saturated deep sediments and also on the influence of gas in the sediments of the FRD in causing liquefaction induced seabed instability. It also demonstrates that the tidal drawdown constitutes a critical factor in triggering flow liquefaction of gaseous sandy sediments.

7.2. Modelling Tidal Variations for One-Dimensional Flow Conditions

Tides are surface waves with long periods and impose periodic loading on the seabed. When tides propagate over a porous bed, such as a sand bed, water flows into and out of the porous medium. The phenomenon has been studied by several researchers as pore water pressure variations in the ground due to tide changes for a variety of boundary conditions. Many studies have concentrated on the influence of tides on ground water levels in coastal aquifers (Ferris, 1951; Money, 1986). Pontin (1986) discussed the computations of pore water pressures in areas protected from tidal flooding by dykes and sheet pile walls. Farrel (1994) presented the results of analytical studies for the ground water variations that arise from tidal flows through leaky marine structures. Vuez and Rahal (1994) presented the results of laboratory studies on clay samples subjected to cyclic sinusoidal loading simulating tidal variations. The measured pore pressures were used to predict the compressibility characteristics of pore fluids and soil skeleton and the coefficient

of permeability. However, most of these studies addressed the generation of pore pressures in the deposits due to tidal variations only in intertidal areas.

A theory to estimate the pore pressure distribution in saturated sediments below an estuary due to tidal loading can be found in the theory for ground water hydraulics. The mechanism of pore pressure variation is described by a general differential equation of motion of ground water flow in storage aquifers. The solution of the equation can estimate the pore pressures in soils for different boundary conditions. Verruijt (1969) developed a storage equation to describe the phenomenon of unsteady flow through a compressible porous medium in plane strain conditions. The basic assumption in the theory is that the interaction between an external load and internal pore water pressure is a direct consequence of the degree of elasticity in the porous framework, that is, the soil obeys Hook's Law. The movement of the pore fluid is assumed to obey Darcy's Law.

Tide loading can cause deformation of the seabed due to changes in total vertical stress. When the tidal wave length is large enough compared with the thickness of the permeable sea bed, the flow of water can be treated as a one-dimensional boundary value problem. The changes in pore water pressure are expressed in terms of the conservation principle applied to the mass of water in the pores of the sediment during its deformation. The net rate of flow of water expelled from an element of soil has to be equal to the net change of volume of the pores of the sediment. The modeling equation was given by Vuez and Rahal (1994) and can be expressed as

$$\frac{1}{c_{vg}}\frac{\partial u}{\partial t} = \frac{\partial^2 u}{\partial z^2} + \frac{1}{c_v}\frac{\partial \sigma}{\partial t} \qquad (7.1)$$

in which c_{vg} and c_v are the consolidation coefficients of gaseous sediments and saturated sediments respectively and are given by

$$c_{vg} = \frac{k}{\gamma_w(n\beta + m_v)} \quad \text{and} \tag{7.2,a}$$

$$c_v = \frac{k}{\gamma_w m_v} \tag{7.2,b}$$

where

k = coefficient of permeability of soil skeleton

n = porosity of the soil structure

β = compressibility of pore fluid

m_v = compressibility of soil skeleton

u = pore water pressure

σ = total stress due to tidal loading = $\frac{\gamma_w H}{2}\sin(\omega t)$,

in which, H is the tidal wave height and ω is the frequency

Equation (7.1) includes the effect of the compressibility of pore fluid. Normally an increment of total stress on a soil is carried partly by the pore fluid as pore pressure and partly by the soil skeleton as effective stress, depending on their relative compressibilities. In saturated soils the compressibility of the soil skeleton is almost infinitely greater than that of the pore water, and thus essentially all of a stress increment applied to a saturated soil is carried by the pore fluid. In partly saturated soil, a stress increment is shared by both the pore fluid and the soil skeleton.

7.3. Evaluation of Tidal Drawdown on Saturated Sediments

In saturated soils, the compressibility of the pore fluid is negligible. Hence, the compressibility term, β, for the pore fluid is negligible in the Equation (7.2,a). Therefore the consolidation Equation (7.1) due to tidal loading on saturated sediments is of the form

$$\frac{\partial u}{\partial t} = c_v \frac{\partial^2 u}{\partial z^2} + \frac{\partial \sigma}{\partial t} \qquad (7.3)$$

Equation (7.3) describes the pore water pressure response for the propagation of tide cycles over a saturated porous bed. The solution of the equation results in the variation of pore pressures in saturated sediments for the tidal change in the FRD at the time of failure in 1985.

The tides in the Strait of Georgia are mixed semi-diurnal tides, with extreme tidal range exceeding 5.4 m (McKenna et al., 1992). From highs and lows obtained at a tide station near Point Atkinson, tidal fluctuations were computed and corrected to Sand Heads based on the Tide Tables, published by the Department of Fisheries and Oceans, Ottawa, Canada. Figure 7.1 presents the tide conditions between 1 June 1985 and 11 July 1985. The maximum tidal variations during the period of failure in 1985 is about 5 m with a period of about 16 hr. The time span of the tide from its peak to its low is about 8 hr.

In Chapter 5, it has been demonstrated that the stress state of the fresh deposits at Sand Heads have a potential to liquefy. A highly stressed zone (shear stress) in the fresh deposits has been identified within the slope of the FRD. The critical stress state (p' = 220 kPa; q = 205 kPa) occurs at a depth of 36 m from the mudline. This stress state is close to the collapse surface. The sediments in the upper depths may be experiencing excess pore pressures due to tidal drawdown, but the stress state of the sediments in the upper depths is further away from the collapse surface. Moreover, the magnitudes of excess pore pressures at the 36 m depth will be greater than the pressures at shallow depths. Therefore, it is reasonable to study the influence of tides on the sediments at the depth of 36 m.

The solution of Equation (7.3) is obtained using finite-difference methods. The application of the method for the boundary value problem is discussed in Appendix B. The pore pressure response due to the tidal variation of 5 m on saturated sediments is shown in Figure 7.2,a. It illustrates that the pore pressure increases in association with the flood tide and dissipates with the ebb tide. The tide-induced pore pressures are in phase with the tidal variation. The pore pressure response is a function of magnitude of tidal loading and permeability and compressibility characteristics of the porous medium. It also shows that no residual pore pressures remain during low tide conditions. Hence, there are no changes in the effective stress conditions. The evaluation of the stress path in p'-q space for the stress changes due to the tidal drawdown of 5 m is presented in the Figure 7.2,b and indicates that the effective stress state remains unchanged. The one-dimensional undrained analysis demonstrates that tidal drawdown can not trigger flow liquefaction of deep saturated sand deposits at the mouth of the Fraser River. However, gas has been found in the samples of pore fluids in marine environments. Degradation of organic matter, such as biological organisms and effluent discharges, in the environment results in the generation of gas. The gas desaturates the sediments. The influence of tidal drawdown on unsaturated sediments and its consequence on the liquefaction stability of deposits have not been studied. The following section investigates the effect of tidal drawdown on unsaturated sediments.

7.4. Effect of Tidal Drawdown on Gaseous Sediments

It has been observed that gases expand and come out of solution in undisturbed samples of marine soils because of the release of the confining stress. When gas expands within a sample, the physical as well as engineering properties of the soils may change. The unit weight, the degree of saturation and the strength and compressibility of soil are irreversibly altered (Poulos, 1988). The presence of methane gas is quite common in marine soils.

Methane has been observed in the pore fluid samples of the FRD (Christian, 1995; personal communication). Esrig and Kirby (1977) have examined the relationship between the in-situ degree of saturation and the degree of saturation which would be measured in a sample at atmospheric pressure. Estimates of the degree of saturation in the samples showed lower values than those that must be present in the field. They also observed that the degrees of saturation in the field were always greater than 85%.

As mentioned previously, an increment of total stress on partly saturated soils is shared by both the soil skeleton and the pore fluid depending on their relative compressibilities. Fredlund and Rahardjo (1993) present the response of pore fluid with air for the changes in total stress as shown in Figure 7.3 and suggests that the degree of saturation in the occluded zone (zone 2) will be between 80% - 100%. In zone 2, the air bubbles are of spherical form and are occluded in the pore fluid. The pore air and pore water pressures are assumed to be equal in the occluded zone (Fredlund and Rahardjo, 1993; Sparks, 1963). Hence, the normal definition of the effective stress principle for saturated soils remains unchanged for soils with occluded air bubbles in the pore water. However, the presence of bubbles renders the pore fluid compressible.

Figure 7.4 illustrates that the compressibility of an air-water mixture is predominantly influenced by the compressibility of the free air portion (Fredlund and Rahardjo, 1993). When the voids of a soil mass are completely filled with water (S=100%), the pore fluid compressibility is negligible. However, the inclusion of even 1% air in the soil is sufficient to significantly increase the pore fluid compressibility. As the percentage of air increases to about 15% (S = 85%) the compressibility of the pore fluid can be as much as the compressibility of soil skeleton. The presence of gas bubbles, such as methane, in pore water may change the compressibility of the gas-water mixture. However, it is assumed that the compressibility of pore air-water mixture and the compressibility of gas-water

mixture are of the same magnitudes. This assumption is reasonable because the isothermal compressibility of air/methane is equal to the inverse of the absolute air/methane pressure.

The one-dimensional consolidation phenomenon due to the tidal variations on the gaseous sediments takes into account the compressibility of pore fluid, that is, Equation 7.1 models the phenomenon.

7.4.1. Evaluation of Tidal Drawdown on Gaseous Sediments in the FRD

The mathematical model of the effect of tidal variations on gaseous sediments (Equation 7.1) requires a knowledge of the porosity of the soil skeleton and the compressibility of the pore fluid. Koppejan et al. (1948) observed that the porosity of river delta deposits in Netherlands was about 48%. Andresen and Bjerrum (1967) suggested that the natural porosities of sand deposits are about 44%. An exact estimate of marine sand deposits is difficult. It is estimated in Chapter 5 that the in-situ void ratio of the sand deposits at the depth of 36 m is about 0.98, which corresponds to the porosity of 49%. Hence, the value of 0.49 is used in the present analysis.

The in-situ degree of saturation in the marine sediments ranges between 85% to 100%. The exact value of degrees of saturation is not possible to predict, unless an investigation to collect samples of pore water is carried out. Moreover, no data regarding the in-situ degree of saturation was available at the time of the failure in 1985. Hence, it is reasonable to investigate the influence of pore fluid compressibilites on the response of sediments for tidal variations over the range of degrees of saturation (100% - 85%). It was demonstrated that low tides can not initiate flow liquefaction failures in saturated sediments. Hence, the analysis can be carried out at different degrees of saturation (99% - 85%). However, small percentages of gas may go into solution in the pore fluid during flood tide. When the gas

dissolves in the solution, the pore fluid can be treated as fully saturated. Figure 7.3 shows that there is a one to one response between the total stress and the pore fluid response at the transition stage (from zone 2 to zone 3), that is, the total stress will be fully carried by the fluid. Hence, the present analysis considers the degrees of saturation of the sediments between 98% to 85%.

Table 7.1 presents the values of different pore fluid compressibilities over the range of degrees of saturation, obtained from Figure 7.4. For fully saturated sediments (S = 100%), the compressibility of pore fluid is negligible. However, the compressibility of pore fluid for the degrees of saturation between 98% to 85% is considerable relative to the compressibility of the FRD sand skeleton, which is obtained from laboratory testing of the sand samples.

The total stress due to tidal variations is shared by the soil and the fluid depending on their compressibilities. The ratio of the consolidation coefficients ($r=c_{vg}/c_v$), that appears in Equation 7.1 determines the stress shared by both the soil and the fluid. For fully saturated sediments, the ratio, r is 1. Hence, the total stress is carried by the pore fluid. However, the values of the ratio decrease gradually by small magnitudes for different degrees of saturation as shown in Table 7.1. Consequently, the change in the pore pressure variation for different degrees of saturation will be small for tidal loading.

Equation 7.1 describes the pore fluid response in gaseous sediments for tidal loading. As previously discussed, the maximum tidal variation at the time of the flow slide in the FRD was about 5 m with a period of 16 hr. The pore fluid response is obtained using finite difference methods for a degree of saturation of 98%. The finite difference equations are presented in Appendix C. Figure 7.5 presents the response of the pore fluid with a gas of 2% for a depth of 36 m. It can be observed that the tide-induced pore pressures are out of

phase by about 1 hr 25 min. in gaseous sediments. A residual pore pressure of about 13 kPa can be observed at low tide. The amplitude change of pore pressure is about 30% of the total stress variation.

During high tide the increase in total stress on the sediments is shared partly by the pore fluid and partly by the soil skeleton as effective stress because of their relative compressibilities. Thus, there will be an increase in the effective stress conditions in the sediments during high tide. When the tide falls to its low value, there is residual pore pressure remaining at low tide. The residual pore pressure changes the effective stress conditions. A partially drained condition prevails in the sediments during low tide.

In the analysis the pore pressure response is assumed to be influenced by the tidal change under a drained condition, that is, a hydrostatic condition. In real soils, there may be an initial excess pore pressure before the rise of the tide from the mean value. However, the present results are supported by the fact that the phase lag and excess pore pressures are consistent with field observations. Karlsrud and Edgers (1980) presented a reference for in-situ measured pore pressures in soft sea beds with the presence of gas. In one case at 3.5 m depth below the mudline, the maximum pore pressure in the sediment occurred 6 hours after peak tide, at the same time as low tide. The amplitude of pore pressure change was about 50% of the total variation. Christian (1995, personal communication) observed a phase lag of about 55 minutes in the pore pressure response at a depth of 5.5 m from the mudline in the FRD. However, the percentage of gas is unknown at the time of observation.

Deposits in deltas will have degrees of saturation ranging between 85% to 100%. The influence of the saturation is reflected in the excess pore pressures that exist during low tide conditions. Over this range, the magnitudes of the excess pore pressures increase with a

decrease of degree of saturation . The smaller the degree of saturation the greater the time lag. However, the variation of the excess pore pressures with the decrease in saturation is not pronounced. For the tide of 5 m with a period of 16 hr, excess pore pressures of about 13 kPa and 17 kPa are observed at low tide conditions for 98% and 85% saturations respectively. This is because the compressibility ratio of soil skeleton and pore fluid does not change significantly at lower degrees of saturation (Table 7.1). Hence, a stress path evaluation for the changes in pore pressures at S =98% is reasonably valid to embody the effect of different degrees of saturation.

7.4.2. Stress Path Evaluation

As discussed, the critical stress state point in the slope at the FRD before failure in 1985 is at a depth of 36 m with the stress values of p' = 220 kPa and q= 205 kPa. Sedimentation in the delta builds up shear stresses and brings the stress state close to the collapse surface and the contractant state boundary surface. Another mechanism is necessary to bring the critical state of the soil on to the boundary surface to trigger liquefaction failure. It is observed that tidal drawdown results in residual pore pressures in gaseous sediments. The pore pressures will change the effective stress state of the sediments. The influence of tidal drawdown can be evaluated for the critical stress state by incorporating the partially drained pore pressures, obtained from the theoretical study.

Figure 7.6,b presents the stress path showing the effect of tidal drawdown on the critical stress state for a degree of saturation of 98%. The stress path shows that the shear stress is unchanged during the tidal drawdown. Tidal activity will not apply any shear stresses on the sediments, whereas surface waves can induce shear stresses in the sediments. Kramer (1988) assumed that tidal drawdown on coastal deposits induces shear stress changes. The

observation that shear stress is unchanged due to tidal drawdown makes the assumption invalid for explaining deep seated flow liquefaction failures.

From Figure 7.5, it is observed that the pore pressures are partially dissipated during the rise of the tide. This indicates that the mean effective stress, p', increases with the rising tide and is shown in Figure 7.6,b. The mean confining stress increases from a value of 220 kPa to 236 kPa. Figure 7.5 indicates that residual pore pressures remain as the tide recedes to its low value. The stress path during this phase (Figure 7.6,b) shows that the mean confining stress decreases from the value of 236 kPa to about 200 kPa with a constant shear stress value. At the extreme low tide stage, the mean confining stress reaches its lowest value along the constant shear stress path.

During the partial dissipation of pore pressures, volume changes also occur in the sediments, that is, changes in void ratio occur due to tidal variation on the gaseous sediments. It was determined in Chapter 5 that the void ratio of the critical stress state of the sediments in the FRD is about 0.98. Due to the changes in the effective stress state during the tidal range of 5 m, the changes in the void ratios are determined and the path of the void ratio changes is plotted in Figure 7.6,a. in e-p' space. During the rise of tide, the increase in effective stress of the sediments represents a decrease in the void ratio from 0.98 to 0.977, that is, a small amount of consolidation occurs in the sediments. During low tide, the excess pore pressure decreases the effective stress in the sediments . The corresponding change in the void ratio is also presented in the Figure 7.6(a) which indicates that the void ratio increases by a small amount during the phase of low tide.

In the e-p'-q space, the path of the critical stress state lies essentially in a constant shear stress plane. The stress path resulting from tidal drawdown on gaseous sediments (Figure 7.6,a) is analogous to the stress path derived for a rise of the water table in loose saturated

sands. Catastrophic liquefaction flow slides have been triggered in loose saturated materials, such as coal stocks (Eckersly, 1990) and waste dumps (Dawson et al, 1992) when following the latter stress path. The materials experienced decrease in void ratio during the drained stress path and failed (liquefied). Figure 7.6,a shows that the void ratio increases slightly for the increasing tide and decreases during low tides. However, the change in the void ratio may not be significant. Figure 7.6,b shows that the path remains in a constant shear stress plane. The influence of this stress path on the Contractive State Boundary Surface (CSB) can be evaluated.

7.4.3. Implication of the Stress path on the Contractant State Boundary Surface

The CSB is the surface constituting all the post peak portions of undrained stress paths (Alarcon-Guzman et al, 1988; Ishihara, 1991). Sasitharan et al. (1993) demonstrated that any attempt to cross the CSB results in collapse of the structure of sediments and leads to rapid generation of pore pressures causing liquefaction failures of the saturated sediments. They showed that a sample brought on to the CSB under fully drained conditions collapsed catastrophically on the CSB and failed in an undrained manner, that is, the sample liquefied. The stress path of the sample remained essentially in the constant shear stress plane. The sample was consolidated along a drained stress path until it reached the CSB. On the boundary surface the stress path attempted to penetrate the boundary, but collapsed, rapidly generating pore pressures.

The observed stress path from the tidal variation of 5 m on the gaseous sediments (S = 98%) is also in the constant shear stress plane. During low tide conditions, the sediments expand slightly and the stress path reaches the CSB during this phase and attempts to cross the boundary. The structural collapse of the sediments occurs during this

attempt. Consequently, the sediments fail in an undrained manner. Figure 7.7 shows the CSB defined for an undrained test at a void ratio of 1.0. The stress path tries to penetrate the CSB at the extreme low tide conditions and eventually, the sediments of the critical stress state liquefy. Thus, the establishment of the stress path explains the triggering of flow liquefaction.

7.5. Development of Flow Slides

It has been observed in Chapter 5 that the stress state of the fresh deposits of the FRD has a potential for flow liquefaction. The triggering of liquefaction of gaseous sediments at the critical stress state during low tides will cause the development of an initial flow slide in the sediments. The loss in shear strength in the liquefied material will result in an initial flow slide. A model developed by Gu et al. (1993) describes the development of flow slides effectively. The initial flow slide leaves behind laterally unsupported contractive gaseous sediments. These sediments will be experiencing excess pore pressures during low tides. However, these pore pressures may not be sufficient to bring the state of the sediments on to the CSB. An undrained stress redistribution from the previously liquefied material strain softens the unsupported sediments, which results in a flow slide. Progressive failure of the deposits continues generating retrogressive flow slides. The slides cease to progress when a dense state of deposits or a stable back scarp is encountered. The mechanism explaining the triggering of flow liquefaction is consistent with the occurrence of retrogressive flow slides in river deltas during low tides.

From the analysis, it is seen that liquefaction flow slides could be triggered in gaseous sediments during low tides. At the time of the liquefaction flow slide that occurred in 1985 in the FRD, the data regarding the degree of saturation was not available. However, a minimum amount of 2% of gas may become critical for the triggering of flow liquefaction.

The extreme low tides of about 5 m could also be critical. These two mechanisms, in association with the high driving shear stresses resulting from rapid sedimentation, are critical in triggering liquefaction flow slides in the Fraser River Delta.

7.6 Summary

The effect of tidal drawdown on saturated sediments has been investigated as a triggering mechanism for liquefaction failures in the FRD. The tidal effect is treated as a one-dimensional consolidation problem subjected to time dependent loading. An undrained analysis demonstrates that the effective stress state does not change in saturated sediments with the tidal loading. The influence of gas in the sediments is also studied for the tidal loading. In-situ degrees of saturation in the marine environment vary from 85% to 100%. Gas in occluded form induces additional compressibility of the pore fluid relative to the compressibility of the soil skeleton. During low tide conditions, the presence of gas gives rise to residual pore pressures in the sediments and a time lag. The residual pore pressures induce effective stress changes in the sediments.

An evaluation of the stress path for the effective stress changes has been carried out. The resulting stress path becomes a critical path in triggering flow liquefaction of the sediments. The stress path continues to stay in a constant shear stress plane and attempts to cross the contractant state boundary during the extreme low tides. This attempt results in the collapse of the structure of the sediments in the FRD and initiates a flow slide. The stress path in the constant shear stress plane indicates the path of partially drained sediments. Progressive failure of the unsupported deposits generates retrogressive flow slides in the delta. The development of these retrogressive flow slides is consistent with the occurrences of flow slides in river deltas around the world.

Permeability of deposits (m/sec)	$1.44 * 10^{-4}$				
Compressibility of FRD sand (m_v) (1/kPa)	$1.3 * 10^{-4}$ (obtained from laboraotry tests on FRD sand samples)				
Degree of saturation, S (percentage)	100	98	95	90	85
Compressibility of pore fluid (β) (1/kPa)	$4.58 * 10^{-7}$ (negligible)	$4.5 * 10^{-4}$	$5.63 * 10^{-4}$	$7.3 * 10^{-4}$	$8.44 * 10^{-4}$
Consolidation coefficient of gaseous sediments (c_{vg})	0.11	$4.33 * 10^{-2}$	$3.76 * 10^{-2}$	$3.14 * 10^{-2}$	$2.82 * 10^{-2}$
Ratio of compressibilities [$r = c_{vg}/c_v = m_v/(n\beta+m_v)$]	1	0.41	0.35	0.295	0.265

Table 7.1. Compressibilities of pore fluid at different degrees of saturation and ratio of compressibilties

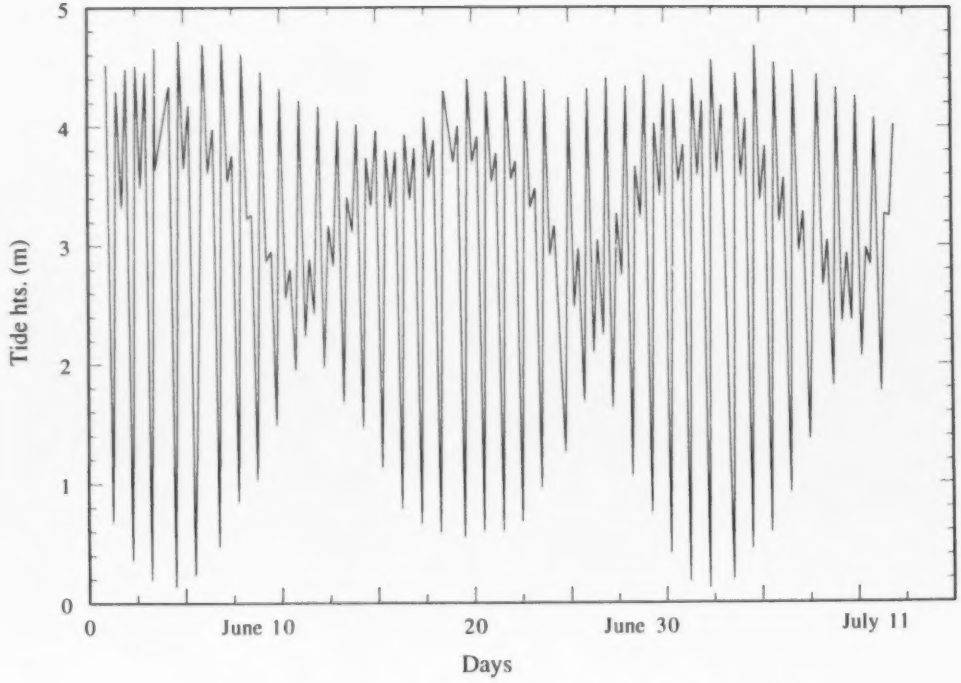

Figure 7.1. Tide conditions @ Sand Heads - June, July 1-11

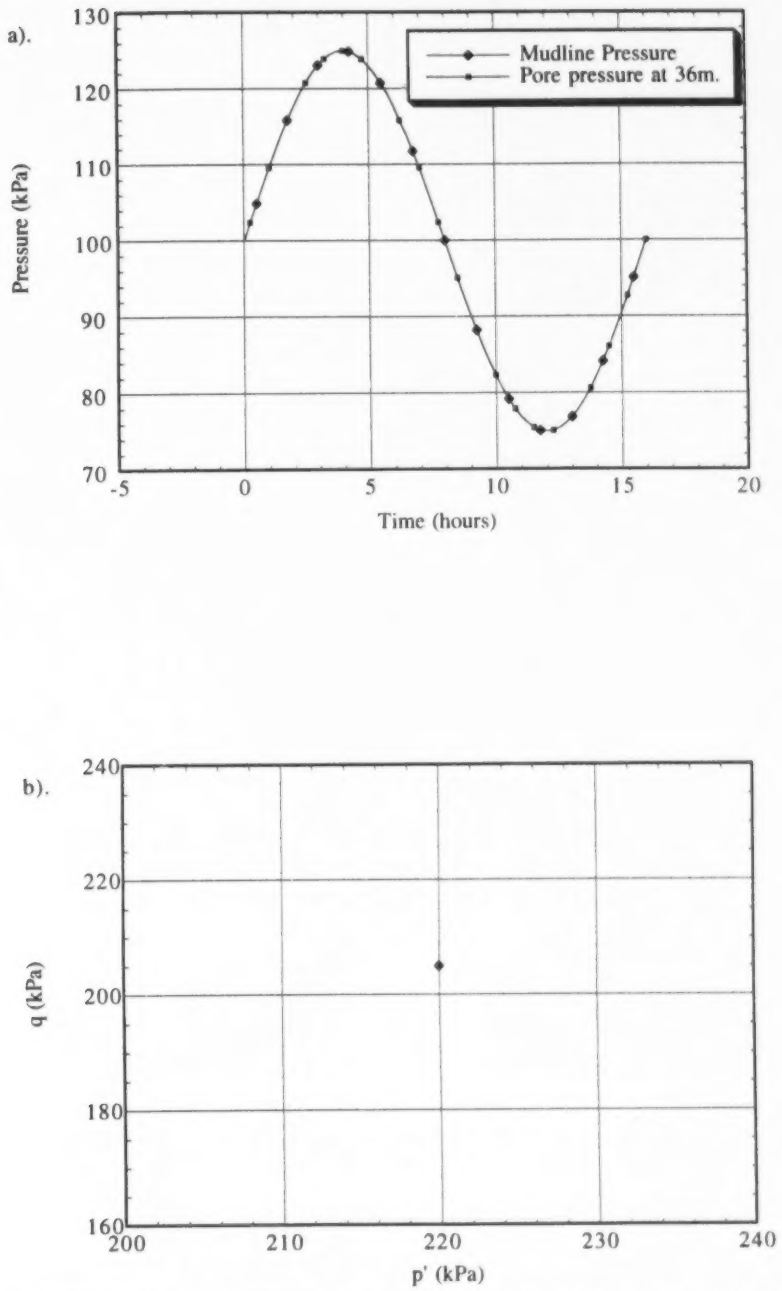

Figure 7.2. Influence of a tide of 5m with a period of 16hr on saturated sediments
a). Variation of pressures b). Stress path due to a tide of 5m (when S=100%)

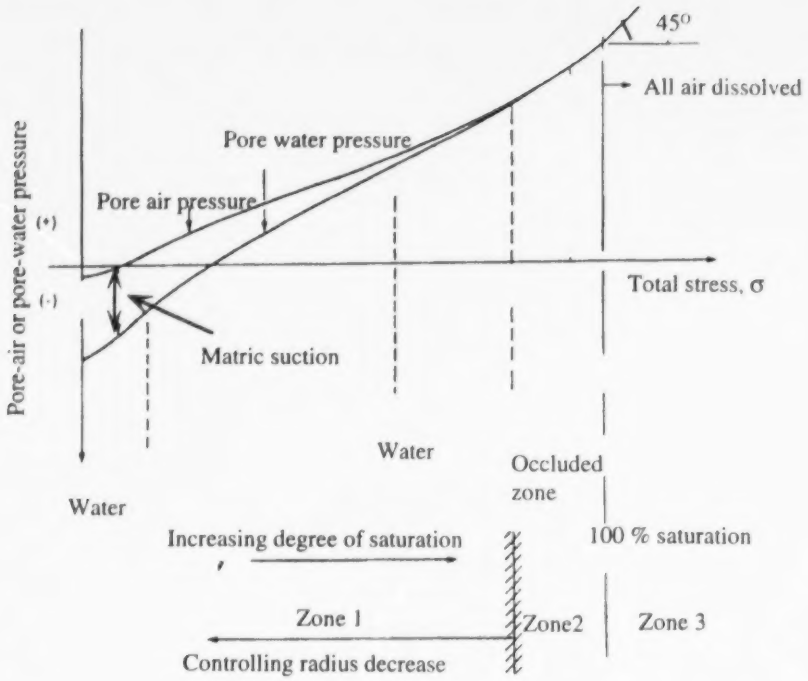

Figure 7.3 Pore air and pore water pressure responses to a change in total stress during undrained compression (after Fredlund and Rahardjo, 1993)

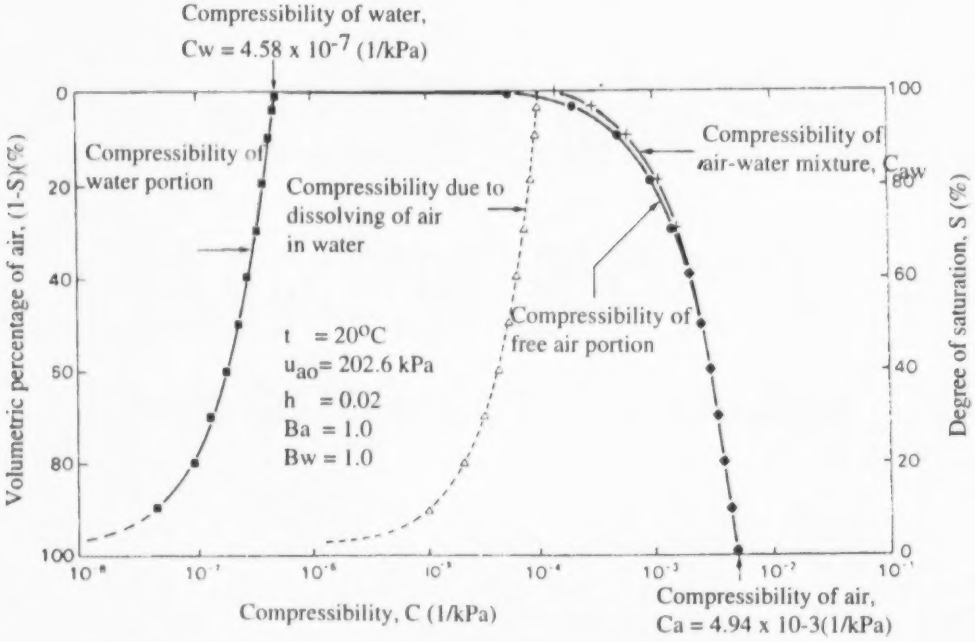

Figure 7.4 Components of compressibility of an air-water mixture (after Fredlund and Rahardjo, 1993)

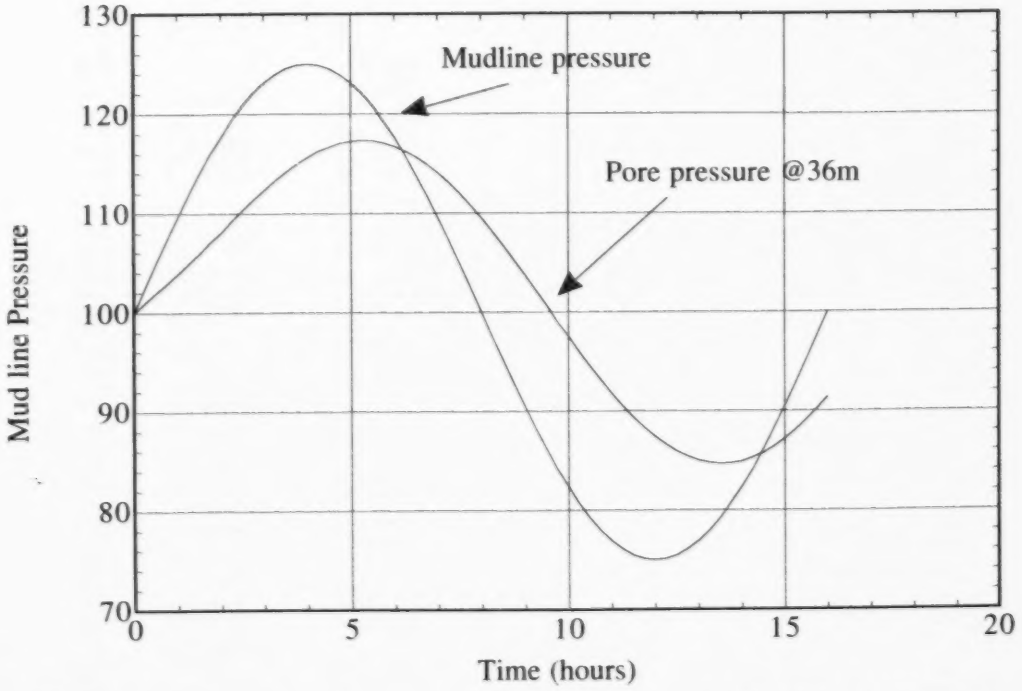

Figure 7.5. Variation of pressures for a tide of 5m with 16 hr periods (S = 98%)

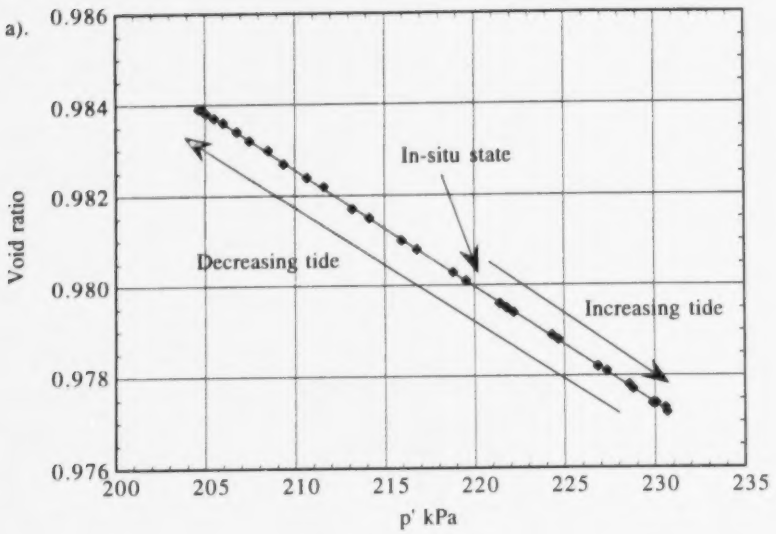

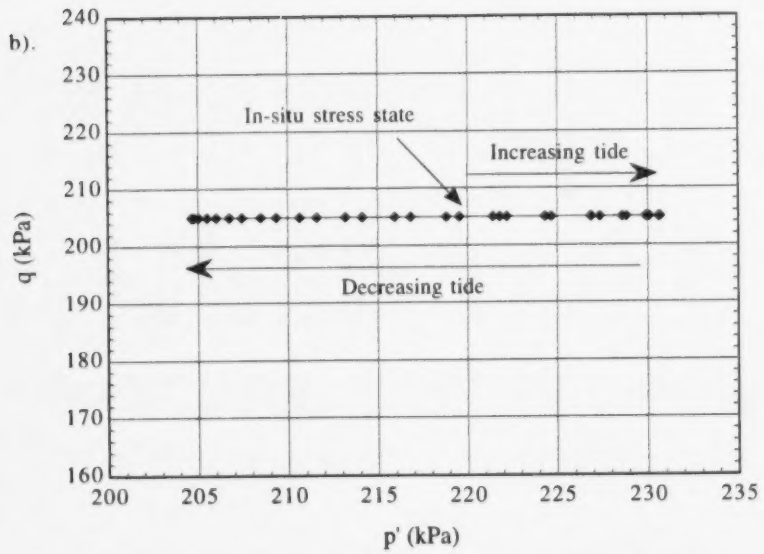

Figure 7.6. Stress path due to a tide of 5m. (When S=98%)
a). e-p' space b). p'-q space

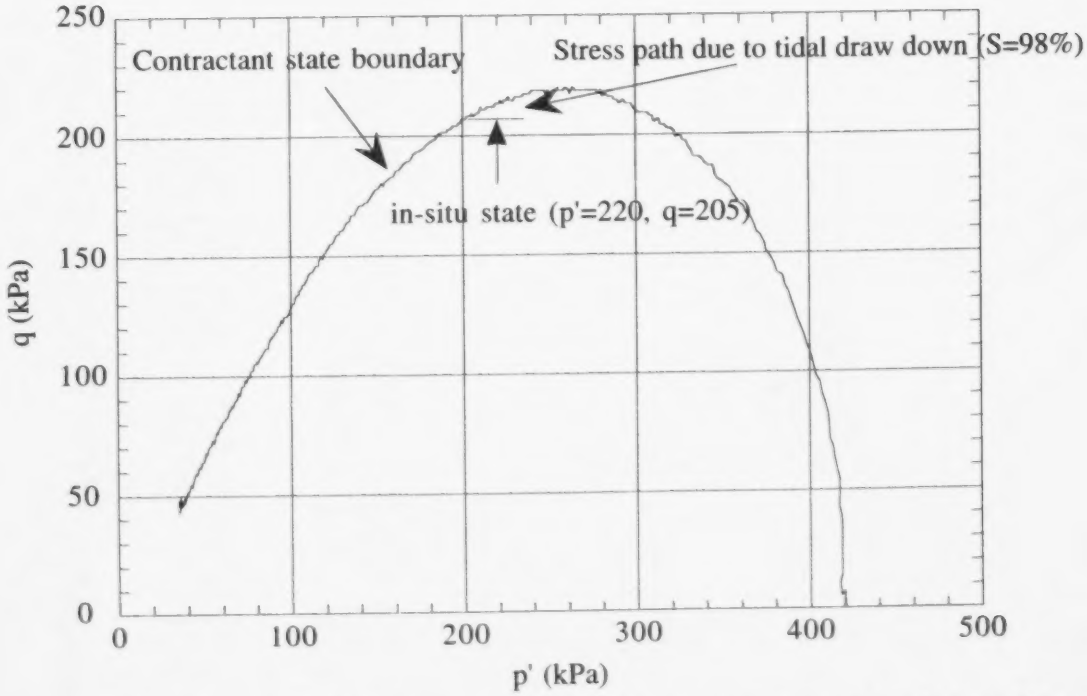

Figure 7.7. Influence of tidal drawdown on Contractant state boundary surface

8.0 Summary and Conclusions

8.1 Summary of Thesis

Liquefaction flow slides are quite common in active river deltas and fjords. The flow slides are caused by triggering of flow liquefaction in loose sandy soils at the mouths of the rivers. These flow slides can be triggered either by dynamic loading or by static loading. Most of the flow slides in the world that are triggered by static loading occur during low tide conditions. In the Fraser River Delta, the occurrence of flow slides appears to be spread over the whole year. The stability of coastal structures is a major concern associated with liquefaction flow slides in the FRD. Different environmental processes, such as rapid sedimentation, surface waves, tides, gas generation in the sediments of deltas, currents, and dredging, can contribute to the triggering of liquefaction flow slides. Triggering of flow liquefaction can initiate retrogressive flow slides. In the literature an explanation for the triggering of flow liquefaction due to static effects in river deltas is not well established and the contributions of the environmental processes for the triggering are not quantified. An investigation exploring the contributions of the environmental processes for initiating a liquefaction flow slide that occurred in 1985 in the FRD was carried out.

The background for explaining the triggering phenomenon requires a knowledge of the behaviour of sands. Chapter 2 discusses the behaviour of sands. An approach by Castro (1969) for defining liquefaction provided a clear understanding of the mechanism. Castro (1969) referred to the state of loose sand during flow liquefaction as steady state. A steady state is unique to a void ratio of a sand and the steady state strength is the available undrained shear strength of the sand. The analysis explaining the triggering of the 1985 liquefaction flow slide in the FRD is based on steady state concepts. Steady state differentiates states of sands either contractive or dilative. A contractive sand possesses a

potential for flow liquefaction, provided that the in-situ shear stress is greater than the steady state strength of the sand. Further developments in steady state concepts helped in building a framework to explain flow liquefaction of saturated sands. A powerful concept of the collapse surface helped to understand the mechanisms of flow liquefaction failures. A contractant state boundary surface controls the behaviour of contractive sands. Any attempt to cross the boundary by a soil state can result in flow liquefaction of the soil, and hence, a flow slide in slopes. For flow liquefaction to occur, an undrained condition is not a pre-requisite. A dilatant state boundary surface controls the behaviour of dilative soils. However, some dilative sands exhibit a contractant behaviour followed by a dilatant behaviour at large strains. These soils do not undergo flow liquefaction.

For quantifying the contributions of the triggering mechanisms, the characteristics of the FRD were studied. The physical setting of the FRD was discussed in Chapter 3. The sedimentation in the FRD is influenced by fluvial processes and oceanographical processes. The processes contribute to the deposition of sand at the mouth of the Fraser River. The maintenance of morphological features in the delta confirm that the flow slides are a recurrent phenomenon in the FRD.

The analysis explaining triggering of liquefaction flow slides in the FRD requires knowledge of the strength characteristics of the FRD sand including the steady state parameters, such as the slope of the steady state line in the e-p' plane as well as the slope in the p'-q plane. The characteristics of the FRD sand are discussed in Chapter 4. Consolidated undrained triaxial compression tests and consolidated drained triaxial tests were carried out on FRD sand samples for determining the sand characteristics. Samples were prepared by both moist tamping and water pluviated techniques. Very loose samples can be obtained by moist tamping. Water pluviation resulted in dilative samples. The slope of the steady state line is relatively flat indicating that the sand is moderately compressible.

At higher confining stresses the sand exhibits a bilinear behaviour in the steady state line indicating that particle crushing is occurring at higher confining stresses. The slopes of the collapse surface and the contractant state boundary surface were obtained from undrained stress paths of the tests.

Shear wave velocity is a parameter that can be used for characterizing uncemented and relatively fresh sediments and is a function of confining stress and void ratio. Shear wave velocity can be determined both in the laboratory and in the field. Bender elements were used on laboratory specimens for measuring shear wave velocities of FRD sand samples. The shear wave velocities were coupled to the steady state line in the e-p' plane which resulted in a chart for the characterization of the in-situ state of the FRD sediments. The results of in-situ tests were also discussed in Chapter 4. CPT and SCPT profiles show that the sediments in the delta are loose sands interbedded with silts. Evaluation of CPT profiles indicate that the loose sands are susceptible to flow liquefaction.

Using the physical characteristics of the FRD, the steady state characteristics of the FRD sand and the results of in-situ tests, evaluation of the triggering mechanisms was carried. Chapter 5 discussed the effect of sediment deposition as a triggering mechanism for the liquefaction flow slide in 1985. When a slope failure (flow slide) occurs in FRD, the scar will be replenished by river borne-clastics. The sedimentation occurs in parallel planes from the backscarp to the final configuration of the slope, that is, a stress state is built up in the slope which constitutes a critical stress state for a possible flow liquefaction failure. The stress state can be established using a finite element model which can simulate the sequential construction of the slope. The program SIGMA/W was used in which the accretion of the slope was modeled by the addition of finite elements in parallel layers. In the model drained linear elastic effective stress parameters were used as constitutive model

parameters. The evaluation of the stress path indicated that shear stresses are built up in the slope due to sedimentation.

The stress state has to be brought on to the collapse surface and the contractant state boundary for triggering flow liquefaction. The stress path can not be evaluated for this unless the in-situ steady state strength (undrained shear strength) of the deposits is known. Alternately, the path of maximum shear stress for each increment of loading was examined. Densification due to consolidation is induced on the previously deposited sediments due to fresh layers. The maximum shear stress path shifts to a new position in the p'-q plane which describes the stress state in the slope. Using in-situ shear wave velocity from SCPT and the chart developed in Chapter 4, this in-situ state of the sand was evaluated. The evaluation shows that the deposits are contractant and have void ratios comparable to those obtained from moist tamping techniques. The driving stress state was observed to be higher than the steady state strength which indicates that the fresh deposits in the FRD are contractant and have a potential to liquefy. A zone of high shear stress was identified within the slope. Progressive failure is more likely to occur when this zone is triggered to flow liquefaction. It also confirms that sedimentation alone may not trigger flow liquefaction of the sediments, but does build up shear stresses.

Another mechanism that could trigger flow slides in the FRD is surface waves. A theoretical investigation was carried out evaluating the effect of surface waves as a triggering mechanism and was also supported by a field investigation of in-situ porewater pressures for surface waves. Two probes were designed, constructed and installed to monitor pore pressures for the surface waves. Results from the field study suggested that the pore pressures were not significant to cause any deep seated failures. The theoretical investigation was based on a concept of threshold shear strain. Surface waves can cause both transient and residual pore pressures. The two types of pore pressures can be

distinguished by the concept of the threshold shear strain. Residual pore pressures start building up when the shear strain associated with a wave exceeds a value of about $10^{-2}\%$. Wave conditions at the time of 1985 failure were predicted using wind data and hindcasting. A maximum significant wave height of 2.7 m with a period of 5.32 sec and a wave length of 40 m was obtained. The shear strain associated with the maximum wave was calculated and observed to be less than the threshold shear strain. It was concluded that the surface waves in the Fraser River Delta can not build up residual pore pressures. However, small magnitudes of transient pore pressures can be created by the waves in the deposits. The consequence of these small pore pressures is that the surface waves could only trigger flow liquefaction of the sediments in the upper few meters of depth. This theoretical study supports the field observations that wave induced pore pressures are significant only in the upper 2 to 3 m.

Many static liquefaction flow slides occurred during low tides in river deltas. It was believed that seepage pressures during low tides were triggering liquefaction flow slides in river deltas. In the literature the effect of the tidal drawdown on the stability of sand deposits in river deltas was not quantified. Storage of porewater is required in ground aquifers for the development of residual pore pressures during low tides. Storage equations are available in groundwater hydraulics for different boundary conditions. These equations can model the phenomenon of tidal variations as a one-dimensional consolidation problem. Solution of a differential equation describing the phenomenon results in pore pressure variation for different boundary conditions.

An increase in total load is shared by soil skeleton and pore fluid depending on their compressibilities. The compressibility of pore fluid is negligible for fully saturated sediments. Hence, all the load is shared by the pore fluid in fully saturated sediments as an undrained loading. An undrained analysis for a tidal fluctuation of 5 m with a period of

16 hr was performed. The tide characteristics at the time of failure in 1985 were obtained from data collected at a base station (Point Atkinson) and corrected to the location of the failure. The undrained analysis showed that there was no residual porewater pressure due to the tide. That is, the effective stress state remains unchanged. It was concluded that tides can not trigger flow liquefaction failure in fully saturated sediments.

Gas is generated in the sediments of the FRD due to degradation of organic matter and this desaturates the sediments. The phenomenon of tidal drawdown on gaseous sediments was investigated as a one-dimensional consolidation problem in Chapter 7. Normally, the in-situ degrees of saturation in marine sediments vary between 100% -85%. During this stage, the gas will be in occluded form and in this zone, the principle of effective stress is applicable. The in-situ degree of saturation was unknown at the time of failure in 1985, therefore a range of degrees of saturation was assumed (98% - 85%). The ratio of compressibilities controls the sharing of total load by both the pore fluid and the soil skeleton. A residual pore pressure was observed from the analysis at low tide condition for unsaturated sediments (S=98%). The residual pore pressures change the effective stress state of the gaseous sediments. The magnitudes of residual pore pressures increase with a decrease in degree of saturation. However, the range of residual pore pressures will be small for the range of degrees of saturation between 98% to 85%. Hence, a degree of saturation of 98% was assumed to represent the wide ranges of in-situ degrees of saturation.

The stress path resulting from the changes of effective stress due to the residual pore pressures was evaluated at the location of high shear stresses. The location was identified from the stress analysis of the slope in Chapter 5. The stress path remains in a constant shear stress plane. During the flooding tide, the effective stress increases because of partial consolidation of the soil skeleton and there will be a small decrease in void ratio. During

the low tide, the residual pore pressures increase resulting in the decrease of the effective stress and increase in void ratio. The stress path is critical for triggering flow liquefaction of the sediments at the location of high shear stresses. This stress path resulting from tidal drawdown is anologus to the stress path derived for a rise in the water table in loose sands. It is confirmed in the literature that decreasing effective confining stresses of laboratory prepared loose samples of sand result in the collapse of soil leading to flow liquefaction. The stress path of gaseous sediments resulting from the effect of tidal drawdown constitutes a critical path to explain the triggering of flow liquefaction of the sediments in the FRD. The implication of the stress path on the contractant state boundary (CSB) was examined. The stress path at the time of low tide attempts to cross the CSB and leads to flow liquefaction. The initial liquefaction of the sediments will spread progressively in an undrained manner because of stress redistribution, leading to a flow slide. Progressive failure continues developing retrogressive flow slides and stops when dense deposits are encountered.

Currents associated with tides and dredging are also believed to contribute to the initiation of flow liquefaction of the sediments. Erosion due to currents may cause local over steepening resulting in undained local failures. Hence, it is not thought to be a contributing mechanism for a major failure. Uncontrolled dredging operations may also induce local oversteepening in the sediments. Therefore, it may lead to local undrained failures at shallow depths.

The environmental conditions in the FRD suggest that the failure could have occurred on 2 July 1995 when there was an extreme tide variation of about 5 m. The environmental processes, such as sedimentation, low tide conditions and gas in the sediments, contributed to the failure. This conclusion is based on the assumption that the sediments in the delta had degrees of saturation between 98% to 85%. Exact data would only be available from

the analysis of the pore fluid. The samples of pore fluid in the Fraser River Delta showed the presence of gas in the sediments.

8.2 Conclusions

The following conclusions can be drawn from the investigation of the flow slide that occurred in the FRD in 1985.

1. Moist tamping methods of preparation of sand samples are found to represent in-situ state of recently deposited loose sandy sediments.
2. An evaluation of sedimentation in the delta as a triggering mechanism shows that the sedimentation may not initiate flow liquefaction failures, but it can build up shear stresses and bring the stress state of the sediments close to the collapse surface.
3. Surface waves in the FRD can not initiate deep seated failures, however, they can trigger shallow flow liquefaction failures.
4. An investigation of the effect of tidal drawdown on saturated sediments in the FRD shows that the effective stress state of the sediments remain unchanged and the tidal drawdown can not trigger flow liquefaction of the saturated sediments.
5. Gas in the sediments of the FRD induces desaturation in the sediments. The effect of tidal drawdown on gaseous sediments reveals that there will be residual pore water pressures in the sediments during low tide conditions and can lead to triggering of flow liquefaction failures during extreme low tide conditions.
6. Progressive failure of sediments develop retrogressive flow slides.
7. Currents and dredging operations may initiate local undrained shallow flow liquefaction failures.

8.3 Recommendations

To protect the foundations of coastal structures from liquefaction flow slides, the following recommendations are made to the Canadian Coast Guard.

Liquefaction flow slides are recurrent in the Fraser River Delta. The foundations of coastal structures are at a risk due to potential instability. Sedimentation in the delta contributes to the failures. Most of the sedimentation in the delta occurs during spring and summer. The sedimentation results in high driving shear stresses in the slope. The in-situ stress state can be estimated in the slope for the effect of sedimentation and this can warn about the potential for further failure. When the replenished sediments in the previous failure scar have a maximum driving shear stress higher than the steady state strength of the sediments, there exists a potential for flow liquefaction in the replenished sediments. The potential for flow slides can be minimized. It is standard practice to dredge out the sediments in the navigation channel for the maintenance of draft for ships. This dredging can be further extended to the fore slope of the delta to reduce the shear stresses developed due to sedimentation. Controlled dredging is necessary to avoid local flow liquefaction failures. The possiblility of flow slides can be minimized by dredging the sediments along with continuous bathymetric profiling.

Tides are natural phenomena in the delta. Tide tables provide data of predicted tidal variation over a year. Extreme low tides make the sediments vulnerable to flow liquefaction failures. However, the presence of gas in the sediments is required for the deep failures. Close observation of the tidal data for the extreme conditions can also provide a warning of possible liquefaction failure. Pore fluid sampling and analysis of the gas content is also required to assess tidal triggering in a more precise manner.

8.4 Further Research

In-situ testing of sediments with the measurement of shear wave velocities at different locations can help identify liquefaction prone deposits.

In this thesis, evaluations of the triggering mechanisms were presented. The studies suggest the conditions under which a flow liquefaction can be triggered. The present work did not address the lateral extents of the failures. In the literature, numerical models incorporating strain softening parameters are discussed to explain lateral extension. These models explain the stress redistribution in liquefied soils which lead to the development of a flow slide. These models may further explain the development of retrogressive flow slides. Application of the models for estimating the lateral extent of the liquefaction failures in the FRD can be carried out.

The evaluation of sedimentation in causing flow liquefaction failures has been investigated for a K_O of 0.43, that is, (1- sin ϕ'). The analysis may not differ considerably to the field K_O conditions. However, further research can be carried out for possible K_O conditions in the FRD.

The evaluation of the influence of tidal activity on gaseous sediments is carried out assuming that the compressibility of porewater with gas is similar to the the compressibility of porewater with air. The difference may not be significant, but a further research work is recommended to study the influence of gas composition in the porewater on the compressibility of porewater.

Laboratory tests are recommended to investigate the crtitical gas content for triggering flow liquefaction failures on loose saturated sands with small amounts of gas subjected to tidal loading conditions .

Bibliography

Alarcon-Guzman, A., Leonards., G. A. and Chameau, J. L., (1988). "Undrained monotonic and cyclic strength of sands." Journal of Geotechnical Engineering, ASCE, Vol. 114, GT. 10, pp. 1089-1109.

Andresen, A. And Bjerrum, L., (1967). "Slides in subaqueous slopes in loose sand and silt." In *Marine Geotechnique*, Edited by A. F. Richards, Urbana, Illinois, University of Illinois Press, pp. 221-239.

Bea, R. G.., Wright, S. G.., Sircar, P. and Niedoroda, A. W.., (1983). "Wave-induced slides in South Pass Block 70, Mississippi Delta." Journal of Geotechnical Engineering, ASCE, Vol. 109, pp. 619-644.

Been, K. H., and Jeffries, M. G..(1985). "A state parameter for sands." Geotechnique, Vol. 35, pp. 99-112.

Been, K., Jefferies, M. G.. and Hachey, J., (1991). "The critical state of sands." Geotechnique, Vol. 41, No. 3, pp. 365-381.

Bennet, R. H.., Burns, J. T., Clarke, T. L.., Faris, J. R.., Forde, E. B.. and Richards, A. F.. (1980). "Piezometer probes for assessing effective stress and stability in submarine sediments." In *Marine Slides and Other Mas Movements*, edited by Saxov. S and Nieuwenhuis, J. K., Plenum press, pp. 129-162.

Bjerrum, L, (1971). Subaqueous slope failures in Norwegian fjords. Norwegian Geotechnical Institute Publication No. 88, p.8.

Casagrande, A., (1936). "Characteristics of cohesionless soils affecting the stability of earthfills." Journal of the Boston Society of Civil Engineers, Vol. 23, No.1, pp. 257-276.

Castro, G., (1969). "Liquefaction of sands." Harvard Soil Mechanics Series No. 81, Harvard University, Cambridge.

Castro, G. (1975). "Liquefaction and cyclic mobility of saturated sands." Journal of Geotechnical Engineering Division, ASCE, Vol. 101, GT 6, pp. 551-569.

Castro, G. and Poulos, S. J., (1977). "Factors affecting liquefaction and cyclic mobility." Journal of Geotechnical Engineering, ASCE, Vol. 103, GT 6, pp. 501-516.

Chaney, R. C. and Fang, H. Y., (1991). Liquefaction in the coastal environment: an analysis of case histories. Marine Geotechnology, Vol. 10, pp. 343 - 370.

Chari, T. R.., Dawe, C. R.., and Barbour, S. A., (1986). "Model studies of wave-seabed interactions." 5th International Conference of Offshore Mechanics and Polar Engineering, Vol. 1, pp. 566-573.

Christian, J.T., Taylor, P. K., Yen, J. K. C. and Erali, D. R.., (1974). "Large diameter underwater pipeline for nuclear power plant designed against soil liquefaction." Offshore Technology Conference, Preprint, Vol. 2, pp. 597-602.

Christian, H., Mulder, T, Courtney, R. C., Mosher., D. C., Barrie, J. V., Currie, R. G.., Olynyk, H. W., and Monahan, P.A. (1994). "Slope Instability on the Fraser River Delta Foreslope., Vancouver, British Columbia." 47th Canadian Geotechnical Conference, Halifax. pp. 155-165.

Christian, H. A., Woeller, D. J., Weemees, I. And Robertson, P. K., (1994). "Use of SASW and SCPT to evaluate seismic liquefaction potential of the Fraser Delta foreslope, Vancouver, British Columbia." Proceedings, 47th Canadian Geotechnical Conference, pp. 166-175.

Clague, J.J., Luternauer, J.L., and Hebda, R.J., (1983). "Sedimentary environs and postglacial history of the Fraser River Delta and lower Fraser Valley, British Columbia." Canadian Journal of Earth Sciences. Vol. 20, pp. 1314-1320.

Coleman, J.M. (1976). *Deltas: Processes of deposition & Models for Exploration* Published by Continuing Education Publication Company Inc., Champaign, IL.

Cunning, J. (1994). "Shear wave velocity measurement of cohesionless soils for evaluation of in-situ state". M.Sc.. thesis, Department of Civil Engineering, University of Alberta, Edmonton..

Dawson, T.H., Suhayada, J.N., And Coleman, J.M., (1981). Correlation of field measurements with elastic theory of seafloor response to surface waves. Proceedings 13th Annual Offshore Technology Conference, p 3973, Vol. 1, Houston, TX, pp. 201-210.

Dawson, R.F., Morgenstern, N.R. and Gu, W.H., (1992). "Instability mechanisms initiating flow failures in mountainous mine waste dumps." Study for Energy, Mines and Resources, Canada.

Demars, K.R. and Vanover, E.A., (1985). "Measurement of wave-induced pressures and stresses in a sandbed." Marine Geotechnology, Vol. 6, pp. 29-59.

Dyvik, R. and Madshus, C., (1985). "Laboratory measurements of G_{max} using bender elements." Proceedings, Advances in the art of testing soils under cyclic conditions, American Society of Civil Engineers, Detroit, Michigan, pp. 186-196.

Eckersley, J., (1990). "Instrumented laboratory flow slides." Geotechnique, Vol. 40, N0.3, pp. 489-502.

Esrig, M.I. and Kirby, R.C. (1977). "Implications of gas content for predicting the stability of submarine slopes". Marine Geotechnology, Vol. 2, pp. 81-100.

Evans, M.D., Seed, H.B. and Seed, R.B., (1992). "Membrane compliance and liquefaction of sluiced gravel specimens." Journal of the Geotechnical Engineering Division, ASCE, Vol.. 118, GT6, pp. 856-867.

Farrel, E.R. (1994). "Analysis of groundwater flow through leaky marine retaining structures". Geotechnique, Vol. 44, pp. 255-263.

Fear, C. and Robertson, P.K, (1994). "Estimating the undrained shear strength of sand: A theoretical framework." Canadian Geotechnical Journal, (in press).

Ferris, J.G. (1951). "Cyclic water level fluctuations as a basis for determining aquifer transmissivity." International Association of Hydrological Sciences, Vol. 2 pp. 148 -155.

Field, M.E., Gardner, J.V., Jennings, A.E., and Edwards, B.D., (1982). "Earthquake-induced sediment failures on a 0.25° slope, Klamath River Delta, California." Geology., Vol. 10, pp. 542-546.

Finn, W.D.L, Siddharthan, R and Martin, G.R., (1983). "Response of seafloor to ocean waves". Journal of Geotechnical Engineering, ASCE, Vol. 109, pp. 556-572.

Fredlund, D.G. and Rahardjo, H. (1993). *Soil Mechanics for Unsaturated Soils.* John Wiley & Sons Inc.

Gu, W.H., Morgenstern, N.R. and Robertson, R.K., (1993). "Progressive failure of the lower San Fernando dam." Journal of the Geotechnical Engineering Division, ASCE Vol. 119, pp. 333-348.

Hardin, B.O. And Drnevich, V.P., (1972). Shear modulus and damping of soils : design equations and curves. Journal of Soil Mechanics and Foundation Division, ASCE, Vol. 98(SM7), pp. 667-692.

Hart , B.S. (1993). Large-scale in-situ rotational failure on a low-angle delta slope: the Fore Slope Hills, Fraser Delta, British Columbia, Canada. Geo-Marine Lectures, Vol. 13, pp. 219-226.

Hart, B.S, Prior, D.B, Barrie, J.V., Currie, R.G. and Luternauer, J.L. (1992). "A river mouth submarine channel and failure complex, Fraser River Delta, Canada." Sedimentary Geology, Vol. 81, pp. 73- 87.

Heezen, B.C. and Ewing, M., (1952). "Turbidity currents and submarine slumps and the Grand Banks earthquake." American Journal of Science, Vol. 250, pp. 849-873.

Heezen, B.C. and Ewing, M., (1955). "Orleansville earthquake and turbidity currents." American Association of Petroleum geologists bulletin, Vol. 39, pp. 2505-2514.

Henkel, D.J. (1970). The role of waves in causing submarine landslides. Geotechnique, 20(1), pp. 123-150.

Holish, L.L., and Hendron., D.H., (1975). "Liquefaction considerations for two submerged essential service cooling ponds." 1975 Structural Design of Nuclear Power Plant Facilities, Vol. 1-B, New York: American Society for testing and materials, pp. 897 - 931.

Houtz, R.E. and Wellman, H.W., (1962). "Turbidity current at Kadavu Passage, Fiji." Geological Magazine, Vol. 99, pp. 57-62.

Hungr, O. and Morgenstern, N.R., (1984). "Experiments on the flow behaviour of granular materials at high velocity in an open channel." Geotechnique, Vol. 34, No. 3, pp. 405-413.

Hutchinson, J.N., (1988). "Morphology and geotechnical parameters of landslides in relation to geology and hydrogeology." Proceedings of 5th International symposium on landslides, Vol. 1, pp. 3-35.

Ishihara, K. (1993). "Liquefaction and flow failure during earthquakes." Geotechnique, Vol. 43, pp. 349-416.

Ishihara, K., Tatsuoka, F. and Yasuda, S, (1975). "Undrained deformation and liquefaction of sand under cyclic Stresses." Journal of Soils and Foundations, Vol. 15, No.1, pp. 29-44.

Ishihara, K., Verdugo, R. and Acacio, A.A., (1991). "Characterization of cyclic behavior of sand and post-seismic stability analysis." 9th Asian Regional Conference on Soil Mechanics and Foundation Engineering, Bangkok, Thailand, Vol. .2, pp. 17-40.

Ishihara, K. and Yamazaki, A.(1984). "Wave-induced liquefaction in seabed deposits of sand." *Seabed Mechanics*, edited by B. Denness, London, pp. 139-148.

Johns, M.W., Prior, D.B., Bornhold, B.D., Coleman, J.M. and Bryant, W.R. (1986). "Geotechnical aspects of a submarine slope failure, Kitimat fjord, British Columbia." Marine Geotechnology, Vol. 6, pp. 243-279.

Karlsrud, K. and Edgers, L. (1980). "Some aspects of submarine slope stability". *Marine Slides and Other Mas Movements,* edited by Saxov. S and Nieuwenhuis, J.K., Plenum press, pp. 61-81.

Kraft, Jr., L.M., Gavin, T.M. and Bruton, J.C., (1992). Submarine flow slide in Puget Sound. Journal of Geotechnical Engineering, Vol. 118, GT10, pp 1577-1591.

Kramer, S.L., (1988). Triggering liquefaction flow slides in coastal soil deposits. Engineering Geology, Vol. 26, pp. 17-31.

Kramer, S.L. and Seed, H.B., (1988). "Initiation of soil liquefaction under static loading conditions". Journal of Geotechnical Engineering, ASCE, Vol. 114, pp. 412-430.

Koppejan, A.W., Van Wamelan, B.M., and Weinberg, L.J.H. (1948). "Coastal flow slides in the Dutch province of Zeeland." Proceedings of the Second International Conference on Soil Mechanics and Foundation Engineering, Rotterdam, Vol. 5, pp. 89-96.

Kostaschuk, R.A., Stephan, B.A., and Luternauer, J.L., (1989). "Sediment dynamics and implications for submarine landslides at the mouth of the Fraser River, British Columbia." Current Research, Part E, Geological Survey of Canada, Paper 89-1E, pp. 207-212.

Kostaschuk, R.A., Luternauer, J.L., Mckenna, G.T. and Moslow., T.F. (1991). "Sediment transport in a submarine channel system: Fraser River Delta, Canada." Journal of Sedimentary Petrology, Vol. 62, No. 2, pp. 273-282.

Lade, P.V., (1993). "Initiation of static instability in the submarine Nerlerk berms." Canadian Geotechnical Journal, Vol. 30.

Lee, H.J., Schwab, W.C. and Booth, J.S. (1993). "Submarine landslides: An Introduction." in *Submarine Landslides: Selected Studies in the U. S. Exclusive Economic zone*, U.S. Geological survey bulletin 2002. Edited by Schwab, W.C., Lee, H.J. and Twichell, D.C., pp. 1-13.

Lee, K.L. and Seed, H.B., (1967). "Drained strength characteristics of sands." Journal of Soil Mechanics and Foundation Division, ASCE, Vol. 93, No. SM6, 117-141.

Liu, P.L. (1973). "Damping of water waves over porous bed". Journal of Hydraulics Division, ASCE, Vol.99, pp. 2263-2271.

Luternauer, J.L., (1980). "Genesis of morphological features on the western delta front of the Fraser River, British Columbia" - status of knowledge in *The Coast Line of Canada* edited by McCann. S. B. Geological Survey of Canada, Paper 80, pp. 381-396.

Luternauer, J.L., Barrie, J.V., Christian, H.A., Clague, J.J., Evoy, E.W., Hart, B.S., Hunter, J.A., Killeen, P.G., Kostaschuk, R.A., Mathewes, R.W., Monahan, P.A., Moslow, T.F., Mwenifumbo, C.J., Olynuk, H.W., Patterson, R.T., Pullan, S.E., Roberts, M.C., Robertson , P.K., Tarbotton, M.R., and Woeller, D.J., (1994). "Fraser River Delta geology, geohazards and human impact." *Handbook of Lower Mainland Geoscience*. (Submitted to the Geological Survey of Canada).

Luternauer, J.L. and Finn, W.D.L., (1983). "Stability of the Fraser River Delta front." Canadian Geotechnical Journal, Vol. 20, pp. 603-616.

Madsen, O.S., (1978). "Wave induced pore pressures and effective stresses in a porous bed." Geotechnique, Vol. 28, No. 4, pp. 377-393.

Mallard, W. and Dalrymple, R.A. (1977). "Water waves propagating over a deformable bottom." Proceedings 9th Annual Offshore Technology Conference, Houston, Texas, pp. 141-146.

Mathews, W.H. and Shepard, F.P., (1962). "Sedimentation of Fraser River delta, British Columbia." American Association of petroleum Geology, Bulletin 46, pp. 1416-1438.

Mckenna, G.T. and Luternauer, J.L., (1987). First documented failure at the Fraser River Delta front, British Columbia. In *Current Research* , Part A, Geological Survey of Canada, Paper 87 - 1A , pp. 919-924.

McKenna, G.T. Luternauer, J.L. and Kostaschuk, R.A., (1992). "Large-Scale mass wasting events on the Fraser River Delta front near Sand Heads, British Columbia." Canadian Geotechnical Journal, Vol. 29, pp. 151 -156.

McRoberts, E.D. and Sladen, J.A. (1990). "Observations on static and cyclic sand liquefaction methodologies." Prediction and performance in Geotechnical, 43rd Canadian Geotechnical Conference, Quebec, pp. 215-226.

Menard, H.W. (1964). "*Marine Geology of the Pacific*" New York, McGraw-Hill Book Company.

Middleton, G.V. and Hampton, M.A. (1976). "Subaqueous sediment transport and deposition by sediment gravity flows" in *Marine Sediment Transport and Environmental Management.* D.J. Stanley and D.J.P. Swift, pp. 197-218.

Milliman, J.O., (1980). "Sedimentation in the Fraser River and its estuary, British Columbia." Esturine and Coastal Marine Science, Vol. 10, pp. 609-633.

Monahan, P.A., Luternauer, J.L., and Barrie, J.V., (1993). "A delta plain sheet sand in the Fraser River delta, British Columbia, Canada." Quaternary International, Vol. 20. pp. 27-38.

Money, M.S. (1986). "Tidal variations of groundwater level in an esturine aquifer." in *Groundwater in engineering geology*, edited by Cripps, J.C., Bell, G. and Culashaw, G., Geological Society, Engineering Geology Special Publication, No.3, pp. 81-85.

Morgenstern, N.R., (1967). "Submarine slumping and the initiation of turbidity currents." *Marine Geotechnique*, Edited by A.F.Richards, Urbana, Illinois, University of Illinois Press, pp. 189-210.

Morgenstern, N.R., (1994). "Observations on the collapse of granular materials." 42nd Annual Geotechnical Engineering Conference, Minneapolis, Minnesota, pp. 1-18

Morrison, K.I., (1984). "Case history of very large submarine landslide, Kitimat, British Columbia." IV International symposium on landslides. Vol. 2. pp. 337-342.

Moslow, T.F., Luternauer, J.L., and Kostaschuk, R.A., (1991). "Patterns and rates of sedimentation on the Fraser River delta slope, British Columbia." in Current Research, Part E, Geological Survey of Canada, Paper 91- 1E, pp. 141 -145.

Nataraja, M.S. and Gill, H.S., (1983). "Ocean wave induced liquefaction analysis." Journal of Geotechnical Engineering Division, ASCE, Vol. 109, pp. 573-590.

Okusa, S., Nakamura, T, and Fukue, M. (1984). "Measurement of wave-induced pore pressures and coefficients of permeability of submarine sediments during reversing flow." *Seabed Mechanics*, edited by Bruce Denness, London, pp. 113-122.

Pontin, J.M.A. (1986). "Predictions of groundwater pressures and uplift below excavations in tidal limits." in *Groundwater in engineering geology*, edited by Cripps, J.C., Bell, G. and Culashaw, G., Geological Society, Engineering Geology Special Publication, No. 3, pp. 353-366.

Postama., G. (1986). Classification for sediment gravity flow deposits based on flow conditions during sedimentation. Geology, Vol. 14, pp. 291-294.

Poulos, S.J., (1981). "The Steady state of deformation." Journal of Geotechnical Engineering Division, ASCE, Vol. 107, GT5, pp. 553-562.

Poulos, H.G., (1988). *Marine Geotechnics,* Published by Prentice-Hall Inc., 473 p.

Putnam, J.A., (1949). "Loss of wave energy due to percolation in a permeable sea bottom." Transactions, American Geophysics Union, Vol. 38, pp. 662-666.

Robertson, P.K., (1994). "Suggested Terminology for liquefaction: An internal CANLEX report." University of Alberta, Alberta, Canada. pp. 1-20.

Robertson, P.K, and Campanella, R.G. (1983). "Interpretation of cone penetration tests. Part I: Sand." Canadian Geotechnical Journal, Vol. 20, pp. 718-733.

Robertson, P.K, Woeller, D.J., Kokan, M., Hunter, J. and Luternauer, J., (1992,a). "Seismic techniques to evaluate liquefaction potential." 45th Canadian Geotechnical Conference, Toronto. Vol. 5, pp. 1-7.

Robertson, P.K, Woeller, D.J., and Finn, W.D.L, (1992, b). "Seismic cone penetration tests for evaluating liquefaction potential under cyclic loading." Canadian Geotechnical Journal, Vol.29, pp. 689-695.

Roscoe, K.H., Schofield, A.N., and Wroth, C.P. (1958). " On the yielding of soils." Geotechnique, Vol. 8, No.1, pp. 22 -53.

Sasitharan, S. (1994). "Collapse behaviour of very loose sand." Ph.D. thesis, Department of Civil Engineering, University of Alberta, Edmonton.

Sasitharan, S., Robertson, P.K., Sego, D.C. and Morgenstern, N.R., (1993). "Collapse behaviour of sand." Canadian Geotechnical Journal, Vol. 30, pp. 569-577.

Sasitharan, S., Robertson, P.K., Sego., D.C. and Morgenstern., N.R., (1994). "A state boundary surface for very loose sand and its practical implications." Canadian Geotechnical Journal, Vol. 31, No. 3, pp. 321-334.

Schawarz, H.U. (1982). "Subaqueous slope failures - experiments and modern Occurrences." *Contributions to Sedimentology* . Edited by Fuchtbauer, F, Lisitzyn, A.P., Milliman, J.D. and Seibold, E., Stuttgart.

Scotton, S. (1977). *The outer banks of the Fraser River Delta, engineering properties and stability considerations.* Unpublished Thesis, Department of Civil Engineering, University of British Columbia, Vancouver.

Seed, H.B., (1968). "Landslides during earthquakes due to soil liquefaction." Journal of the Soil Mechanics and Foundation Division, ASCE, Vol. 94, SM 5, pp. 1053-1122.

Seed, H.B., (1979). "Soil liquefaction and cyclic mobility evaluation for level ground during earthquakes". Journal of Geotechnical Engineering, ASCE, Vol. 105, No. 2, pp. 201-255.

Seed, H.B. And Rahman, M.S. (1978). Wave-induced pore pressure in relation to ocean floor stability of cohesion less soils. Marine Geotechnology 3, pp. 123-150.

Seed, H.B., Idriss, I.M., and Arango, I., (1983). "Evaluation of liquefaction potential using field performance data." ASCE, Vol. 109, GT3, pp. 458-482.

Sego, D.C., Robertson, P.K., Sasitharan, S., Kilpatrick, B.L. and Pillai, V.S. (1994). "Ground freezing and sampling of foundation soils at Duncan Dam." Canadian Geotechnical Journal. Vol. 31, pp. 939-950.

Shepard, F.P., and Milliman, J.D. (1978). "Sea-floor currents on the foreset slope of the Fraser River delta, British Columbia (Canada)." Marine Geology, Vol. 28, pp. 245-251.

Shore Protection Manual, (1984). 4th edition. Publication by Department of the Army, Waterways Experiment Station, Corps of Engineers, Coastal Engineering Research Center, Washington, DC.

Skopek, P., Morgenstern, N.R., Robertson, P.K. and Sego, D.C., (1993). "Collapse of dry sand." Submitted to Canadian Geotechnical Journal.

Skopek, P., Morgenstern, N.R., and Robertson, P.K., (1994). "State boundary surface for very loose sand." Submitted to Canadian Geotechnical Journal.

Skopek, P., Morgenstern, N.R., and Robertson, P.K., (1994). "Effective stress approach to evaluate flow liquefaction." Submitted to Canadian Geotechnical Journal.

Sladen, J.A., D'Hollander, R.D. and Krahn, J., (1985,a). "The Liquefaction of sands - a collapse surface approach." Canadian Geotechnical Journal, Vol. 22, pp. 564-578.

Sladen, J.A., D' Hollander, R.D., and Krahn, J.,(1985,b). "Back analysis of the Nerlerk Berm liquefaction slides." Canadian Geotechnical Journal, Vol. 22, pp. 579-588.

Sladen, J.A., and Hewitt, K.J., (1989). "Influence of placement method of the in-situ density of hydraulic fills." Canadian Geotechnical Journal, Vol. 26, pp. 453-466.

Sleath, J.F.A. (1970). "Wave-induced pressures in beds of sand." Journal of Hydraulics Division, ASCE, Vol. 96, pp. 367-379.

Sparks, A.D.W. (1963). "Theoretical considerations of stress equations for partly saturated soils." Proceedings, 3rd Africa Regional Conference of Soils Mechanics and Foundation Engineering, Salisbury, Vol. 1, pp. 215-218.

Stokoe, K.H. II , Roesset, J. M, Nazarian, S, Rix, G.J., Mok, Y. J,. Sanchez-Salinero, Sheu, J. C. (1987). In-situ testing of hard-to-sample soils. XIII CGT, Confernze di Geotechnica di Torino, 10-12 November.

Terzaghi, K, (1956). "Varieties of submarine slope failures." Proceedings of 8th Texas Conference on Soils and Foundation Engineering., University of Texas, Austin, pp. 1-41.

Terzaghi, K., (1962). "Discussion of " Sedimentation of Fraser River Delta, British Columbia." by Mathwes and Shepard, 1962." American Association of Petroleum Geology Bulletin ,Vol. 46, pp. 1438-1443.

Terzaghi, K. and Peck, R.B. (1948). *Soil Mechanics in Engineering Practice*, New York, John Wiley & Sons. 566 p.

Thomson, K., (1975). "Longshore current generation by internal waves in the Straight of Georgia." Canadian Journal of Earth Sciences, Vol. 12, pp. 472-488.

Thomson, K., (1981). *Oceanography of the British Columbia Coast*, Canadian Specialty Publication of Fisheries and Aquatic Sciences, 56, 291 p.

Tiffin, D.L., Murray, J.W., Mayers, I.R. and Garrison, R.E. (1971). Structure and origin of Foreslope Hills, Fraser Delta, British Columbia. Canadian Petroleum Geology Bulletin, Vol. 19, pp. 589-600.

Tsui, Y.S. and Helfrich, S.C., (1983). "Wave-induced pore pressures in submerged sand layer." Journal of Geotechnical Engineering Division, ASCE, Vol. 109, pp. 603-618.

Vaid, Y.P., and Chern, J.C., (1985). "Cyclic and monotonic undrained response of saturated sands." Advances in the Art of Testing Soils under Cyclic Conditions. ASCE National Convention, Detroit, pp. 120-147.

Vaid, Y.P. and Thomas, J, (1995). "Liquefaction and postliquefaction behaviour of sand." Journal of Geotechnical Engineering, ASCE, Vol. 121, No. 2, February, pp. 163-173.

Varnes, D.J., (1958). "Landslides types and processes, in Eckel, E.D.," ed., *Landslides and Engineering Practice; Highway Research Board* Special Report 29, pp. 20-47.

Verruijt, A. (1969). "Elastic storage of aquifers." in *Flow Through Porous Media,* edited by DeWiest, R.J.M., Chapter 8, Academic Press, pp. 331-376.

Vuez, A. and Rahal, A. (1994). "Cyclic loading for the measuring of soil consolidation parameters." Proceedings, Settlement'94, Texas A&M University, College Station, pp. .762-774.

Wiegel, R.L. (1964). *Oceanographical Engineering.* ; Prentice-Hall., Englewood Cliffs, N.J.

Yamamoto , T., Koning, H.L.,Sellmeijer, H. and Hijum, E.V., (1978). "On the response of a poro-elastic bed to water waves." Journal of Fluid Mechanics, Vol. 87, pp. 193-206.

Zen, K. and Yamazaki, H. (1990). "Mechanism of wave-induced liquefaction and densification in seabed." Journal of Soils and Foundations, Vol. 30, pp. 90-104.

Appendix A

Methods of Sample Preparation

Two techniques are used for preparing samples of the Fraser River Delta sand for laboratory testing. The basic requirements of any of the methods are firstly to obtain homogeneous samples with uniform distribution of void ratio and secondly to be able to prepare samples having the lowest possible density. It has been observed that different methods of sample preparation create different fabrics, thereby yielding different response to load application.

1. Moist Tamping Method

A known weight of dry sand is mixed with water thoroughly to achieve a moisture content of about 5 percent. Because of capillarity effects between particles, the moist sand can be used to prepare a very loose structured sample with a void ratio higher than the ASTM derived maximum void ratio. A membrane is stretched on the inside face of a split mould which is attached to the base pedestal of the testing apparatus. A vacuum of about 25 kPa is applied to the split mould to maintain the stretched membrane taut to the inside face of the mould. The moist sand is placed in 4 to 5 layers into the split mould. Each layer is compacted with a small flat-bottom tamper weighing 150 grams falling between 10 to 15 mm. The number of blows is increased for each additional layer for obtaining uniform density in the sample. This method of preparation ensures a very loose structure of the sample. The number of blows can be increased for preparing a dense sample. If the tamping energy is small, the sample will be so loose that volume contraction will occur

upon subsequent saturation with water. Hence the optimum amount of energy should be applied in preparing a loose sample.

After the sample is enclosed by the membrane with a top cap, a vacuum of 25 kPa is applied through the sample and the split mould is dismantled. The sample dimensions are measured. The top cell is placed on the base of the test apparatus. The cell is mounted in the frame. A cell pressure of 25 kPa is applied and the vacuum is disconnected. Carbon dioxide is percolated through the sample and de-aired water is flushed through it. During the saturation process, volume changes in the sample are recorded.

After flushing a back pressure is applied to saturate the sample. During the back pressure saturation, the pore pressure and the cell pressure are monitored simultaneously to determine the pore pressure parameter, B. When the B value reaches 0.99 or greater, the sample is considered to be fully saturated.

2. Water Pluviation Method

A known weight of sand is boiled with water in a flask to de-air the mixture. The mixture is allowed to cool at room temperature. A membrane is stretched taut to the inside face of a split mould which is attached to the base pedestal of the test apparatus. The membrane cavity is filled with de-aired water. A rubber stopper with a glass nozzle is used to seal the flask after filling it with de-aired water to the brim. The glass nozzle is also filled with de-aired water. The flask is inverted into the membrane cavity. Sand starts depositing in the mould by replacing the de-aired water. The upward flow of the de-aired water creates turbulence and suspends fine particles. Segregation of sand is a problem with this technique. After the deposition of the sand the top cap is placed and the membrane is stretched on to the top cap. A vacuum of 20 -25 kPa is applied through the sample while

ensuring that the vacuum does not disturb the sample. Sample measurements are made. The top cell is placed on the base of the testing apparatus. The cell is mounted on the frame. A cell pressure of about 25 kPa is applied and the vacuum is disconnected. Back pressure is applied for saturation. During the back pressure saturation, the pore pressure and the cell pressure are monitored simultaneously to determine the pore pressure parameter, B. When the B value reaches 0.99 or greater, the sample is considered to be fully saturated.

Appendix B

Modeling Tidal Loading on Saturated Sediments

Modeling of tidal variations for one-dimensional conditions can be given by

$$\frac{1}{c_{vg}}\frac{\partial u}{\partial t} = \frac{\partial^2 u}{\partial z^2} + \frac{1}{c_v}\frac{\partial \sigma}{\partial t} \qquad \text{(B.1)}$$

This general equation describes the pore pressure response in sediments with a compressible pore fluid for a time dependent loading. For saturated sediments, the compressibility of the pore fluid can be assumed negligible. Hence, the equation will be of the form,

$$\frac{\partial u}{\partial t} = c_v \frac{\partial^2 u}{\partial z^2} + \frac{\partial \sigma}{\partial t} \qquad \text{(B.2)}$$

The solution of Equation (B.2) for the boundary value problem can be obtained using finite difference equations. In Equation B.2, the first two terms represent the basic differential equation, that is, the one dimensional consolidation equation by Terzaghi. Braja M. Das (1987) presents the finite difference equations for the basic equation.

For arbitrary reference excess pore pressure u_R, time t_R and depth z_R, the equation can be expressed in non-dimensional form as

$$\frac{1}{t_R}\frac{\partial \bar{u}}{\partial \bar{t}} = \frac{c_v}{z_R^2}\frac{\partial^2 \bar{u}}{\partial \bar{z}^2} \tag{B.3}$$

If the reference time t_R is selected in such a way that $t_R = z_R^2/c_v$, Equation B.3 takes the form

$$\frac{\partial \bar{u}}{\partial \bar{t}} = \frac{\partial^2 \bar{u}}{\partial \bar{z}^2} \tag{B.4}$$

The left-hand side of Equation (B.4) can be written in finite difference form as

$$\frac{\partial \bar{u}}{\partial \bar{t}} = \frac{1}{\Delta \bar{t}}(\bar{u}_{0,\bar{t}+\Delta\bar{t}} - \bar{u}_{0,\bar{t}}) \tag{B.5}$$

where $\bar{u}_{0,\bar{t}}$ and $\bar{u}_{0,\bar{t}+\Delta\bar{t}}$ are the nondimensional pore pressure at point 0 (Figure B.1), at nondimesional times t and t+Δt. Similarly, the right-hand side can be expressed in finite difference form

$$\frac{\partial^2 \bar{u}}{\partial \bar{z}^2} = \frac{1}{(\Delta z)^2}(\bar{u}_{1,\bar{t}} + \bar{u}_{3,\bar{t}} - 2\bar{u}_{0,\bar{t}}) \tag{B.6}$$

Equating Equations B.5 and B.6 and rearranging

$$\bar{u}_{0,\bar{t}+\Delta\bar{t}} = \frac{\overline{\Delta t}}{(\Delta \bar{z})^2}(\bar{u}_{1,\bar{t}} + \bar{u}_{3,\bar{t}} - 2\bar{u}_{0,\bar{t}}) + \bar{u}_{0,\bar{t}} \tag{B.7}$$

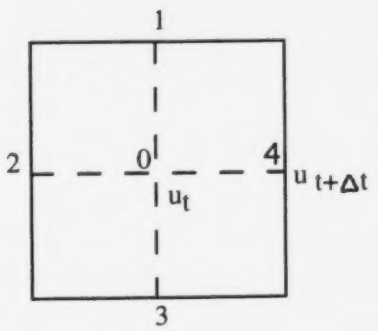

Figure B.1

For Equation B.7 to converge, $\Delta\bar{t}$ and $\partial\bar{z}$ must be chosen such that $\frac{\overline{\Delta t}}{(\Delta\bar{z})^2}$ is less than 0.5. At the interface of an impervious layer, the suffix 3 can be replaced by the suffix 1 in Equation B.7. The above equations can be used for modeling the tidal variations as a time dependant loading. σ in Equation B.2 represents the sinusoidal loading due to a tide, that is,

$$\sigma = (\gamma_w H/2) \sin \omega t \qquad (B.8)$$

For saturated sediments, the ratio, r, c_{vg}/c_v is equal to one. The loading term, $\partial\sigma/\partial t$, wil be added/subtracted to the pore pressure response at different depths and at different time steps depending on the stage of the tide during calculation.

It is of interest to study the pore pressure response of saturated sediments for a tide of 5 m with a period of 16 hr and at a depth of 36 m in the Fraser River Delta. It is assumed that the time step,t_R, is 15 minutes and z_R is 36 m. Hence, $\Delta\bar{z} = 0.5$ for a depth step of 18 m. Table 7.1 presents the value of c_v for saturated sediments as 0.11.

Therefore, $\frac{\overline{\Delta t}}{(\Delta\bar{z})^2}$ is calculated as 0.308 which is less than 0.5.

The final equation will be

$$\bar{u}_{0,\bar{t}+\Delta\bar{t}} = 0.308(\bar{u}_{1,\bar{t}} + \bar{u}_{3,\bar{t}} - 2\bar{u}_{0,\bar{t}}) + \bar{u}_{0,\bar{t}} + \frac{\partial\sigma}{\partial t} \qquad \text{(B.9)}$$

This equation can be solved for the pore pressure response on saturated sediments for the 5 m tide.

Appendix C

Modeling Tidal Loading on Gaseous Sediments

Equation B.1 presents the modeling equation for one-dimensional condition. The solution for the boundary value problem results in the pore pressure response of gaseous sediments for tidal loading. In nondimensional terms, the governing equation can be written from Equation B.9 as

$$\bar{u}_{0,\bar{t}+\Delta\bar{t}} = \frac{\Delta\bar{t}}{(\Delta\bar{z}^2)}(\bar{u}_{1,\bar{t}} + \bar{u}_{3,\bar{t}} - 2\bar{u}_{0,\bar{t}}) + \bar{u}_{0,\bar{t}} + \frac{c_{vg}}{c_v}\frac{\partial\sigma}{\partial t} \qquad \text{(C.1)}$$

Table presents values of the ratio ($r = c_{vg}/c_v$) for different degrees of saturation. As the first case of the analysis, a degree of saturation of 98% is considered to represent the in-situ degree of saturation of the sediments in the Fraser River Delta. For the 98% saturation, the ratio, r, is 0.41. Other requirement, such as $\frac{\Delta\bar{t}}{(\Delta\bar{z}^2)} < 0.5$, is to be satisfied in the analysis.

The pore pressure response of gaseous sediments is to be obtained for the tide of 5 m with a period of 16 hr period. It is assumed that the time step, t_R, is 15 minutes and the reference depth, z_R, is 36 m. Hence, $\Delta\bar{z} = 0.25$ for a depth step of 9 m. Table 7.1 presents the value of c_{vg} for the 98% saturated sediments as 4.11×10^{-2} m^2/sec.

Therefore, $\frac{\Delta\bar{t}}{(\Delta\bar{z}^2)}$ is calculated as 0.48 which is less than 0.5. Using Equation C.1, the pore pressure response can be obtained for the 5 m tide.